Université de Montréal

Équations différentielles à retard et leur application en hématopoïèse, avec étude du cas de la neutropénie cyclique

par

Samuel Bernard

Département de mathématiques et de statistique

Faculté des arts et des sciences

Thèse présentée à la Faculté des études supérieures

en vue de l'obtention du grade de

Philosophiæ Doctor (Ph.D.)
en Mathématiques appliquées

décembre 2003

Université de Montréal

Faculté des études supérieures

Cette thèse intitulée

Équations différentielles à retard et leur application en hématopoïèse, avec étude du cas de la neutropénie cyclique

présentée par

Samuel Bernard

a été évaluée par un jury composé des personnes suivantes :

Robert Brunet
(président-rapporteur)

Jacques Bélair
(directeur de recherche)

Michael C. Mackey
(co-directeur)

Michel Delfour
(membre du jury)

Glenn Webb
(examinateur externe)

André Garon
(représentant du doyen de la FES)

Thèse acceptée le:

RÉSUMÉ

Le système hématopoïétique est responsable de la production des cellules sanguines. Chaque jour, le corps humain produit 10^{12} cellules sanguines à partir des cellules souches hématopoïétiques (CSH). Les équations aux dérivées partielles (EDP) avec structure d'âge et de maturité ainsi que les équations différentielles à retard se révèlent efficaces dans la modélisation des contrôles du système hématopoïétique. Ces deux types d'équations sont utilisés dans une série de quatre articles présentés dans cette thèse.

Le premier article porte sur la stabilité des équations différentielles linéaires avec distribution de retards (EDLDR). Un théorème donne des conditions suffisantes pour qu'une EDLDR soit stable en ne connaissant que l'espérance E et la forme générale de la distribution : si la distribution a une asymétrie à gauche alors l'équation est stable si l'équation correspondante avec un retard discret (EDR) en E est stable. Autrement dit, l'EDLDR est stable si l'EDR correspondante est stable.

Le deuxième article présente un modèle de production de neutrophiles et traite plus précisément de l'origine de la neutropénie cyclique. Ce désordre sanguin présente une oscillation de la population de neutrophiles sous la moyenne. Le modèle à deux compartiments et à deux retards tient compte des CSH et des neutrophiles mûrs. Après une estimation rigoureuse des paramètres et une analyse de la dynamique du modèle, l'hypothèse selon laquelle la source des oscillations se trouve dans le bassin des CSH est confirmée ici. Le modèle permet ainsi de conclure que la hausse de l'apoptose (mort programmée) des précurseurs des neutrophiles induit une pression indue sur la différenciation des CSH, provoquant en retour une hausse de la prolifération de ces cellules, ce qui déstabilise le système.

Le troisième article présente une analyse approfondie des bifurcations du modèle proposé dans le deuxième article. La transition de valeurs normales des paramètres à des valeurs pathologiques mène à des bifurcations de Hopf surcritiques ainsi que des bifurcations col-nœud de cycles limites.

Le dernier article introduit un système d'EDP linéaires structurées en âge et en maturité permettant d'analyser les données provenant d'expériences de traquage de cellules proliférantes. Le modèle permet l'estimation des paramètres cinétiques des cellules.

MOTS-CLÉS

équation différentielle à retard, stabilité linéaire, bifurcation de Hopf, multistabilité, apoptose, cycle cellulaire, différenciation cellulaire, équation aux dérivées partielles, modèle structuré en âge-maturité, distribution de temps de maturation

SUMMARY

The hematopoietic system is responsible for the production of blood cells. The human body produces 10^{12} blood cells each day from a pool of hematopoietic stem cells (HSC). Age and maturity structured partial differential equations (PDE), and delay differential equations are well suited to modeling hematopoietic system control mechanisms. These two types of equations are used in a series of four articles presented in this thesis.

The first article deals with the stability of linear differential equations with distributed delays (LDEDD). A theorem gives sufficient conditions for a LDEDD to be stable when only the expectation E and general shape of the distribution are known : if the distribution is left skewed, then the equation is stable if the corresponding equation with a discrete delay (DDE) in E is stable. That is to say, the LDEDD is stable if the corresponding DDE is stable.

The second article presents a neutrophil production model. The origin of cyclical neutropenia is studied. Cyclical neutropenia is a hematological disorder in which a below average oscillation in neutrophil count is seen. This two-compartment model with two delays takes into account the HSC and mature neutrophil count. After rigorous parameter estimation and analysis of the model dynamics, the hypothesis that the source of oscillation is the stem cell pool is confirmed. The model allows us to conclude that the increase of apoptosis (programmed cell death) of neutrophil precursors induces an overpressure on the HSC differentiation, provoking an increase of the HSC proliferation, which destabilizes the system.

The third article uses the above-mentioned model and an exhaustive bifurcation analysis of the model is performed. The transition from normal to pathological parameter values induces supercritical Hopf bifurcations and saddle-node bifurcations of limit cycles.

The last article introduces a system of linear PDEs with age and maturity structure to analyse data coming from proliferative cell tracking experiments. The model allows the estimation of cell kinetic parameters.

KEYWORDS

delay differential equation, linear stability, Hopf bifurcation, multistability, apoptosis, cell cycle, cell differentiation, partial differential equation, maturity and age-structured model, distribution of maturation times

TABLE DES MATIÈRES

LISTE DES FIGURES

LISTE DES TABLEAUX

LISTE DES SIGLES

Sigles français	Sigles anglais	Signification
CSH	HSC	Cellule souche hématopoïétique
GB	WBC	Globule blanc
EDP	PDE	Équation aux dérivées partielles
EDR	DDE	Équation différentielle à retard
CFSE	CFSE	CarboxyFluorescein diacetate Succinimidyl Ester
Epo	Epo	Érythropoïétine
G-CSF	G-CSF	Facteur de croissance hématopoïétique-granulocytique
Tpo	Tpo	Thrombopoïétine
LMC	CML	Leucémie myéloïde chronique
MV	PV	Maladie de Vaquez
NC	CN	Neutropénie cyclique
TGM	MGT	Temps de génération moyen

À MariÈve

REMERCIEMENTS

Je tiens tout d'abord à remercier mes deux directeurs, Jacques Bélair et Michael C. Mackey, qui m'ont initié à cette discipline de la dynamique non linéaire. Grâce à leur expérience et leur dynamisme, ma conception de la science a complètement changé.

Jacques Bélair, professeur pour qui rien n'est impossible, m'a fait découvrir un des domaines d'application mathématiques les plus intéressants. Je le remercie pour sa confiance en moi, et son appui indéfectible.

Michael C. Mackey est un professeur aux vastes connaissances dont une des plus grandes qualités scientifiques est de ne jamais être satisfait par un modèle ou une théorie. Il m'a inculqué un sens critique et m'a appris à aller directement à l'essentiel, sans faire de compromis pour des raisons de facilité ou d'esthétisme.

Je voudrais aussi remercier les organismes qui m'ont permis de poursuivre mes recherches sans me faire de soucis : l'Institut des sciences mathématiques (ISM), le Centre de recherches mathématiques (CRM), les Mathématiques pour les technologies de l'information et des systèmes complexes (MATISC, Canada), la Faculté des études supérieures de l'Université de Montréal, le Fonds pour la formation des chercheurs et l'aide à la recherche (FCAR, Québec) et le Conseil de recherche en sciences naturelles et en génie (CRSNG, Canada).

J'ai aussi une pensée pour tout le groupe du Département de mathématiques et de statistique de l'Université de Montréal, les étudiants, les professeurs et le personnel de soutien.

Les dernières années passées au Centre de Dynamique Nonlinéaire en Physiologie et en Médecine à l'Université McGill furent pour moi une révélation. Je veux remercier les différents étudiants et stagiaires post-doctoraux qui y sont ou sont passés par là pour

leurs idées et leur esprit : Caroline, Gil, Katsumi, Tiger, Moises, Trine, Christian, Necmettin, Michèle, Laurence, Sherwin, Eric et particulièrement Laurent Pujo-Menjouet, avec qui j'ai formé une incroyable équipe et qui a bien voulu prendre le temps de relire cette thèse. Ses judicieux commentaires ont permis de la rendre un peu plus compréhensible.

Je remercie aussi le jury pour son intérêt.

Merci à ma famille, qui m'a toujours soutenu et encouragé ; ma mère mes frères et sœur.

Enfin, un merci sincère à MariEve qui m'a accompagné tout au long de mon cheminement.

Chapitre 1

INTRODUCTION

1.1. HÉMATOPOÏÈSE

L'hématopoïèse se définit comme la production de cellules sanguines. Bien qu'il soit établi que toutes les cellules sanguines proviennent d'une même source, les cellules souches hématopoïétiques, les mécanismes régissant cette production sont encore mal compris. Il semble toutefois clair que la production des érythrocytes et thrombocytes est contrôlée par des mécanismes de feedback faisant intervenir des cytokines (protéines de type hormonales) comme l'érythropoïétine (Epo) ou la thrombopoïétine (Tpo) (Mahaffy et al., 1998; Santillan et al., 2000). Cependant la régulation de la leucopoïèse (formation des globules blancs) est moins bien comprise, de même que les mécanismes locaux de régulation des cellules souches hématopoïétiques (Haurie et al., 1998, 1999a,b, 2000; Hearn et al., 1998; Rubinow et Lebowitz, 1975; MacDonald, 1978; Mackey, 2001). Grâce à leur caractère dynamique, la neutropénie cyclique et autres désordres hématologiques périodiques nous permettent de mieux cerner la nature de ces processus de régulation (von Schulthess et Mazer, 1982). Dans cette introduction, nous passerons en revue différentes maladies hématologiques dynamiques ainsi que divers modèles utilisés pour décrire les caractéristiques particulières de ces désordres. Nous verrons que la plupart de ces modèles nécessitent l'utilisation d'équations différentielles à retard ou encore, de modèles structurés en maturité pour décrire l'évolution de ces maladies. Dès les années soixante-dix, ces systèmes ont été utilisés pour la description de l'hématopoïèse (MacDonald, 1978; Rubinow et Lebowitz, 1975) jusqu'à tout récemment dans la modélisation de l'érythropoïèse (Bélair et al.,

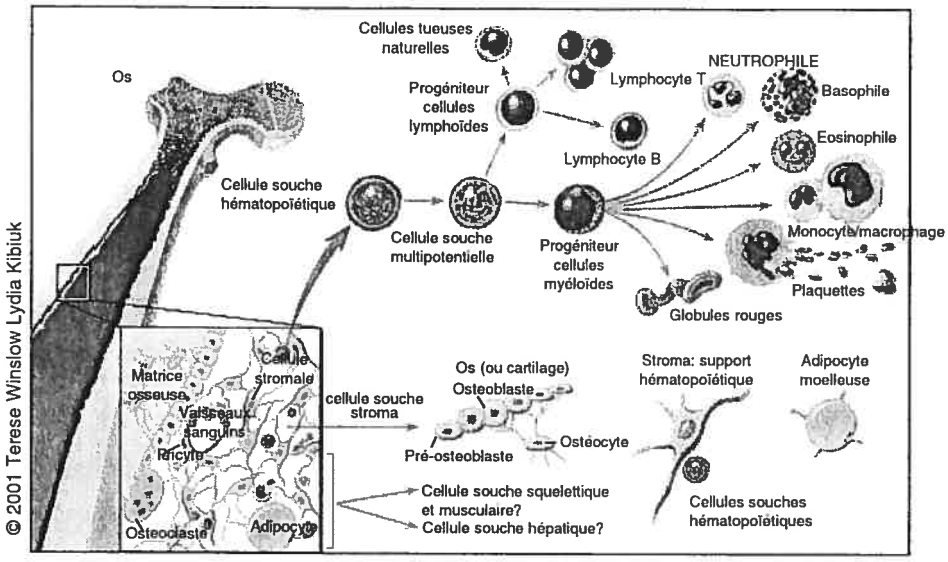

FIG. 1.1. Différentes cellules sanguines. Figure prise du site web du National Institutes of Health (NIH).

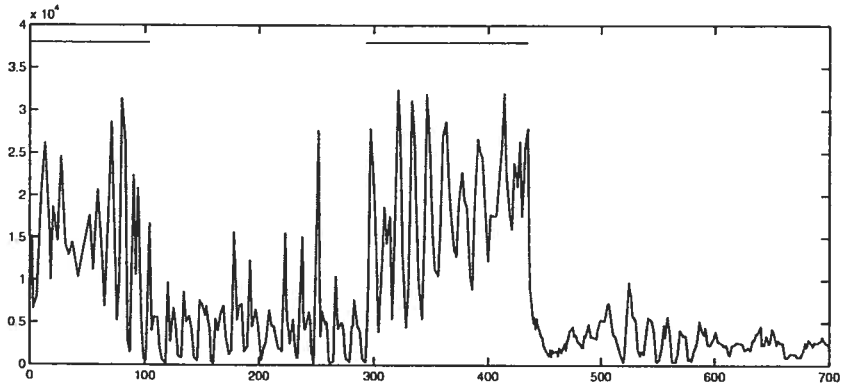

FIG. 1.2. Données expérimentales d'Oprah, un colley gris atteint de neutropénie cyclique. Les lignes en haut indiquent les phases de traitement au G-CSF. Données de Haurie et al.

1995; Mahaffy et al., 1998) ou de la thrombopoïèse (Santillan et al., 2000; Bélair et Mackey, 1987). Les équations à retard sont aussi largement utilisées dans d'autres domaines des sciences biologiques, notamment les réseaux neuronaux (Bélair et al., 1996; Campbell et al., 1995; Bélair et Campbell, 1994), la pharmacodynamique (Milton et al., 1995), la dilatation de la pupille (Longtin et Milton, 1988, 1989a,b; Longtin et al., 1990) ou le stockage d'information (Mensour et Longtin, 1995).

1.2. DÉSORDRES HÉMATOPOÏÉTIQUES PÉRIODIQUES

La neutropénie cyclique (NC) est une maladie hématologique rare caractérisée par une oscillation dans le nombre de neutrophiles en circulation dans le sang. La population passe d'un niveau normal et chute à un niveau indécelable suivant une période de 19 à 21 jours chez l'humain (Guerry et al., 1973; Dale et Hammond, 1988; Haurie et al., 1998), pouvant même aller jusqu'à 40 jours (Haurie et al., 1998). Ces oscillations du nombre de neutrophiles sont accompagnées généralement d'oscillations dans d'autres lignées cellulaires comme les plaquettes, les lymphocytes et les réticulocytes (Haurie et al., 2000). Tous les patients atteints de NC ont une mutation du gène de l'élastase des neutrophiles (Dale et al., 2000; Aprikyan et al., 2002) associée à un arrêt de la maturation et de la prolifération des précurseurs myéloïdes, probablement dû à une élévation du taux d'apoptose (Aprikyan et al., 2001).

La neutropénie cyclique existe aussi chez une race canine ; le colley gris (Lund et al., 1967) qui naît atteint de cette maladie congénitale. Ceci permet d'avoir beaucoup de données cliniques provenant de cet animal ; le défi étant de transférer chez l'humain les mécanismes de cette maladie compris chez le chien. La période d'oscillation chez le colley gris est typiquement de l'ordre de 11 à 15 jours (Haurie et al., 2000), soit environ 60% de la période moyenne chez l'humain.

En plus de la neutropénie cyclique, on retrouve un certain nombre de désordres hématologiques périodiques dans la littérature scientifique. Par exemple, la leucémie myéloïde (ou myélogène) chronique périodique (LMC) est une maladie caractérisée par une granulocytose et une splénomégalie (Grignani, 1985). Dans la majorité des cas, les cellules hématopoïétiques contiennent une translocation entre les chromosomes 9 et 22 ; ce dernier est appelé chromosome Philadelphia (Ph). En général, si aucun soin n'est apporté, la forme aiguë de la maladie finit par se développer. Différents cas rapportés dans la littérature scientifique ont été passés en revue par Fortin et Mackey (1999). Les périodes d'oscillations varient entre 30 et 100 jours.

La polyglobulie (ou polycythémie) essentielle, aussi appelée maladie de Vaquez (MV), est caractérisée par une prolifération accrue et incontrôlée de tous les progéniteurs hématopoïétiques. Il a été rapporté deux cas de MV avec oscillation du nombre de réticulocytes, de plaquettes et de neutrophiles. Les périodes étaient de 27 jours pour

les plaquettes, 15 jours pour les neutrophiles et 17 jours pour les réticulocytes (Morley, 1969).

Des oscillations sont aussi clairement vues dans les population des plaquettes, réticulocytes et neutrophiles dans les cas d'anémie aplastique (Mackey, 1978a; Morley, 1979) ainsi que chez un patient atteint de pancytopénie (Birgens et Karl, 1993) avec périodes de 40 et 100 jours respectivement.

La chimiothérapie, les radiations ou encore l'administration de cytokines peuvent aussi induire des oscillations dans le nombre de cellules sanguines. La cyclophosphamide a induit des cycles de 11 à 17 jours chez des chiens (Morley et Stohlman, 1970) et de 5,7 jours chez l'humain (Dale et al., 1973). Une érythropoïèse cyclique a été induite chez des souris anémiques de souche W/W^v et $S1/S1^d$ par du strontium-89 (Gurney et al., 1981; Gibson et al., 1984, 1985). La période était de 16 jours. Des oscillations dans le nombre de cellules sanguines induites par des traitements d'hydroxycarbamide (hydroxyurée) ont aussi été aperçues chez des patients atteints de MV et de LMC (Bennett et Grunwald, 2001; Steensma et al., 2001). Un patient atteint de MV a eu des oscillations du nombre de plaquette avec une période de 29 jours tandis que deux patients atteints de LMC ont eu des oscillations du nombre de globules blancs, de plaquettes et du niveau d'hémoglobine, avec des périodes moyennes de 74 et 64 jours.

Le G-CSF (granulocyte-colony stimulating factor) est fréquemment utilisé pour stimuler la reconstitution de la moelle osseuse et lutter contre une neutropénie transitoire après une transplantation ou un traitement de chimiothérapie, et peut induire des oscillations dans le nombre de neutrophiles (Dale et al., 1993).

Enfin, des oscillations dans le nombre de neutrophiles, de monocytes et de lymphocytes CD-8+ ont été observées chez des sujets en santé (Carulli et al., 2000).

Ces cas rapportés dans la littérature scientifique suggèrent qu'un délicat mécanisme de contrôle est à l'œuvre dans le système hématopoïétique et que certaines pathologies ainsi que des médicaments peuvent entraîner la déstabilisation de celui-ci.

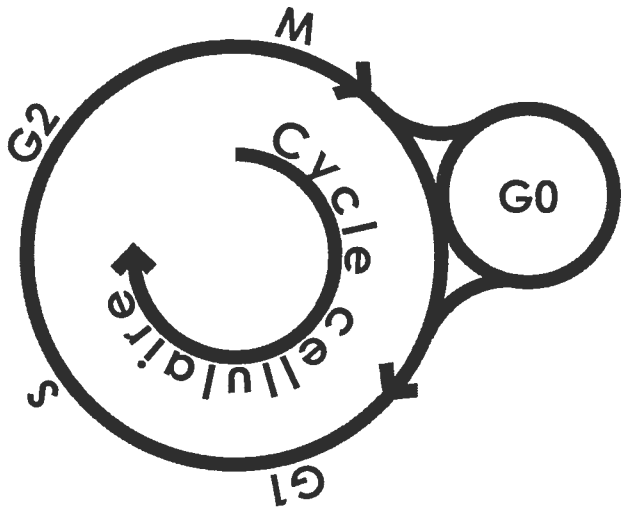

FIG. 1.3. Le cycle cellulaire.

1.3. APPROCHE MATHÉMATIQUE DU CYCLE CELLULAIRE

Le cycle cellulaire correspond à la période qui va de la naissance d'une cellule par division d'une cellule mère jusqu'à sa propre division. Le cycle cellulaire est traditionnellement constitué d'une phase de synthèse S de l'ADN, et d'une phase de mitose M. Deux phases intermédiaires G_1 et G_2 (G pour « gap ») précèdent les phases S et M, et sont considérées comme des points d'arrêt qui permettent à la cellule de vérifier que les mécanismes de division sont fonctionnels. Une autre phase G_0, qui suit la phase M, a une durée variable et les cellules dans cette phase sont au repos, ou hors du cycle cellulaire.

En général, l'approche utilisée pour modéliser la dynamique du cycle cellulaire tient compte de l'âge, de la maturité de la cellule ou parfois des deux. Les propriétés dynamiques des cellules dépendent de leur état de différenciation. Il importe donc d'inclure cette variable dans la construction d'un modèle. Deux classes de modèles peuvent être utilisées : stochastiques ou déterministes. Les modèles stochastiques peuvent être basés sur des processus de Markoff, où une cellule à l'état j a une probabilité de changer d'état (de se diviser ou d'avancer dans le cycle cellulaire) avec une distribution $\lambda_j \exp(-\lambda_j t)$, $t \geq 0$, $j = 1,...,k$. Chaque état j peut représenter une position dans le cycle cellulaire, et une cellule se divisera lorsqu'elle aura passé les k états, ou phases,

pour se retrouver en phase $j = 1$. Supposant les paramètres identiques, $\lambda_j \equiv \beta$, la distribution T des temps de divisions suivra une loi chi carré à $2k$ degrés de liberté χ^2_{2k} de paramètre β (Kendall, 1948) :

$$T \; : \; \frac{(\beta t)^{k-1}\beta e^{-\beta t}}{(k-1)!} \tag{1.3.1}$$

Cette distribution correspond aussi à une loi gamma, qui est très importante dans la modélisation de processus de naissance et de maturation. La loi déterministe τ est une autre distribution de temps de maturation fréquemment utilisée. Smith et Martin (1973) l'ont utilisée dans un modèle de cycle cellulaire où le temps T de division est $W + \tau$, avec W une variable aléatoire exponentielle de paramètre β représentant une phase de repos et τ une constante positive représentant une phase active où la cellule entre en division cellulaire. Si nous incluons aussi une probabilité pour les cellules au repos de quitter par différenciation et pour les cellules actives de quitter par apoptose, suivant respectivement des lois exponentielles de paramètre μ et γ, les équations donnant N l'espérance du nombre de cellules au repos et P l'espérance du nombre de cellules actives s'écrivent,

$$\frac{dN}{dt} = -[\mu+\beta]N(t) + 2\exp(-\gamma\tau)\beta N(t-\tau), \tag{1.3.2}$$

$$\frac{dP}{dt} = -\gamma P + \beta N - \exp(-\gamma\tau)\beta N(t-\tau). \tag{1.3.3}$$

Ce modèle a été intensément étudié ou utilisé par plusieurs auteurs dans des applications sur les phénomènes de résonance en chimiothérapie (Andersen et Mackey, 2001), pour déterminer des paramètres hématopoïétiques (Mackey, 2001), dans le cadre de modèles structurés en âge-maturation décrits par des équations aux dérivées partielles avec (Adimy et Pujo-Menjouet, 2001; Pujo-Menjouet et Rudnicki, 2000; Mackey et Rudnicki, 1994, 1999; Dyson et al., 1996a,b, 1997, 2000a,b) ou sans retards (Lebowitz et Rubinow, 1969), entre autres. Les EDP structurées en âge ou en maturité sont un autre moyen d'approcher la modélisation de la dynamique cellulaire. En définissant les densités de cellules au repos et en prolifération $n(t,a)$ et $p(t,a)$ respectivement, considérons les équations de transport suivantes,

$$\frac{\partial n(t,a)}{\partial t} + \frac{\partial n(t,a)}{\partial a} = -(\beta(a)+\mu(a))n(t,a), \tag{1.3.4}$$

$$\frac{\partial p(t,a)}{\partial t}+\frac{\partial p(t,a)}{\partial a}=-(\alpha(a)+\gamma(a))p(t,a), \tag{1.3.5}$$

où les fonctions $\alpha(a),\beta(a),\mu(a),\gamma(a)$ sont respectivement les taux de division, d'entrée en prolifération, de mortalité ou de différenciation et d'apoptose. Ces équation quasi-linéaires se résolvent par la méthode des caractéristiques, et nous trouvons,

$$n(t,a)=n(t-a,0)\exp\left[-\int_0^a \beta(\xi)+\mu(\xi)\mathrm{d}\xi\right], \tag{1.3.6}$$

$$p(t,a)=p(t-a,0)\exp\left[-\int_0^a \alpha(\xi)+\gamma(\xi)\mathrm{d}\xi\right]. \tag{1.3.7}$$

Soit $g_\beta(a)$ la densité de probabilité qu'une cellule d'âge a quitte la phase de repos vers la phase proliférative. Alors la proportion de cellules restantes dans la phase de repos d'âge supérieur à a est égale à la probabilité que ces cellules quittent la phase de repos après l'âge a. D'où,

$$\exp\left[-\int_0^a \beta(\xi)\mathrm{d}\xi\right]=\int_a^\infty g_\beta(\xi)\mathrm{d}\xi. \tag{1.3.8}$$

Prenant le logarithme de chaque côté et différenciant, nous obtenons,

$$\beta(a)=\frac{g_\beta(a)}{\int_a^\infty g_\beta(\xi)\mathrm{d}\xi}. \tag{1.3.9}$$

La fonction $g_\beta(a)$ est appelée fonction génératrice de distribution. Par exemple, si $g_\beta(a)=\beta\exp(-\beta a)$ est une loi exponentielle de paramètre β, alors le taux de réintroduction est $\beta(a)\equiv\beta$, ce qui correspond à l'exemple ci-dessus. L'autre distribution utilisée dans l'exemple précédent est la distribution de Dirac centrée en τ, et en ce cas $g_\alpha(a)=\delta(a-\tau)$ et,

$$\alpha(a)=\frac{\delta(a-\tau)}{\int_a^\infty \delta(\xi-\tau)\mathrm{d}\xi}, \tag{1.3.10}$$

et donc,

$$\alpha(a)=\begin{cases}0, & \text{si } a<\tau\\ \infty, & \text{si } a=\tau.\end{cases} \tag{1.3.11}$$

Cette dernière équation implique que toute les cellules se divisent à l'âge τ, ce qui induit les conditions limites suivantes,

$$\begin{aligned}\alpha(a)&=0 \qquad a\in[0,\tau)\\ p(t,a)&=0 \qquad a\geq\tau\\ n(t,0)&=2p(t,\tau_-)\end{aligned}. \tag{1.3.12}$$

L'autre condition limite est donnée par la transition des cellules au repos vers la phase proliférative,

$$p(t,0) = \int_0^\infty \beta(\xi) n(t,\xi) \mathrm{d}\xi. \tag{1.3.13}$$

Définissons

$$\begin{aligned} N(t) &\equiv \textstyle\int_0^\infty n(t,\xi)\mathrm{d}\xi, \\ P(t) &\equiv \textstyle\int_0^\tau p(t,\xi)\mathrm{d}\xi. \end{aligned} \tag{1.3.14}$$

Lorsque $\beta(a) = \beta$, $\mu(a) = \mu$, $\gamma(a) = \gamma$, la Condition (1.3.13) devient $p(t,0) = \beta N(t)$ et la réduction des Équations (1.3.4, 1.3.5) en équations différentielles à retard devient possible. En intégrant les Équations (1.3.4, 1.3.5) par rapport à a, nous obtenons,

$$\int_0^\infty \frac{\partial n(t,a)}{\partial t}\mathrm{d}a + \int_0^\infty \frac{\partial n(t,a)}{\partial a}\mathrm{d}a = -(\beta+\mu)\int_0^\infty n(t,a)\mathrm{d}a, \tag{1.3.15}$$

et,

$$\int_0^\tau \frac{\partial p(t,a)}{\partial t}\mathrm{d}a + \int_0^\tau \frac{\partial p(t,a)}{\partial a}\mathrm{d}a = -\gamma\int_0^\tau p(t,a)\mathrm{d}a. \tag{1.3.16}$$

Ceci mène à,

$$\frac{\mathrm{d}N(t)}{\mathrm{d}t} + n(t,a)|_{a=0}^{a=\infty} = -(\beta+\mu)N(t), \tag{1.3.17}$$

$$\frac{\mathrm{d}P(t)}{\mathrm{d}t} + p(t,a)|_{a=0}^{a=\tau_-} = -\gamma P(t). \tag{1.3.18}$$

Les Conditions (1.3.12) et (1.3.13) nous donnent,

$$\frac{\mathrm{d}N(t)}{\mathrm{d}t} - 2p(t,\tau_-) = -(\beta+\mu)N(t), \tag{1.3.19}$$

$$\frac{\mathrm{d}P(t)}{\mathrm{d}t} + p(t,\tau_-) - \beta N(t) = -\gamma P(t). \tag{1.3.20}$$

La densité des cellules prolifératives en τ_- est donnée par l'Équation 1.3.7, et

$$p(t,\tau_-) = p(t-\tau,0)\exp(-\gamma\tau) = \beta\exp(-\gamma\tau)N(t-\tau). \tag{1.3.21}$$

Les Équations (1.3.19, 1.3.20) se réduisent alors aux Équations (1.3.2, 1.3.3). Pour spécifier totalement le problème défini par ces équations différentielles à retard, il faut imposer des conditions initiales. Des précautions particulières doivent être apportées à la définition des conditions initiales. Pour garantir une solution unique du problème (1.3.2, 1.3.3), il faut poser les fonctions initiales au temps $t = t_0$,

$$X(t_0+\theta) \equiv \begin{pmatrix} N(t_0+\theta) = \varphi_1(\theta) \\ P(t_0+\theta) = \varphi_2(\theta) \end{pmatrix}, \ \theta \in [-\tau, 0], \tag{1.3.22}$$

La continuité de φ_j, $j = 1,2$, garantit la différenciabilité des solutions sur les intervalles $(t_0 + k\tau, t_0 + (k+1)\tau)$, et il est donc suffisant de considérer $\varphi_j \in C = C[-\tau, 0]$, l'espace des fonctions continues sur l'intervalle $[-\tau, 0]$. La solution formelle est alors $X_t^\varphi \in C$ où $X_t^\varphi(\theta)$ est la solution évaluée au temps $t+\theta$, $(N(t+\theta), P(t+\theta))^T$ avec condition initiale $X_{t_0}^\varphi = (\varphi_1, \varphi_2)^T$. Chaque condition initiale $\varphi \in C$ définit une solution unique X_t^φ. En pratique, les fonctions $N(t)$ et $P(t) \in \mathbb{R}$ sont souvent considérées comme solutions. Cet abus de langage sera utilisé tout au long du présent ouvrage, d'une part pour simplifier l'écriture, mais aussi parce que l'analyse numérique se fait dans ce contexte. Il ne faut cependant pas perdre de vue que les états des solutions d'équations différentielles à retard se situent dans un espace de dimension infinie.

Définissons les conditions initiales en $t = 0$ suivantes pour les Équations (1.3.4, 1.3.5),

$$\begin{aligned} n(0,a) &= n_0(a) \quad a \in [0,\infty), \\ p(0,a) &= p_0(a) \quad a \in [0,\tau). \end{aligned} \tag{1.3.23}$$

L'Équation (1.3.21) indique que les solutions des EDP doivent être valides sur l'intervalle $t \in [-\tau, 0]$, et donc la condition initiale $p(0,a) = p_0(a)$ ne peut être posée arbitrairement. D'une part, nous avons,

$$N(\theta) = \int_0^\infty n(\theta,\xi)\mathrm{d}\xi = \left[\int_0^\infty n_0(\xi-\theta)\mathrm{d}\xi\right] e^{-(\beta+\mu)\theta}. \tag{1.3.24}$$

D'autre part, des Équations (1.3.13) et ci-dessus,

$$\begin{aligned} P(\theta) &= \textstyle\int_0^\tau p(\theta,\sigma)\mathrm{d}\sigma, \\ &= \textstyle\int_0^\tau p(\theta-\sigma,0)e^{-\gamma\sigma}\mathrm{d}\sigma, \\ &= \textstyle\int_0^\tau \beta N(\theta-\sigma)e^{-\gamma\sigma}\mathrm{d}\sigma, \\ &= \textstyle\beta\int_0^\tau\int_0^\infty n_0(\xi+\sigma-\theta)e^{-(\beta+\mu)(\theta-\sigma)-\gamma\sigma}\mathrm{d}\xi\mathrm{d}\sigma, \end{aligned} \tag{1.3.25}$$

où $\theta \in [-\tau, 0]$. Les conditions initiales pour les Équations (1.3.2, 1.3.3) s'écrivent donc,

$$N(\theta) = \varphi(\theta) = e^{-(\beta+\mu)\theta}\int_0^\infty n_0(\xi-\theta)\mathrm{d}\xi,\ \theta \in [-2\tau, 0], \tag{1.3.26}$$

$$P(\theta) = \int_0^\tau \beta\varphi(\theta-\sigma)e^{-\gamma\sigma}\mathrm{d}\sigma. \tag{1.3.27}$$

La fonction $\varphi(\theta)$ peut être choisie arbitrairement dans $C^1[-2\tau,0]\cap\{\varphi(\theta)\geq 0\}$ avec la relation suivante,

$$n_0(-\theta)=\left(\frac{d\varphi(\theta)}{d\theta}+(\beta+\mu)\varphi(\theta)\right)\exp(\beta+\mu), \tag{1.3.28}$$

et une condition initiale sur la condition initiale,

$$\varphi(-2\tau)=e^{2\tau(\beta+\mu)}\int_0^\infty n_0(\xi+2\tau)d\xi. \tag{1.3.29}$$

Les liens entre les modèles structurés en âge et en maturité et les équations différentielles à retard sont étroits. Il convient de ne pas perdre de vue ce lien lors de la formulation des conditions initiales, ceci risquant d'entraîner des solutions pour les EDD qui ne correspondent pas aux solutions des EDP.

1.4. Modèles de production de cellules sanguines

La plupart des modèles de production de cellules sanguines ont la forme générale :

$$\frac{dx(t)}{dt}=-\alpha x(t)+F(\tilde{x}(t)). \tag{1.4.1}$$

où $\tilde{x}$ représente l'histoire de x. Le terme $-\alpha x$ représente une perte linéaire due à l'élimination des cellules de l'organisme. La fonction F, une boucle de feedback négatif qui agit avec retard, représente la production de nouvelles cellules. Les différentes propriétés de stabilité de l'Équation (1.4.1) ont été étudiées notamment dans (Anderson, 1991, 1992; Mackey et an der Heiden, 1982; Boese, 1989; Kuang, 1994; Hayes, 1950; Cooke et Grossman, 1982).

L'histoire $\tilde{x}$ peut prendre la forme d'un retard discret :

$$\tilde{x}(t)=x(t-\tau)\equiv x_\tau(t), \tag{1.4.2}$$

ou encore d'une distribution de retards :

$$\tilde{x}(t)=\int_0^\infty x(t-\tau)f(\tau)d\tau. \tag{1.4.3}$$

La plupart des auteurs se sont penchés sur des modèles faisant intervenir des retards discrets, souvent pour des raisons de simplicité mais aussi parce que les mécanismes physiologiques sont assez méconnus.

En plus des articles cités plus haut, un certain nombre de livres traite de la stabilité et des oscillations survenant dans les équations à retard. Parmi ceux-ci mentionnons

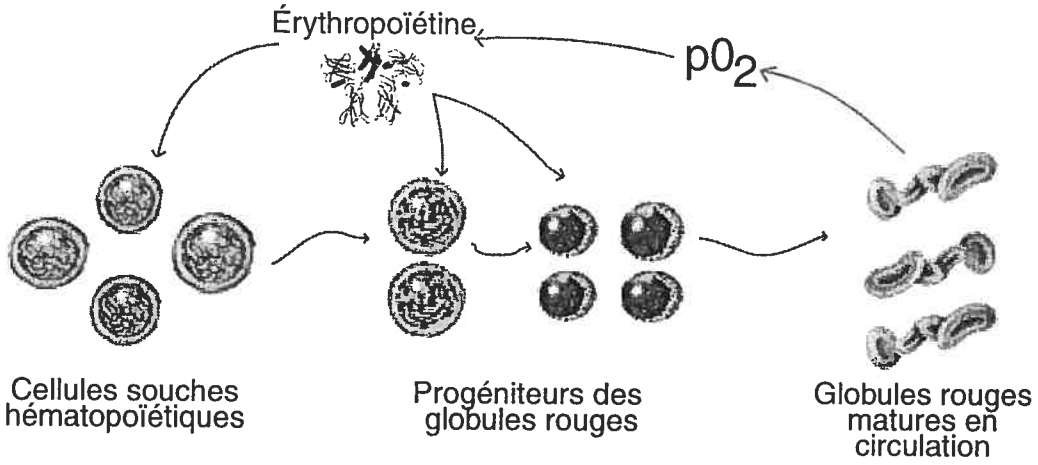

FIG. 1.4. Contrôle de la production des globules blancs par l'érythropoïétine.

les monographies de El'sgol'ts (El'sgol'ts, 1966), Mackey et Glass (Mackey et Glass, 1988), Kuang (Kuang, 1993), Halanay (Halanay, 1966) et Gopalsamy (Gopalsamy, 1992), entre autres.

1.4.1. Modèle d'érythropoïèse

Une quantité de modèles d'érythropoïèse ont été développés au cours des quarante dernières années (Kirk et al., 1968; Loeffler et al., 1989; Loeffler et Pantel, 1990; Monot et al., 1975; Mylrea et Albrecht, 1971; Vácha et Znojil, 1975; Wichmann et al., 1976, 1989; Wulf et al., 1989; Znojil et Vácha, 1975; Bélair et al., 1995; Mahaffy et al., 1998).

Le modèle considéré par Mahaffy et al. (1998) se réduit à un système de trois équations différentielles avec deux retards, dont un dépend de l'état du système,

$$\begin{aligned} \frac{dM(t)}{dt} &= e^{\beta\mu_1} S_0(E(t-T)) - \gamma M(t) - Q, \\ \frac{dE(t)}{dt} &= f(M(t)) - kE(t), \\ \frac{d\nu_F(t)}{dt} &= 1 - \frac{Qe^{-\beta\mu_1} e^{\gamma\nu_F(t)}}{S_0(E(t-T-\nu_F(t)))}. \end{aligned} \tag{1.4.4}$$

Dans ce modèle, les auteurs supposent une condition limite mouvante, où les cellules mûres les plus âgées sont activement éliminées par des macrophages. Il est supposé que ces macrophages sont rassasiés, c.-à-d. qu'ils éliminent un quantité maximale d'érythrocytes par jour, les plus âgés étant détruits les premiers. Les variables M, E et ν_F

représentent respectivement la population des globules rouges mûres, la concentration d'érythropoïétine (Epo) et l'âge maximal des globules rouges qui sont activement éliminés de l'organisme par les macrophages. Le terme Q représente le taux constant de destruction par ces macrophages, et cache la variable ν_F, ce qui découple le système 1.4.4. En effet, l'hypothèse de satiété des macrophages induit la condition limite constante,

$$Q = (1 - \dot{\nu}_F(t))e^{-\gamma\nu_F(t)}S_0(E(t - T - \nu_F(t))). \tag{1.4.5}$$

Le premier terme de l'équation pour M représente la production d'érythrocytes en fonction de la concentration d'Epo E au temps $t - T$, un retard T dû à la prolifération et à la maturation des érythrocytes. La production d'Epo, quant à elle, est régulée négativement par le compte des érythrocytes $f(M(t))$. Les simulations numériques du modèle ont permis de reproduire l'évolution du niveau d'érythrocyte après un don de sang et de simuler l'anémie hémolytique auto-immune chez le lapin.

1.5. Contrôle périphérique de la production des neutrophiles et neutropénie cyclique

Nombre de modèles mathématiques ont été proposés pour expliquer l'origine des oscillations des populations des différentes cellules sanguines chez les patients atteints de neutropénie cyclique et par le fait même de mieux comprendre les mécanismes de régulation de la production des neutrophiles dans les cas non pathologiques. Chez certains auteurs, cette production est gérée par une boucle de feedback négatif au niveau des précurseurs des neutrophiles (Glumenson, 1973, 1975; Fokas et al., 1991; Rubinow, 1969; Rubinow et al., 1971; Rubinow et Lebowitz, 1975, 1976a,b; Smeby et Benestad, 1980; Steinbach et al., 1980; Wheldon, 1975; Wichmann et Loffler, 1988). Il a été suggéré qu'une déstabilisation de cette boucle soit la source des oscillations du nombre de neutrophiles dans la neutropénie cyclique (Kazarinoff et van den Driessche, 1979; King-Smith et Morley, 1970; MacDonald, 1978; Morley et al., 1969; Morley et Stohlman, 1970; Morley, 1970; Reeve, 1973; Schmitz et al., 1990, 1994, 1995; Wichmann et al., 1988; von Schulthess et Mazer, 1982; Shvitra et al., 1983). Cependant, il a été montré qu'une déstabilisation de ce feedback ne peut causer ces oscillations (Hearn et al., 1998; Mackey et al., 2003b), la conclusion étant que l'origine des oscillations

se trouverait dans une déstabilisation du système de régulation des cellules souches hématopoïétiques. Ceci expliquerait le fait que les autres lignées de cellules oscillent aussi avec la même période que les neutrophiles. Plusieurs données cliniques montrent de plus que la neutropénie cyclique serait causée par une élévation du taux d'apoptose chez les précurseurs des neutrophiles (Dale et al., 2000; Aprikyan et al., 2001).

1.5.1. Modèle avec forçage périodique et boucle de feedback

Le modèle utilisé par Haurie et al. (2000) est de la forme

$$\dot{x} = -\alpha x + \mathcal{M}_0(\tilde{x}(t), t), \tag{1.5.1}$$

où

$$\tilde{x}(t) = \int_{\tau_m}^{\infty} x(t-s)g(s)ds. \tag{1.5.2}$$

Ici, l'histoire $\tilde{x}$ est pondérée par la distribution de retards $g(s)$. La production $\mathcal{M}_0$ au temps t dépend donc de la valeur de x sur l'intervalle $(-\infty, t-\tau_m]$.

La distribution de retards est due au fait que les précurseurs des neutrophiles ne mûrissent pas tous à la même vitesse. Les plus rapides vont mûrir en τ_m jours tandis que les plus lents mettront beaucoup plus de temps à transiter vers le bassin des cellules mûres.

Selon les donnés expérimentales, une distribution particulièrement bien adaptée à la maturation des précurseurs est la distribution gamma :

$$g_q(\xi) = \frac{\beta^{q-1}}{\Gamma(q-1)}(\xi - \tau_m)^{q-2} e^{-\beta(\xi-\tau_m)}. \tag{1.5.3}$$

Cette distribution, en plus d'avoir la forme voulue, a plusieurs propriétés mathématiquement intéressantes, la plus évidente étant que l'équation caractéristique associée au système linéaire est un polynôme quand $\tau_m = 0$.

1.5.2. Effet du G-CSF

Le G-CSF est la principale cytokine impliquée dans la régulation du niveau des neutrophiles. Elle agit de quatre façons (Haurie et al., 1999a; Hammond et al., 1990; Avalos et al., 1994) :

(1) augmente le taux de différentiation des cellules souches vers les précurseurs des neutrophiles : μ croît,

(2) augmente le taux de proliferation : β croît,

(3) diminue la durée du cycle cellulaire : τ décroît,

(4) diminue le taux d'apoptose : γ décroît.

Le G-CSF est éliminé, en partie, en se liant aux récepteurs en surface des neutrophiles et de ses précurseurs. Ceci suggère que le G-CSF, comme d'autres cytokines, est impliqué dans la boucle de feedback contrôlant la production de cellules mûres.

1.6. Organisation de la présente thèse

Nous avons survolé différents aspects du contrôle de l'hématopoïèse ainsi que les applications des équations différentielles à retard en biologie et en médecine. Les applications sont surtout utiles dans la modélisation de boucles de feedback. Un des systèmes où les retards semblent avoir une importance primordiale est l'hématopoïèse. Bien qu'il y ait d'autres options pour expliquer l'origine des oscillations, par exemple une origine génétique (Horwitz et al., 1999), l'hypothèse d'un déséquilibre dynamique dans les mécanismes de régulation est prometteuse.

Le présent travail est organisé comme suit. Les Chapitres 2, 3, 4, 5 se composent de quatre articles écrits dans le cadre des études supérieures effectuées au cours des cinq dernières années. Les références des articles inclus dans la thèse sont les suivantes.

1° Bernard, S., Bélair, J., et Mackey, M.C., (2001) Sufficient conditions for stability of linear differential equations with distributed delays. Discrete Contin. Dyn. Syst. Ser. B. 1 : 233-256.

2° Bernard, S., Bélair, J., Mackey, M.C., (2003) Oscillations in Cyclical Neutropenia : New Evidence Based on Mathematical Modeling, J. Theor. Biol. 223 : 283-298.

3° Bernard, S., Bélair, J., Mackey, M.C., Bifurcations in a model of blood cell production, accepté en juin 2003 pour publication dans C. R. Biologies.

4° Bernard, S., Pujo-Menjouet, L., Mackey M.C., (2003) Analysis of Cell Kinetics Using a Cell Division Marker : Mathematical Modeling of Experimental Data, Biophys. J. 84 : 3414-3424.

Les contributions des auteurs sont définies au début de chaque chapitre et les accords et autorisations de publication sont inclus dans l'Annexe B.

Le Chapitre 2 porte sur l'analyse de la région de stabilité d'équations différentielles avec distribution de retards (Bernard et al., 2001). Le Chapitre 3 porte sur le développement d'un modèle de production de globules blancs, l'estimation des paramètres physiologiques, l'analyse du modèle et les simulation numériques (Bernard et al., 2003b). Ce modèle est formé de deux équations différentielles à retards discrets. Cet article, qui est le cœur du présent ouvrage, donne une interprétation dynamique des symptômes vus dans certaines maladies hématologiques dynamiques telles que la neutropénie cyclique. Le Chapitre 4 porte sur l'analyse de bifurcation du modèle de production de cellules sanguines présenté dans le Chapitre 3, et nous trouvons des conditions physiologiquement réalistes pour l'existence d'oscillations dans le compte des cellules sanguines (Bernard et al., 2003a). Enfin, le Chapitre 5 utilise un système d'équations aux dérivées partielles pour analyser la prolifération de cellules traquées par un marqueur fluorescent et présente d'étonnants résultats numériques et permet d'évaluer des paramètres dynamiques des cellules autrement très difficiles à obtenir (Bernard et al., 2003c). Dans le Chapitre 6, nous faisons un retour sur les différents aspects de la thèse et nous commentons les enjeux soulevés par les résultats présentés ici.

L'Annexe A présente les codes en `Matlab` utilisés dans le Chapitre 5 pour calculer les solutions exactes des équations de population et pour produire les figures.

L'Annexe B présente les accords des auteurs pour inclure les articles qui composent la présente thèse ainsi que les autorisations des éditeurs de ces articles.

Chapitre 2

SUFFICIENT CONDITIONS FOR STABILITY OF LINEAR DIFFERENTIAL EQUATIONS WITH DISTRIBUTED DELAYS

AUTEURS : SAMUEL BERNARD, JACQUES BÉLAIR ET MICHAEL C. MACKEY

2.1. CONTRIBUTION DE L'AUTEUR À L'ARTICLE

Cet article contient une section qui a été écrite par les coauteurs (Section 2.6). Le reste, c.-à-d. les résultats concernant les conditions suffisantes pour la stabilité d'équations différentielles à retard, ainsi que les exemples et l'application à un modèle de production de globules blancs, est de moi.

2.2. CONDITIONS SUFFISANTES POUR LA STABILITÉ D'ÉQUATIONS DIFFÉRENTIELLES LINÉAIRES AVEC RETARDS DISTRIBUÉS

Les équations différentielles à retard ont des applications dans plusieurs domaines, notamment en génie et en biologie où la transmission de l'information et de la réponse d'un système de contrôle ne se fait pas instantanément. Parmi les travaux publiés sur le sujet, peu traitent des équations différentielles avec distribution de retards. L'étude du linéarisé est d'une importance primordiale dans l'étude de bifurcation d'une équation avec retards, distribués ou non. Une équation différentielle scalaire linéaire avec retards distribués peut s'écrire de façon générale comme suit,

$$\dot{x}(t) = -\alpha x(t) - \beta \int_0^\infty x(t-\tau) f(\tau)\, d\tau, \tag{2.2.1}$$

où f est la distribution des retards et α et β sont deux constantes réelles. Si f est un delta de Dirac avec singularité en $\bar{\tau} > 0$, c.-à-d. $f(\tau) = \delta(\tau - \bar{\tau})$, alors l'intégrale dans l'Équation (2.2.1) se réduit au terme $x(t-\bar{\tau})$ et l'Équation (2.2.1) devient une équation différentielle à retard discret. Un résultat standard sur la stabilité de telles équations (Hayes, 1950) dit que la solution triviale de l'Équation (2.2.1) est asymptotiquement stable si et seulement si,

(1) $\alpha > |\beta|$, ou bien

(2) $\beta \geq |\alpha|$ et

$$\bar{\tau} < \tau_{crit} \equiv \frac{\arccos(-\alpha/\beta)}{\sqrt{\beta^2 - \alpha^2}}. \tag{2.2.2}$$

Le résultat principal de cet article (Théorème 2.7.2) donne une borne du même type que l'Équation (2.2.2) pour une distribution de retards avec espérance $\bar{\tau} = \int \tau f(\tau) d\tau$. Il est aussi conjecturé que la borne donnée par l'Équation (2.2.2) est valable pour toutes les distributions de retards, peu importe leur forme. Ce résultat permet en pratique de simplifier certaines équations en remplaçant les distributions de retards par un retard discret $\bar{\tau}$. Ces résultats sont ensuite appliqués à un modèle de production de cellules sanguines comportant une distribution de retards. Une caractérisation des modes d'oscillation est effectuée tant avec le modèle qu'avec les données expérimentales sur lesquelles le modèle était basé. Il est montré que l'entraînement périodique d'une boucle de feedback négatif peut déstabiliser cette boucle périodiquement et induire un second mode d'oscillation, qui apparaît sur la phase descendante du mode principal.

2.3. ABSTRACT

We develop conditions for the stability of the constant (steady state) solutions of linear delay differential equations with distributed delay when only information about the moments of the density of delays is available. We use Laplace transforms to investigate the properties of different distributions of delay. We give a method to parametrically determine the boundary of the region of stability, and sufficient conditions for stability based on the expectation of the distribution of the delay. We also obtain a result based on the skewness of the distribution. These results are illustrated on a recent model of peripheral neutrophil regulatory system which include a distribution

of delays. The goal of this paper is to give a simple criterion for the stability when little is known about the distribution of the delay.

2.4. INTRODUCTION

Delay differential equations (DDE) have been studied extensively for the past 50 years. They have applications in domains as diverse as engineering, biology and medicine where information transmission and/or response in control systems is not instantaneous. For a good introduction to the subject, see (El'sgol'ts, 1966). Much of the work that has been done treats DDEs with one or a few discrete delays.

A number of realistic physiological models however include distributed delays and a problem of particular interest is to determine the stability of the steady state solutions. For applications in physiological systems see (Haurie et al., 2000; Mackey et an der Heiden, 1982, 1984; Mackey et Glass, 1979, 1988). Although results concerning DDEs with particular distributed delays (for extensive results about the *gamma* distribution see (Boese, 1989)) have been published, there has been no systematic study of this problem when little is known about the density of the delay distribution: most notably, results on sufficient conditions for stability of solutions of equations such as those considered in the present paper are given in (Gopalsamy, 1992; Kuang, 1993).

The problem of stability is very important in physiology and medicine. One class of diseases is characterized by a dramatic change in the dynamics of a physiological variable or a set of variables and there is sometime good clinical evidence that these changes are a consequence of a bifurcation in the underlying dynamics of the physiological control system. In (Mackey et Glass, 1988) it was proposed that these diseases be called *dynamical diseases*. In many cases, one variable starts (or stops) to oscillate. In order to treat these diseases, it is useful to know the parameter which causes the oscillation (or the suppression thereof). An example of a dynamical disease is cyclical neutropenia which is the subject of Section 2.9.

In Section 2.5 we briefly set the stage for the type of problem that we are considering. In Section 2.6, we define our notion of stability and discuss how to perimetrically determine the region of stability of a simple DDE for three particular distributions of delay: when the delay is a single discrete delay, a uniformly distributed delay and a

distribution with the gamma density. In Section 2.7 we introduce a sufficient condition to have stability based on the expected delay and the symmetry of the distribution of delays. In Section 2.8 we give some examples again turning to the single delay, and the uniformly and gamma distributed cases. In Section 2.9 we apply our results to a recently published model for the peripheral regulation of neutrophil production.

2.5. PRELIMINARIES

In this paper we study the stability of the linear differential Equation

$$\dot{x}(t) = -\alpha x(t) - \beta \int_0^\infty x(t-\tau) f(\tau)\, d\tau \tag{2.5.1}$$

where α and β are constants. We show that the symmetry of the distribution f plays an important role in the stability of the trivial solution, and our first result considers the characteristic equation of the DDE (2.5.1) if the density f is symmetric. If f is skewed to the left (meaning that there is more weight to the left of the expectation) then stability is stronger (*i.e.* holds for a wider range of parameter values) than for a single delay.

We restrict the values of α and β to $\beta \geq |\alpha|$ because we are interested in the influence of the distribution f on the stability properties of (2.5.1). It is straightforward to show that if $\beta \leq -\alpha$ then the trivial solution of Equation (2.5.1) is not stable. Moreover if $\alpha > |\beta|$, Equation (2.5.1) is stable for all values of τ. The interesting parameter values are therefore located in the cone $\beta \geq |\alpha|$.

Consider the general differential delay equation

$$\frac{dx(t)}{dt} = \mathcal{F}(x(t), \tilde{x}(t)), \tag{2.5.2}$$

where $\tilde{x}(t)$ is $x(t-\tau)$ weighted by a distribution of maturation delays. $\tilde{x}(t)$ is given explicitly by

$$\tilde{x}(t) = \int_{\tau_m}^\infty x(t-\tau) f(\tau) d\tau \equiv \int_{-\infty}^{t-\tau_m} x(\tau) f(t-\tau) d\tau. \tag{2.5.3}$$

τ_m is a minimal delay and $f(\tau)$ is the density of the distribution of maturation delays. Since $f(\tau)$ is a density, $f \geq 0$ and

$$\int_0^\infty f(\tau) d\tau = 1. \tag{2.5.4}$$

To completely specify the semi-dynamical system described by Equations (2.5.2) and (2.5.3) we must additionally have an initial function

$$x(t') \equiv \varphi(t') \qquad \text{for} \qquad t' \in (-\infty, 0). \tag{2.5.5}$$

Steady states x_* of Equation (2.5.2) are defined implicitly by the relation

$$\frac{dx_*}{dt} \equiv 0 \equiv \mathcal{F}(x_*, x_*). \tag{2.5.6}$$

Definition 2.5.1. If there is a unique steady state x_* of Equation (2.5.2) it is *globally asymptotically stable* if, for all initial functions φ,

$$\lim_{t\to\infty} x(t) = x_*. \tag{2.5.7}$$

The primary consideration of this paper is the stability of the steady state(s), defined implicitly by Equation (2.5.6), and how that stability may be lost. Though we would like to be able to examine the global stability of x_* to perturbations, one must often be content with an examination of the *local* stability of x_*.

Definition 2.5.2. A steady state x_* of Equation (2.5.2) is *locally asymptotically stable* (Hale et Verduyn Lunel, 1991) if, for all initial functions φ satisfying $|\varphi(t') - x_*| \leq \varepsilon$, $0 < \varepsilon \ll 1$,

$$\lim_{t\to\infty} x(t) = x_*. \tag{2.5.8}$$

2.6. Local stability

To examine its local stability, we linearize Equation (2.5.2) in the neighborhood of any one of the steady states defined by (2.5.6), and define $z(t) = x(t) - x_*$ as the deviation of $x(t)$ from that steady state. The resulting linear equation is

$$\frac{dz(t)}{dt} = -\alpha z(t) - \beta \tilde{z}(t), \tag{2.6.1}$$

where

$$\tilde{z}(t) = \int_{\tau_m}^{\infty} z(t-\tau) f(\tau) d\tau \equiv \int_{-\infty}^{t-\tau_m} z(\tau) f(t-\tau) d\tau, \tag{2.6.2}$$

and α and β are defined by

$$\alpha \equiv -\frac{\partial \mathcal{F}(x,\tilde{x})}{\partial x}\Big|_{x=x_*} \qquad \beta \equiv -\frac{\partial \mathcal{F}(x,\tilde{x})}{\partial \tilde{x}}\Big|_{\tilde{x}=x_*}. \tag{2.6.3}$$

If we make the *ansatz* that $z(t) \simeq e^{st}$ in Equation (2.6.1), the resulting eigenvalue equation is

$$s+\alpha+\beta e^{-s\tau_m}\hat{f}(s)=0, \tag{2.6.4}$$

where

$$\hat{f}(s)=\int_0^\infty e^{-s\tau}f(\tau)d\tau \tag{2.6.5}$$

is the Laplace transform of f.

2.6.1. The single delay case

The "usual" situation considered by many authors is that in which there is a single discrete delay. The density f is then given as a Dirac delta function, $f(\tau)=\delta(\tau-\bar{\tau})$. In this case the eigenvalue Equation (2.6.4) takes the form

$$s+\alpha+\beta e^{-s\bar{\tau}}=0. \tag{2.6.6}$$

If $s=\mu+i\omega$, then the boundary between locally stable behaviour ($\mu<0$) and unstable behaviour ($\mu>0$) is given by the values of α, β, and $\bar{\tau}$ satisfying

$$i\omega+\alpha+\beta e^{-i\omega\bar{\tau}}=0, \tag{2.6.7}$$

which has been studied by Hayes (Hayes, 1950). Isolating the real

$$\alpha+\beta\cos(\omega\bar{\tau})=0, \tag{2.6.8}$$

and imaginary

$$\omega-\beta\sin(\omega\bar{\tau})=0 \tag{2.6.9}$$

parts of (2.6.7) it is straightforward to show that $\mu<0$ whenever

(1) $\alpha>|\beta|$, or if

(2) $\beta\geq|\alpha|$ and

$$\bar{\tau}<\tau_{crit}\equiv\frac{\arccos\left(-\frac{\alpha}{\beta}\right)}{\sqrt{\beta^2-\alpha^2}}. \tag{2.6.10}$$

The stability boundary defined by Equation (2.6.10) is shown in Figure 2.2 in Section 2.8 where we have parametrically plotted

$$\beta(\omega)=\frac{\omega}{\sin(\omega\bar{\tau})} \tag{2.6.11}$$

versus

$$\alpha(\omega) = -\omega\cot(\omega\bar{\tau}). \tag{2.6.12}$$

When $\bar{\tau} = \tau_{crit}$ there is a Hopf bifurcation to a periodic solution of (2.6.1) with *Hopf period*

$$T_{Hopf} = \frac{2\pi}{\sqrt{\beta^2 - \alpha^2}}. \tag{2.6.13}$$

2.6.2. The uniform (rectangular) density

Suppose we have the simple situation wherein there is distribution of delays with a uniform rectangular density given by

$$f(\tau) = \begin{cases} 0 & 0 \le \tau < \tau_m \\ \frac{1}{\delta} & \tau_m \le \tau \le \tau_m + \delta \\ 0 & \tau_m + \delta < \tau. \end{cases} \tag{2.6.14}$$

The expected value E of the delay is

$$E = \int_0^\infty \tau f(\tau) d\tau = \frac{\delta}{2}, \tag{2.6.15}$$

so the average delay is

$$< \tau >= \tau_m + E = \tau_m + \frac{\delta}{2} \tag{2.6.16}$$

and the variance (denoted by V) is

$$V = \frac{\delta^2}{12} = \frac{E^2}{3}. \tag{2.6.17}$$

The Laplace transform of f as given by (2.6.14) is easily computed to be

$$\hat{f}(s) = \frac{e^{\delta s} - 1}{\delta s}, \tag{2.6.18}$$

so the eigenvalue Equation (2.6.4) takes the form

$$\delta s(s+\alpha) + \beta e^{-s\tau_m}\left[e^{\delta s} - 1\right] = 0. \tag{2.6.19}$$

This may be rewritten in terms of the expectation E as

$$2Es(s+\alpha) + \beta e^{-s\tau_m}\left[e^{2Es} - 1\right] = 0. \tag{2.6.20}$$

Taking $s = i\omega$ and proceeding as before we obtain parametric equations for $\alpha(\omega)$ and $\beta(\omega)$ as follows:

$$\alpha(\omega) = -\omega \frac{\sin[(\delta - \tau_m)\omega] + \sin(\omega\tau_m)}{\cos[(\delta - \tau_m)\omega] - \cos(\omega\tau_m)}, \tag{2.6.21}$$

and

$$\beta(\omega) = \frac{\delta\omega^2}{\cos[(\delta - \tau_m)\omega] - \cos(\omega\tau_m)}. \tag{2.6.22}$$

Refer to Figure 2.3 to see a graphical representation of the region of stability.

2.6.3. The gamma density

The density of the gamma distribution with parameters (a, m)

$$f(\tau) = \begin{cases} 0 & 0 \leq \tau < \tau_m \\ \frac{a^m}{\Gamma(m)}(\tau - \tau_m)^{m-1} e^{-a(\tau - \tau_m)} & \tau_m \leq \tau \end{cases} \tag{2.6.23}$$

with $a, m \geq 0$, is often encountered (Haurie et al., 2000; Hearn et al., 1998) in applications. The parameters m, a, and τ_m in the density of the gamma distribution can be related to certain easily determined statistical quantities. Thus, the average of the *unshifted* density is given by

$$E = \int_0^\infty \tau f(\tau) d\tau = \frac{m}{a}, \tag{2.6.24}$$

so the average delay is

$$< \tau >= \tau_m + E = \tau_m + \frac{m}{a} \tag{2.6.25}$$

and the variance is

$$V = \frac{m}{a^2}. \tag{2.6.26}$$

Using (2.6.24) and (2.6.26) the parameters m and a can be expressed as

$$a = \frac{E}{V} \tag{2.6.27}$$

and

$$m = \frac{E^2}{V}. \tag{2.6.28}$$

Using the Laplace transform of (2.6.23) the eigenvalue Equation (2.6.4) becomes

$$(s + \alpha)\left[1 + \frac{s}{a}\right]^m + \beta e^{-s\tau_m} = 0. \tag{2.6.29}$$

Equation (2.6.29) can be used to give a pair of parametric equations in α and β defining the local stability boundary ($\mu \equiv \text{Re}\, s \equiv 0$). We start by setting $s = i\omega$ and

$$\tan\theta = \frac{\omega}{a}. \tag{2.6.30}$$

Using de Moivre's formula in Equation (2.6.29) with $s = i\omega$ gives

$$(\alpha + i\omega)(\cos[m\theta]) + i\sin[m\theta]) = -\beta\cos^m\theta(\cos\omega\tau_m - i\sin\omega\tau_m) \tag{2.6.31}$$

Equating the real and imaginary parts of Equation (2.6.31) gives the coupled equations

$$\alpha + \beta r\cos\omega\tau_m = \omega\tan[m\theta], \tag{2.6.32}$$

and

$$\alpha\tan[m\theta] - \beta r\sin\omega\tau_m = -\omega, \tag{2.6.33}$$

where

$$r = \frac{\cos^m\theta}{\cos[m\theta]}. \tag{2.6.34}$$

Equations (2.6.32) and (2.6.33) are easily solved for α and β as parametric functions of ω to give

$$\alpha(\omega) = -\frac{\omega}{\tan[\omega\tau_m + m\tan^{-1}(\omega/a)]} \tag{2.6.35}$$

and

$$\beta(\omega) = \frac{\omega}{\cos^m[\tan^{-1}(\omega/a)]\sin[\omega\tau_m + m\tan^{-1}(\omega/a)]} \tag{2.6.36}$$

respectively. Refer to Figure 2.4 to see the region of stability.

2.6.4. General density case

The method employed above can be generalized for any density. Consider Equation (2.6.4) and let $s = i\omega$. Separating the real and imaginary parts leads to

$$\alpha + \beta\int_0^\infty \cos(\omega\tau)f(\tau)d\tau = 0 \tag{2.6.37}$$

$$\omega - \beta\int_0^\infty \sin(\omega\tau)f(\tau)d\tau = 0. \tag{2.6.38}$$

Define

$$C(\omega) \equiv \int_0^\infty \cos(\omega\tau)f(\tau)d\tau \tag{2.6.39}$$

and

$$S(\omega) \equiv \int_0^\infty \sin(\omega\tau)f(\tau)d\tau. \tag{2.6.40}$$

Then we can solve for α and β to obtain them as parametric functions of ω:

$$\alpha(\omega) = -\omega\frac{C(\omega)}{S(\omega)} \tag{2.6.41}$$

and

$$\beta(\omega) = \frac{\omega}{S(\omega)}. \tag{2.6.42}$$

2.7. STABILITY CONDITIONS

One method to study the stability is to find conditions for which the eigenvalue equation (or *characteristic equation*) has no roots with positive real part. The difficulty with Equation (2.5.1) is that the characteristic equation often involves a transcendental term. A noticeable exception is the unshifted gamma distribution for which the characteristic equation [Equation (2.6.29) with $\tau_m = 0$] is a polynomial. This term, the Laplace transform of the density of the distribution of delays, can be expressed as $C(\omega) + iS(\omega)$ [Equations (2.6.39) and (2.6.40)] on the imaginary axis. The first Lemma gives a bound on the term $C(\omega) = \int_0^\infty \cos(\omega\tau) f(\tau) d\tau$ when the density f is symmetric.

Lemma 2.7.1. *Let f be a probability density such that:*

(1) $f : R \longrightarrow R^+$

(2) $E = \int_{-\infty}^{\infty} \tau f(\tau)\, d\tau$,

(3) $f(E-\tau) = f(E+\tau)$

(The third property implies that f is symmetric about its expectation). Then

(1) for all ω,

$$\left| \int_{-\infty}^{\infty} \cos(\omega\tau)\, f(\tau)\, d\tau \right| \leq |\cos(\omega E)| \ ; \tag{2.7.1}$$

(2) if $\omega < \pi/2E$,

$$\int_{-\infty}^{\infty} \cos(\omega\tau)\, f(\tau)\, d\tau > 0. \tag{2.7.2}$$

PROOF. For the first part of the Lemma, assume that f is piecewise constant and given by

$$f(\tau) = \sum_{i=1}^{N} C_i \chi_{[A_i,B_i]}(\tau)$$

where $\chi_{[A_i,B_i]}$ denotes the indicator function on the interval $[A_i, B_i]$:

$$\chi_{[A,B]}(\tau) = \begin{cases} 0 & \tau \notin [A,B] \\ 1 & \tau \in [A,B] \end{cases}. \tag{2.7.3}$$

Then

$$\begin{aligned}\left|\int_{-\infty}^{\infty}\cos(\omega\tau)f(\tau)d\tau\right| &= \left|\int_{-\infty}^{\infty}\cos(\omega\tau)\sum_{i=1}^{N}C_i\chi_{[A_i,B_i]}(\tau)d\tau\right| \\ &= \left|\sum_{i=1}^{N}C_i\int_{A_i}^{B_i}\cos(\omega\tau)\,d\tau\right| \\ &= \left|\sum_{i=1}^{N}\frac{C_i}{\omega}(\sin(\omega B_i)-\sin(\omega A_i))\right|,\end{aligned}$$

which must be less than $|\cos(\omega E)|$ as we now show.

Using the trigonometric identity

$$\sin(x+y)-\sin(x-y)=2\cos(x)\sin(y),$$

we have

$$\left|\sum_{i=1}^{N}\frac{C_i}{\omega}(\sin(\omega B_i)-\sin(\omega A_i))\right| = \left|\sum_{i=1}^{N}\frac{C_i}{\omega}2\cos(\omega\frac{B_i+A_i}{2})\sin(\omega\frac{B_i-A_i}{2})\right|.$$

By the symmetry of f, we know that $C_i = C_{N-i+1}$, and the distance between the expectation E and the middle of the ith interval is equal to the one between E and the middle of the $(N-i+1)$th interval. That is,

$$\left|E-\frac{A_i+B_i}{2}\right| = \left|E-\frac{A_{N-i+1}+B_{N-i+1}}{2}\right|.$$

Set $E_i = \left|E-\frac{1}{2}(A_i+B_i)\right|$. For $1\le i\le N/2$, we have $\frac{1}{2}(A_i+B_i) = E-E_i$, $\frac{1}{2}(A_{N-i+1}+B_{N-i+1}) = E+E_{N-i+1}$ and $E_i = E_{N-i+1}$. Substitute these values in the summation:

$$\begin{aligned}\left|\sum_{i=1}^{N}\frac{C_i}{\omega}2\cos(\omega\frac{B_i+A_i}{2})\sin(\omega\frac{B_i-A_i}{2})\right| &= \\ \left|\sum_{i=1}^{N/2}2\frac{C_i}{\omega}\sin(\omega\frac{B_i-A_i}{2})(\cos(\omega(E-E_i))+\cos(\omega(E+E_i))\right| &= \\ \left|\sum_{i=1}^{N/2}2\frac{C_i}{\omega}\sin(\omega\frac{B_i-A_i}{2})(2\cos(\omega E)\cos(\omega E_i)\right|\end{aligned}$$

The last equality is obtained by the trigonometric identity

$$\cos(x+y)+\cos(x-y)=2\cos(x)\cos(y).$$

Apply the triangle inequality and bound $|\cos(\omega E_i)|$ by 1 and the sine by its argument to obtain

$$\begin{aligned}
\left|\sum_{i=1}^{N/2} 2\frac{C_i}{\omega}\sin(\omega\frac{B_i-A_i}{2})(2\cos(\omega E)\cos(\omega E_i)\right| &\leq \\
\sum_{i=1}^{N/2}\left|4\frac{C_i}{\omega}\sin(\omega\frac{B_i-A_i}{2})\right||\cos(\omega E)||\cos(\omega E_i)| &\leq \\
\sum_{i=1}^{N/2}\left|4\frac{C_i}{\omega}\sin(\omega\frac{B_i-A_i}{2})\right||\cos(\omega E)| &\leq \\
\sum_{i=1}^{N/2}\left|4C_i\frac{B_i-A_i}{2}\right||\cos(\omega E)| &= \sum_{i=1}^{N}|C_i(B_i-A_i)||\cos(\omega E)|
\end{aligned}$$

Since f is a probability density,

$$\int_{-\infty}^{\infty} f(\tau)d\tau = \sum_{i=1}^{N}\int_{A_i}^{B_i} C_i d\tau = \sum_{i=1}^{N} C_i(B_i-A_i) = 1.$$

So

$$\sum_{i=1}^{N}|C_i(B_i-A_i)||\cos(\omega E)| = |\cos(\omega E)|.$$

Then

$$\left|\sum_{i=1}^{N}\frac{C_i}{\omega}(\sin(\omega B_i)-\sin(\omega A_i))\right| \leq |\cos(\omega E)|.$$

We thus have (2.7.1) when f is piecewise constant. If f is any symmetric probability density, we can approximate it by a sequence of functions $\{f_n\}_{n=1}^{\infty}$, when f_n is a piecewise constant symmetric probability density, with $f_n \to f$ as $n \to \infty$ and $\int_{-\infty}^{\infty}\tau f_n(\tau)d\tau = \int_{-\infty}^{\infty}\tau f(\tau)d\tau = E$. Note that

$$\left|\int_{-\infty}^{\infty}\cos(\omega\tau)\, f_n(\tau)\, d\tau\right| \leq |\cos(\omega E)|$$

for every n, so

$$\begin{aligned}
\lim_{n\to\infty}\left|\int_{-\infty}^{\infty}\cos(\omega\tau)f_n(\tau)d\tau\right| &= \left|\int_{-\infty}^{\infty}\cos(\omega\tau)\lim_{n\to\infty} f_n(\tau)d\tau\right| \\
= \left|\int_{-\infty}^{\infty}\cos(\omega\tau)\, f(\tau)\, d\tau\right| &\leq |\cos(\omega E)|.
\end{aligned}$$

To prove the second part of the Lemma, observe that

$$|\cos(\omega(E-\tau))f(E-\tau)| \geq |\cos(\omega(E+\tau))f(E+\tau)|,$$

so the integral over the positive part is greater than the one over the negative part. □

Remark 2.7.1. We can also prove, under the same hypothesis of Lemma 2.7.1, that

$$\left| \int_{-\infty}^{\infty} \sin(\omega\tau)\, f(\tau)\, d\tau \right| \leq |\sin(\omega E)|\,. \tag{2.7.4}$$

The stability of Equation (2.5.1) depends on all moments of f about its mean. The expectation obviously plays an important role in stability; Anderson (Anderson, 1991, 1992) also showed the importance of the variance (second moment about the mean) in these stability considerations.

We now study the location of the first root of $C(\omega)$. Lemma 2.7.1 states that the first root of $C(\omega)$ is at $\omega = \pi/2E$ whenever the density f is symmetric. It is of primary interest to see how this root changes when the distribution is not symmetric. Around $\omega\tau = \pi/2$, the cosine in $C(\omega) = \int_0^{\infty} \cos(\omega\tau) f(\tau) d\tau$ can be expanded in Taylor series,

$$C(\omega) = \int_{-\infty}^{\infty} \sum_{n=0}^{\infty} \frac{(-1)^{n+1} (\omega\tau - \pi/2)^{2n+1}}{(2n+1)!} f(\tau) d\tau, \tag{2.7.5}$$

leading to the integral of a sum of terms with odd power (odd because we expand around a root). The higher moments about the mean do not necessarily converge and for this reason we can not usually switch the sum and the integral. The first term of this expansion is

$$-\frac{\pi}{2E} \int_0^{\infty} (\tau - E) f(\tau) d\tau = 0 \tag{2.7.6}$$

since the mean E is precisely the value for which this relation hold. The second term is the third moment about the mean (up to a multiplicative factor).

$$\frac{\pi^3}{(2E)^3 3!} \int_0^{\infty} (\tau - E)^3 f(\tau) d\tau. \tag{2.7.7}$$

The third moment is in general the first nonzero term of the Taylor expansion and so the sign of this term has a great importance in determining the position of the root of $C(\omega)$. The *skewness* of a distribution is usually defined as the third moment about the mean divided by the third power of the standard deviation. If the density f is symmetric, all moment about the mean are zero. So a symmetric density has a skewness equal to zero, which is coherent with intuition. But a third moment equal to zero does not imply that the density is symmetric. We require a definition in which a skewness equal to zero means that the density is symmetric. For the purpose of the paper, we will use the following definition of skewness.

Definition 2.7.1. Let f be a probability density with expectation E. The skewness of f, $B(f)$, is defined as

$$B(f) = (-1)^{k+1} \int_0^\infty (\tau - E)^{2k+1} f(\tau) d\tau \tag{2.7.8}$$

where

$$k = \min \left\{ n \left| \int_0^\infty (\tau - E)^{2n+1} f(\tau) d\tau \neq 0 \right. \right\}. \tag{2.7.9}$$

The density f is said to be *skewed to the left* if $B(f) > 0$ and *skewed to the right* if $B(f) < 0$. In the case where $k = \infty$ we define $B(f) = 0$.

Remark 2.7.2. It is clear that f is symmetric if and only if all the moments about its mean are zero, i.e. f is symmetric if and only if $B(f) = 0$. In general, for a non-symmetric density, the third moment about the mean is nonzero, so the definition of $B(f)$ reduces to the standard case (up to a positive multiplicative factor).

We can now look for sufficient conditions for stability of Equation (2.5.1).

Theorem 2.7.2 (Sufficient Conditions). *Let f be a probability density defined on $[0, +\infty)$ with expectation $\int_0^\infty \tau f(\tau) d\tau = E$. Suppose $\beta > |\alpha|$. Then in Equation (2.5.1)*

(1) The solution $x_* = 0$ is asymptotically stable (a.s.) if

$$E < \frac{\pi \left(1 + \frac{\alpha}{\beta}\right)}{c\sqrt{\beta^2 - \alpha^2}} \tag{2.7.10}$$

where $c = \sup\{c | \cos(x) = 1 - cx/\pi, x > 0\} \approx 2.2764$.

(2) If the skewness $B(f) = 0$ we have the stronger sufficient condition for asymptotic stability:

$$E < \frac{\arccos\left(\frac{-\alpha}{\beta}\right)}{\sqrt{\beta^2 - \alpha^2}}. \tag{2.7.11}$$

(3) If the skewness is positive ($B(f) > 0$), then there is a $\delta > 0$ such that condition (2.7.11) holds for $|\alpha| < \delta$.

PROOF. The characteristic equation of (2.5.1) is

$$s + \alpha + \beta \int_0^\infty e^{-s\tau} f(\tau) d\tau = 0. \tag{2.7.12}$$

If $E = 0$, (2.7.12) reduces to $s + \alpha + \beta = 0$ which trivially has no root with positive real part so $x_* = 0$ is asymptotically stable. If an increase in E leads to instability of $x_* = 0$, then a root s of (2.7.12) must intersect the imaginary axis, i.e. there exists E

such that (2.7.12) has pure imaginary roots. We seek roots of the form $s = i\omega$, and because the roots come in conjugate pairs, we can restrict our search to $\omega > 0$. In this case Equation (2.7.12) splits into a real part

$$\alpha + \beta \int_0^\infty \cos(\omega\tau) f(\tau) d\tau = 0, \tag{2.7.13}$$

and an imaginary part

$$\omega - \beta \int_0^\infty \sin(\omega\tau) f(\tau) d\tau = 0. \tag{2.7.14}$$

First note that $\omega \leq \sqrt{\beta^2 - \alpha^2}$ since:

$$\begin{aligned} \left[\int_0^\infty \cos(\omega\tau) f(\tau) d\tau\right]^2 + \left[\int_0^\infty \sin(\omega\tau) f(\tau) d\tau\right]^2 &\leq \\ \int_0^\infty \cos^2(\omega\tau) f(\tau) d\tau + \int_0^\infty \sin^2(\omega\tau) f(\tau) d\tau &= \\ \int_0^\infty f(\tau) d\tau &= 1. \end{aligned}$$

and thus, by Equations (2.7.13) and (2.7.14), $\alpha^2 + \omega^2 \leq \beta^2$.

To show condition (2.7.10), notice that

$$\begin{aligned} \int_0^\infty \cos(\omega\tau) f(\tau) d\tau &\geq \int_0^\infty \left(1 - \frac{c\omega\tau}{\pi}\right) f(\tau) d\tau \\ = \int_0^\infty f(\tau) d\tau - \frac{c\omega}{\pi} \int_0^\infty \tau f(\tau) d\tau &= 1 - \frac{c\omega}{\pi} E. \end{aligned}$$

If $1 - c\omega E/\pi > -\alpha/\beta$, Equation (2.7.13) thus has no root. However, $\omega \leq \sqrt{\beta^2 - \alpha^2}$ so a sufficient condition for (2.7.13) to have no root is

$$E < \frac{\pi\left(1 + \frac{\alpha}{\beta}\right)}{c\sqrt{\beta^2 - \alpha^2}}.$$

For the proof of the second part of Theorem 2.7.2. suppose that f is symmetric about its mean and $\alpha \geq 0$. We want $\int_0^\infty \cos(\omega\tau) f(\tau) d\tau > -\alpha/\beta$ for $0 < \omega \leq \sqrt{\beta^2 - \alpha^2}$. By Lemma 2.7.1, we know that $\int_0^\infty \cos(\omega\tau) f(\tau) d\tau > 0$ for $\omega < \pi/2E$. For $\omega \geq \pi/2E$,

$$\left|\int_0^\infty \cos(\omega\tau)\, f(\tau)\, d\tau\right| \leq |\cos(\omega E)|.$$

This implies that

$$\int_0^\infty \cos(\omega\tau) f(\tau) d\tau \geq \cos(\omega E)$$

whenever $\int_0^\infty \cos(\omega\tau)f(\tau)d\tau < 0$. If $\cos(\omega E) > -\alpha/\beta$ then $E < \omega^{-1}\arccos(-\alpha/\beta)$ and

$$\int_0^\infty \cos(\omega\tau)f(\tau)d\tau > -\alpha/\beta.$$

A sufficient condition for (2.7.12) with $\alpha \geq 0$ to have no root with positive real part is therefore:

$$E < \frac{\arccos\left(\frac{-\alpha}{\beta}\right)}{\sqrt{\beta^2-\alpha^2}}.$$

If $\alpha < 0$, compare the boundary of region of stability $(\alpha(\omega),\beta(\omega))$ defined by Equations (2.6.41) and (2.6.42) and the curve $(\alpha_E(\omega),\beta_E(\omega))$ defined by the boundary of region of stability of the single delay at E. These two curves intersect for $\omega = 0$ at the point $(-1/E, 1/E)$:

$$\lim_{\omega\to 0}\alpha(\omega) = \lim_{\omega\to 0}\frac{-\omega C(\omega)}{S(\omega)} = \lim_{\omega\to 0}\frac{-\omega}{S(\omega)} = -\lim_{\omega\to 0}\beta(\omega)$$

This limit is 1 over the slope of $S(\omega)$ at 0, which is E. This is true for all distributions with expectation E and this is their only intersection point. To have intersection we must get

$$\frac{-\omega C(\omega)}{S(\omega)} = \frac{-\omega\cos(\omega E)}{\sin(\omega E)}$$

and

$$\frac{\omega}{S(\omega)} = \frac{\omega}{\sin(\omega E)}$$

which imply, for $\omega \neq 0$, that $C(\omega) = \cos(\omega E)$ and $S(\omega) = \sin(\omega E)$. These equalities can not occur until $\omega = \pi/2E$. Moreover, when $\omega = \pi/2E$, both curves cross the β-axis and at this point $\beta(\omega) > \beta_E(\omega) = \pi/2E$. These facts imply that the curve $(\alpha(\omega),\beta(\omega))$ lies always above the "sufficient" curve $(\alpha_E(\omega),\beta_E(\omega))$ and condition (2.7.11) holds for $\alpha < 0$.

Now we have to show that if $B(f) \geq 0$, no root crosses the imaginary axis when α is sufficiently small. Consider any density f with positive skewness. Let $p \in [0,1]$, and define

$$f_p = pf(\tau) + (1-p)f(2E-\tau).$$

The function $f_{1/2}$ is a symmetric density and we have shown that:

$$\left|\int_{-\infty}^{\infty}\cos(\omega\tau)f_{1/2}(\tau)d\tau\right| \leq |\cos(\omega E)|.$$

Moreover we have that

$$\int_{-\infty}^{\infty} \cos(\omega\tau) f_p(\tau) d\tau = \int_{-\infty}^{\infty} \sum_{n=0}^{\infty} \frac{(-1)^{n+1} (\omega\tau - \pi/2)^{2n+1}}{(2n+1)!} f_p(\tau) d\tau.$$

By Definition 2.7.1 the first nonzero term of the series evaluated at $\omega = \pi/2E$ is

$$\int_{-\infty}^{\infty} \frac{(-1)^{k+1} (\omega\tau - \pi/2)^{2k+1}}{(2k+1)!} f_p(\tau) d\tau =$$
$$\left(\frac{\pi}{2E}\right)^{2k+1} \frac{1}{(2k+1)!} \int_{-\infty}^{\infty} (-1)^{k+1} (\tau - E)^{2k+1} f_p(\tau) d\tau.$$

For $p > 1/2$, it is clear that $B(f_p) > 0$ so

$$\left(\frac{\pi}{2E}\right)^{2k+1} \frac{1}{(2k+1)!} \int_{-\infty}^{\infty} (\tau - E)^{2k+1} f_p(\tau) d\tau = \left(\frac{\pi}{2E}\right)^{2k+1} \frac{1}{(2k+1)!} B(f_p) > 0.$$

This means that for $p = 1/2 + \varepsilon$, with small $\varepsilon > 0$,

$$\int_{-\infty}^{\infty} \cos(\omega\tau) f_p(\tau) d\tau > 0$$

for ω in a neighborhood of $\pi/2E$. This implies that

$$\int_{0}^{\infty} \cos(\omega\tau) f(\tau) d\tau > 0.$$

Thus, we have shown that

$$B(f) \equiv \int_{0}^{\infty} (\tau - E)^{2k+1} f(\tau) d\tau > 0$$

implies

$$\int_{0}^{\infty} \cos(\omega\tau) f(\tau) d\tau > 0$$

around $\omega = \pi/2E$.

The first root of $C(\omega)$ is thus to the right of $\omega = \pi/2E$ (If this is were not true, there would be a (continuous) family of densities f_μ, $\mu \in [0,1]$, with $B(f_0) = 0$, $B(f_\mu) > 0$ for $\mu > 0$ and $f_1 = f$. There would then exist $\mu = \mu_0 > 0$ where a root of $C_{f_{\mu_0}}(\omega)$ appears before $\pi/2E$. This would mean that at $\mu = \mu_0$, a root of the characteristic equation could suddenly appear in the right half complex plane, which is impossible (see Lemma 1.1 in (Kuang, 1994))).

Thus, an increase in p increases

$$\int_{-\infty}^{\infty} \cos(\omega\tau) f_p(\tau) d\tau,$$

and

$$\int_0^\infty \cos(\omega\tau) f(\tau) d\tau > \int_{-\infty}^\infty \cos(\omega\tau) f_{1/2}(\tau) d\tau.$$

This means that a positive skewness increases the stability of Equation (2.5.1) when $|\alpha|$ is small. □

Remark 2.7.3. We can apply condition (2.7.11) to any density with a (small) positive skewness. By the last part of the proof, a small perturbation which increases the skewness of a symmetric density will not cause roots of characteristic equation to cross the imaginary axis.

Conditions (2.7.10) and (2.7.11) differ only when α is small or negative. If α is of the same order of magnitude as β, the conditions are equivalent. When $\alpha = 0$ we get for conditions (2.7.10) and (2.7.11) respectively:

$$E < \frac{\pi}{c\beta}$$

and

$$E < \frac{\pi}{2\beta}.$$

The difference is a factor of $2/c \approx 0.88$, and the difference decreases when α increases. These two bounds are asymptotic to the line $\beta = \alpha$ so the difference vanishes asymptotically.

2.8. SPECIFIC EXAMPLES

When we know the distribution of the delay in (2.5.1), we can find the region $\mathcal{S}$ of stability in the plane of the parameters α and β. Theorem 2.7.2 gives sufficient conditions to have stability in a region $\mathcal{R}$, which must therefore be included in $\mathcal{S}$. A crucial question is: how does $\mathcal{R}$ approach $\mathcal{S}$? In case of a symmetric density, the approximation of the real bound is good if α in Equation (2.5.1) is small. In any case the stability of (2.5.1) tends to increase when the variance of f increases or the expectation decreases as discussed by Anderson in (Anderson, 1991). If we consider the relative variance R defined (Anderson, 1991, 1992) by

$$R = \frac{V}{E^2},$$

we can see that (in general) $\mathcal{R} \to \mathcal{S}$ as $R \to 0$. For an example in which this is not the case see Boese (Boese, 1989). When $R = 0$, the distribution is a Dirac delta $f = \delta_E(\tau)$, and it is well known (El'sgol'ts, 1966) that for a discrete delay, Equation (2.5.1) is stable if and only if

$$E < \frac{\arccos\left(\frac{-\alpha}{\beta}\right)}{\sqrt{\beta^2 - \alpha^2}}$$

when $|\alpha| < \beta$. Moreover, suppose that the distribution has a minimal delay τ_m ($f(\tau) = 0$ for $\tau < \tau_m$). This distribution has an expectation greater than τ_m. Then one could suppose that this distribution is strictly less stable than the single delay at $\tau = \tau_m$ because all information comes after this time. Generally, increasing the expectation of the delay decreases the stability. But other factors also influence the stability. If the variance and skewness are large enough, the stability is improved. Consider for instance the single delay distribution $\delta_{\bar{\tau}}$ with delay $\bar{\tau} = 1$ and the distribution with two delays at $\tau = 1$ and 3.1:

$$f(\tau) = \frac{9}{10}\delta_1(\tau) + \frac{1}{10}\delta_{3.1}(\tau). \tag{2.8.1}$$

Then the density f is more stable than the single delay at 1! This shows the sometimes non-intuitive nature of the necessary conditions for stability of (2.5.1) [See Figure 2.1 for details].

Let us now compare the stability regions $\mathcal{S}$ and $\mathcal{R}$ for some common distributions: a single delay, a uniform delay and a gamma distribution.

2.8.1. The single delay

The single delay density takes the form $\delta_{\bar{\tau}} = \delta(\tau - \bar{\tau})$ which is the Dirac delta function at the fixed time $\bar{\tau}$. With $f(\tau) = \delta_{\bar{\tau}}(\tau)$, Equation (2.5.1) take the simple form

$$\dot{x}(t) = -\alpha x(t) - \beta x(t - \bar{\tau}), \tag{2.8.2}$$

and the characteristic equation is

$$s + \alpha + \beta e^{-s\bar{\tau}} = 0. \tag{2.8.3}$$

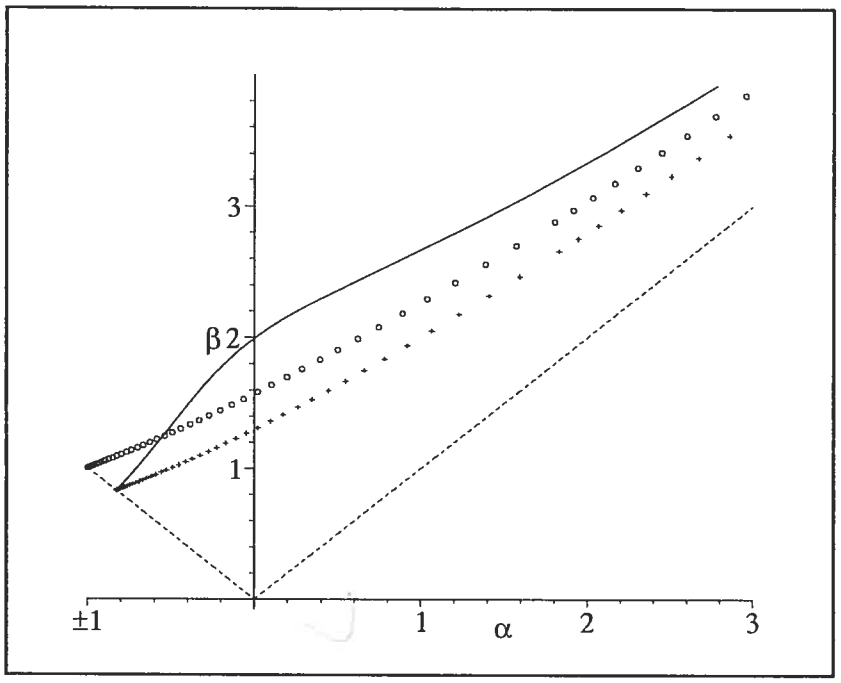

FIGURE 2.1. Comparison of stability boundaries for different distributions of delays. In all cases, the stability region is bounded above by the curve displayed. The solid curve is the boundary of the region of stability with the two discrete delay distribution defined by (2.8.1). The curve with crosses is the sufficient condition computed using condition (2.7.11) of Theorem 2.7.2 and the middle one (circle) defines the stability region of the single delay with $\tau = 1$. The dotted line is the cone $\beta = |\alpha|$.

This density is symmetric and by Theorem (2.7.2), we know that Equation (2.8.2) is stable if

$$\bar{\tau} < \frac{\arccos\left(\frac{-\alpha}{\beta}\right)}{\sqrt{\beta^2 - \alpha^2}}.$$

In this case, this condition is also necessary . Figure 2.2 shows the region of stability, plotted with the method outlined in Section 2.6.1.

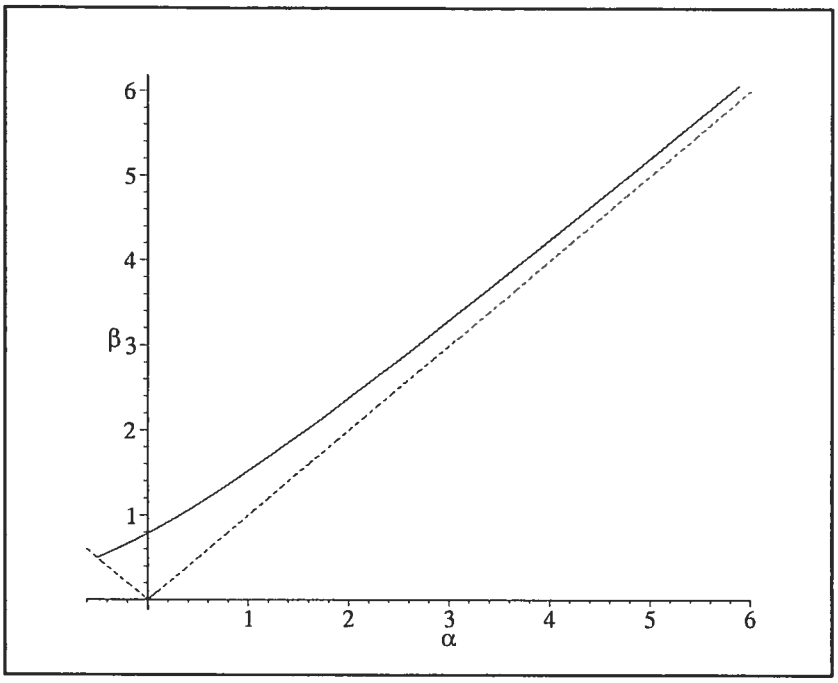

FIGURE 2.2. Upper bound (solid line) of the region of stability for Equation (2.8.2). Here $\mathcal{S} = \mathcal{R}$ and the delay $\bar{\tau} = 2$. Note that the boundary is asymptotic to the line $\beta = \alpha$ (dashed line).

2.8.2. Uniform density

When the delay is uniformly distributed, the density can be written

$$f(\tau) = \begin{cases} 0 & 0 \le \tau < \tau_m \\ 1/\delta & \tau_m \le \tau \le \tau_m + \delta \\ 0 & \tau_m + \delta < \tau \end{cases} \tag{2.8.4}$$

The expectation is $E = \tau_m + \delta/2$. We can apply Theorem 2.7.2, since f is symmetric, to obtain Figure 2.3 when $\tau_m = 2$ and $\delta = 2$.

2.8.3. Gamma density

The shifted gamma distribution with parameters (m, a) is

$$f(\tau) = \begin{cases} 0 & 0 \le \tau < \tau_m \\ \frac{a^m}{\Gamma(m)}(\tau - \tau_m)^{m-1} e^{-a(\tau - \tau_m)} & \tau_m < \tau. \end{cases} \tag{2.8.5}$$

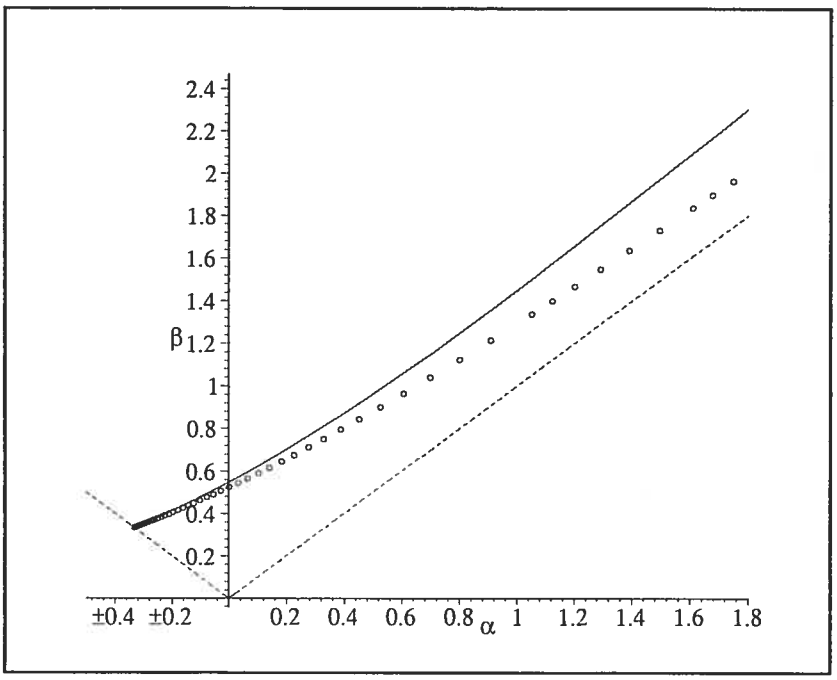

FIGURE 2.3. Stability region for a uniform density on the interval [2,4]. The solid line is the boundary of $\mathcal{S}$, the one with circles is the sufficient condition [Equation (2.7.11)] for stability and the dotted line is the cone $\beta = |\alpha|$.

This distribution has expectation $E = \tau_m + m/a$. The third moment about the mean is

$$\int_0^\infty \frac{a^m}{\Gamma(m)} \tau^{m-1} e^{-a\tau} (\tau - m/a)^3 d\tau = \frac{2m}{a^3} > 0. \tag{2.8.6}$$

Note that the skewness is independent of τ_m because the third moment is taken about the mean which varies with τ_m. The skewness $B(f)$ is positive, so we can apply Theorem 2.7.2. Figure 2.4 shows the difference between the real boundary of $\mathcal{S}$ and the boundary of $\mathcal{R}$. The characteristic equation is

$$s + \alpha + \beta \hat{f}(s) = 0. \tag{2.8.7}$$

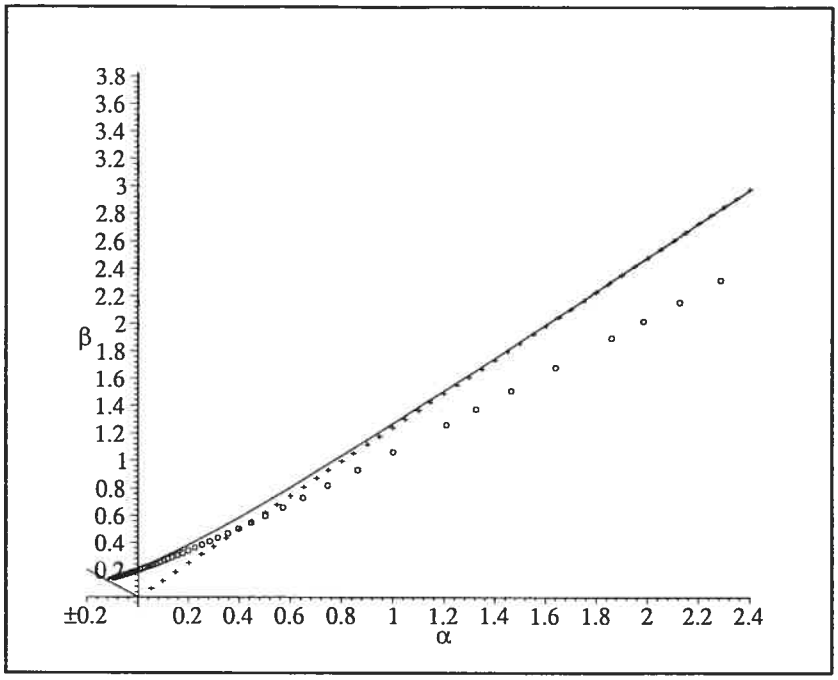

FIGURE 2.4. Region of stability (solid line) for a gamma distribution with parameters $m = 3$, $a = 1$ and $\tau_m = 5$. The curve with circles is the sufficient condition(2.7.11) of Theorem 2.7.2. The upper curve was computed with Equations (2.6.35) and (2.6.36). The asymptote (crosses) comes from Equation (2.8.15).

where $\hat{f}$ denoteS the Laplace transform of f. For the unshifted distribution ($\tau_m = 0$),

$$\hat{f}(s) = \left(1 + \frac{s}{a}\right)^{-m}, \tag{2.8.8}$$

so that we can write Equation (2.8.7) as

$$(s+\alpha)\left(1 + \frac{s}{a}\right)^{m} + \beta = 0. \tag{2.8.9}$$

For large β, there should exist K such that the boundary of the region of stability is asymptotic to $\beta = K\alpha$. This boundary is implicitly expressed by Equation (2.8.7) when $s = i\omega$. Moreover, when β is large, ω should be near π/E. The reason for this is that the imaginary part of $\hat{f}(i\omega)$, $S(\omega)$, takes its first zero near this point, so $S(\pi/E) \approx \omega/\beta \approx 0$. Remember that in the parametric representation of the boundary of S, $\beta(\omega) = \omega/S(\omega)$. If β is very large, since ω is bounded, $S(\omega)$ must be very small.

Substituting $s = i\pi/E = i\pi a/m$ in Equation (2.8.7), we obtain

$$\left(\frac{i\pi a}{m}+\alpha\right)\left(1+\frac{i\pi}{m}\right)^m+\beta\approx 0. \tag{2.8.10}$$

Thus

$$\beta\approx -\alpha\left(1+\frac{i\pi}{m}\right)^m-\frac{i\pi a}{m}\left(1+\frac{i\pi}{m}\right)^m. \tag{2.8.11}$$

When α is large enough, the second term in Equation (2.8.11) is negligible and β is asymptotic to

$$\alpha\left|1+\frac{i\pi}{m}\right|^m. \tag{2.8.12}$$

This term only depends on m. If m increases to infinity, for fixed E, f converges weakly to a Dirac delta function. In this case the asymptote is $\beta=\alpha$ and we see that

$$\left(1+\frac{i\pi}{m}\right)^m\rightarrow e^{i\pi}=-1 \tag{2.8.13}$$

as $m\rightarrow\infty$, which is consistent with the case of the single delay with density given by the Dirac delta function. Thus, for large β and large m, we obtain an informal condition for the stability for the unshifted gamma density:

$$\beta\leq K\alpha=\left|1+\frac{i\pi}{m}\right|^m\alpha. \tag{2.8.14}$$

For the shifted gamma density, we must evaluate $S(\omega)$ at $\pi/E=\pi/(\tau_m+m/a)$. This leads to the condition

$$\beta\leq K\alpha=\left|1+\frac{i\pi}{a\tau_m+m}\right|^m\alpha. \tag{2.8.15}$$

In our example (Figure 2.4), $m=3$, $a=1$ and $\tau_m=5$ so $K=1.24$.

2.9. NEUTROPHIL DYNAMICS

As mentioned in the Introduction, in some diseases a normally approximately constant physiological variable changes its qualitative dynamics and displays an oscillatory nature. This is the case of cyclical neutropenia (CN) in which there is a periodic fall in the neutrophil count from approximately normal to virtually zero and then back up again (Haurie et al., 1998, 2000, 1999b). Haurie *et al.* (Haurie et al., 2000) developed a model for the peripheral regulation of neutrophil production. Their results and other evidence strongly suggest that the origin of the oscillatory behavior in CN is not due to an instability in the peripheral neutrophil regulatory system. Rather, the

oscillations are probably due to a pathological low level oscillatory stem cell input to the neutrophil regulatory system, caused by a destabilization of the hematopoietic stem cell compartment (Mackey, 1978a, 1997). Haurie *et al.* analyzed the data from nine grey collies and found different dynamics between dogs. When the amplitude of the oscillation of the neutrophil is low, the oscillation is approximately sinusoidal. However, when the amplitude increases, a small "bump" appears on the falling phase of the oscillation which increases the neutrophil count before the count falls to zero. Many models of neutrophil production incorporate a negative feedback with delay. However, in a recent modeling study Hearn *et al.* (Hearn et al., 1998) have shown that this feedback alone cannot lead to the oscillations seen in CN. The principal source of oscillation of the neutrophil count comes from the oscillation of the stem cell input which is exterior to the neutrophil regulatory system.

A regulatory model for neutrophil dynamics with *delayed negative feedback* can be written as

$$\dot{x}(t) = -\alpha x(t) + \mathcal{M}_o(\tilde{x}(t)) \tag{2.9.1}$$

where

$$\tilde{x}(t) = \int_{\tau_m}^{\infty} x(t-\tau) f(\tau) d\tau. \tag{2.9.2}$$

The function $\mathcal{M}_o(\tilde{x}(t))$ is the feedback control and is a decreasing function. The constant α is the rate of elimination of neutrophil and f is the distribution of maturation delay. This model, proposed by Haurie *et al* in (Haurie et al., 2000), can be expressed in linearized form as

$$\dot{z}(t) = -\alpha z(t) + \varepsilon I(\bar{\omega}) e^{i\bar{\omega}t} \mathcal{M}_{o*} + \mathcal{M}'_{o*}[1 + \varepsilon I(\bar{\omega}) e^{i\bar{\omega}t}]\tilde{z}(t). \tag{2.9.3}$$

The distribution f is taken to be the shifted gamma defined in Equation (2.6.23) since it offers an excellent fit to the data (Hearn et al., 1998). The term $\varepsilon I(\bar{\omega}) e^{i\bar{\omega}t}$ accounts for the oscillation of the stem cell input. The constant $\mathcal{M}_{o*}$ is the granulocyte turnover rate defined by

$$\alpha x_* = \mathcal{M}_o(x_*) \equiv \mathcal{M}_{o*}. \tag{2.9.4}$$

where x_* is the unique stable steady state of Equation (2.9.1). The other parameters are the period of oscillation of the stem cell input $2\pi/\bar{\omega}$, ε which is assumed to be 1 and

$\mathcal{M}'_{o*}$, the slope of the feedback function at the steady state x_*. The term $I(\bar{\omega})$ depends on a and m:

$$I(\bar{\omega}) = \left(\frac{a}{i\bar{\omega}+a}\right)^{m+1} e^{-i\bar{\omega}\tau_m}. \tag{2.9.5}$$

The value of a is 14.52, m is 8.86 and $\bar{\omega}$ is around 0.45. The maximum value of the oscillation factor $\varepsilon\Re I(\bar{\omega})$ is nearly one, so

$$\max\left|\mathcal{M}'_{o*}[1+\varepsilon I(\bar{\omega})e^{i\bar{\omega}t}]\right| \approx 2\left|\mathcal{M}'_{o*}\right|. \tag{2.9.6}$$

Now if we look at the autonomous part of Equation (2.9.3), we get

$$\dot{z}(t) = -\alpha z(t) + \mathcal{M}'_{o*}[1+\varepsilon I(\bar{\omega})e^{i\bar{\omega}t}]\tilde{z}(t). \tag{2.9.7}$$

When the amplitude of the stem cell input reaches its maximum, we can approximate Equation (2.9.7) using Equation (2.9.6) by

$$\dot{z}(t) = -\alpha z(t) + 2\mathcal{M}'_{o*}\tilde{z}(t). \tag{2.9.8}$$

Since we suppose that $\mathcal{M}_o(\tilde{z}(t))$ is a decreasing function, we know that $\mathcal{M}'_{o*}$ is non-positive. We can therefore apply Theorem 2.7.2 to study the stability of Equation (2.9.8). If $2\mathcal{M}'_{o*} \leq \alpha$, Equation (2.9.8) is always stable. In this case, oscillation in the neutrophil count is due only to the oscillation of the stem cell input in the neutrophil regulatory system and the behavior of the neutrophil count is sinusoidal.

However, in some cases, even if $\mathcal{M}'_{o*} \leq \alpha$, we may have that $2\mathcal{M}'_{o*} \geq \alpha$. Then to study the stability, we can use condition (2.7.11) which gives

$$E < \frac{\arccos(\alpha(2\mathcal{M}'_{o*})^{-1})}{\sqrt{(2\mathcal{M}'_{o*})^2 - \alpha^2}}. \tag{2.9.9}$$

The decay rate α is between 2.18 and 2.48 (days^{-1}), and the expected delay E is between 3.21 and 3.42 days. From data fitting (Haurie et al., 2000), we obtain $\mathcal{M}'_{o*}$ ranging from -0.05 to -2.20. Taking $\alpha = 2.4$, we see that $\left|\mathcal{M}'_{o*}\right| \geq 1.20$ can destabilize Equation (2.9.8). From Table 4 of Haurie *et al.* (reproduced in Table 2.1) the smallest slope $\left|\mathcal{M}'_{o*}\right|$ greater than 1.20 is 1.50. With $\mathcal{M}'_{o*} = -1.50$, a sufficient condition to have stability is

$$E < \frac{\arccos(-0.80)}{\sqrt{3.24}} = 1.39.$$

However, since E is far greater than 1.39 (at least 3.21), we expect that Equation (2.9.8) will not be stable for values of $\left|\mathcal{M}'_{o*}\right| \geq 1.50$. This implies that Equation (2.9.3) will

be destabilized when the amplitude of the stem cell input reaches a threshold which depend on $\mathcal{M}'_{o*}$. From Table 2.1, we can estimate the interval of time during which Equation (2.9.8) will be destabilized. The expected delay E must satisfy

$$E \gg \frac{\arccos\left[\alpha\{\mathcal{M}'_{o*}(1+\Re(\varepsilon I(\bar{\omega}))\}^{-1}\right]}{[\{1+\varepsilon\Re(I(\bar{\omega}))\}^2\mathcal{M}'^2_{o*}-\alpha^2]^{1/2}}. \tag{2.9.10}$$

At worst this condition becomes

$$E \gg \pi[\{1+\varepsilon\Re(I(\bar{\omega}))\}^2\mathcal{M}'^2_{o*}-\alpha^2]^{-1/2}. \tag{2.9.11}$$

We can approximate $\Re(I(\bar{\omega}))$ with Equation (2.9.5) by

$$\Re(I(\bar{\omega})) \simeq 0.96\cos[\bar{\omega}(t-\tau_m)]. \tag{2.9.12}$$

Equation (2.9.11) becomes, with $\alpha = 2.4$,

$$\cos[\bar{\omega}(t-\tau_m)] \gg \frac{2.71}{|\mathcal{M}'_{o*}|} - 1.04. \tag{2.9.13}$$

Given that the density of the maturation delays is concentrated around its expectation (the variance is 0.042), we can replace in our approximation the symbol $\gg$ by the usual $>$. Solving for t gives that t must lie in an interval of length

$$T_{ins} \equiv \frac{2}{\bar{\omega}}\arccos\left(\frac{2.71}{|\mathcal{M}'_{o*}|} - 1.04\right) \tag{2.9.14}$$

The value of T_{ins} for each dog is given in Table 2.1. We find that the peripheral neutrophil regulatory system is destabilized during an average of 4.93 days each period of stem cell input which is of length between 12.6 and 15 days. The effect of this is the small bump seen after the spikes of the neutrophil count.

2.10. Conclusion

We have analysed the influence of the distribution of delays on the stability properties of the null solution of Equation (2.5.1). In general, distributed delays seem to increase the stability of the steady state of a DDE when compared to a discrete delay. With a gamma distribution of the delay, if α and β are sufficiently large, then the steady state will be stable for more values of the parameters than with any equation with a discrete delay.

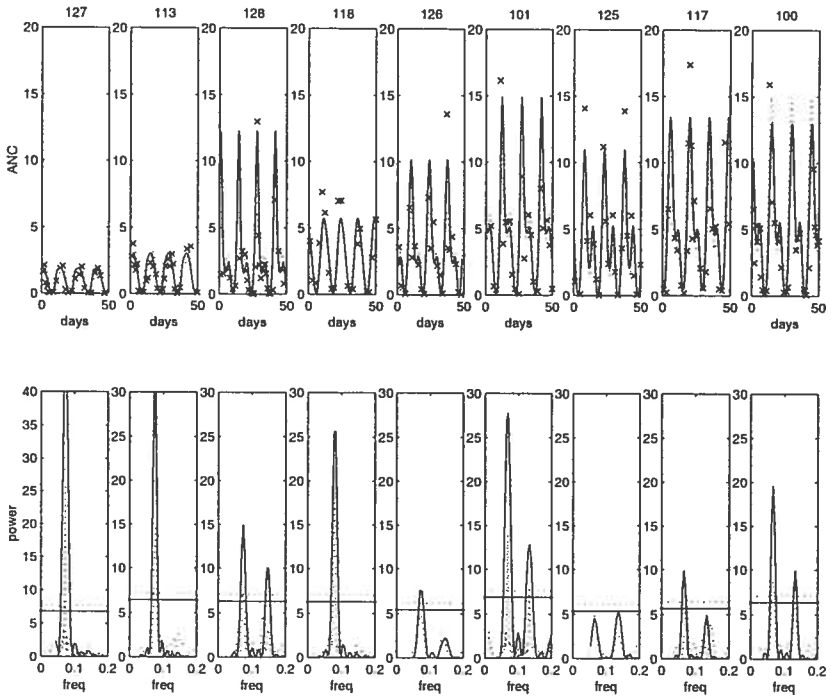

FIGURE 2.5. Simulation results of the model to the absolute neutrophil count (ANC,top) and the Lomb periodogram (bottom) (taken from (Haurie et al., 2000)). The units for ANC are cells$\times 10^{-3}$mm^{-3}. The x's are the data points and the solid lines are the simulation results of Equation (2.9.1). Note the existence of a second harmonic in the Lomb periodogram for all but three dogs (127,113 and 118), which is consistent with the theoretical computation done in Table 2.1.

Theorem 2.7.2 shows that even limited properties of the distribution of delay provide a good indication for the stability when α is relatively small. In many cases, the study of the stability of a differential equation with distributed delays can be reduced to the problem of stability with a discrete delay. When the distribution of delays is known, results of Section 2.6 gives a way to find the boundary of the stability region even if it is not always possible to find an explicit bound in term of intrinsic parameters of the distribution.

Dog	$\mathcal{M}'_{o*}$	$\mathcal{M}'_{o*}$ fit	$\bar{\omega}$	T_{ins}
127	-0.20	-0.10	0.465	0
113	-0.91	-0.05	0.470	0
128	-1.09	-2.00	0.464	5.39
118	-0.48	-0.50	0.500	0
126	-1.00	-1.80	0.463	4.70
101	-1.24	-1.50	0.426	3.27
125	-1.15	-2.20	0.421	6.55
117	-1.05	-1.70	0.438	4.49
100	-1.20	-1.80	0.418	5.20

TABLE 2.1. Data for nine grey collies. The computations for T_{ins} were made using $\mathcal{M}'_{o*}$ fit. Note that with $\mathcal{M}'_{o*}$, only Dog 101 has a slope high enough to destabilize the peripheral regulatory system. This suggests that the fitted values are close to the real ones. The units of $\mathcal{M}'_{o*}$, $\mathcal{M}'_{o*}$ fit and $\bar{\omega}$ are days^{-}1 and T_{ins} is in days. From Haurie *et al.* (Haurie et al., 2000).

In a modeling context, it is often difficult to precisely determine the distribution of delays in the description of a delayed regulated process. Results such as those presented here thus have great interest since they provide *general* bounds on stability regions, irrespective of the particulars of these distributions.

We end this paper with a conjecture which we have found to hold in all cases of distributions of delays that we have studied. Proving it would be very useful and would make the results of Section 2.7 obsolete. In words, it amounts to stating that the most destabilizing distribution of delays is a single Dirac δ function. If true, it could provide, by consideration of simplified models containing single discrete delays, uniform upper bounds on regions of stability in parameter space.

Conjecture 2.10.1. *In the notation of Section 2.7, let f be a probability density defined on R^+ with expectation E. Suppose that ω^* is the first root of $C(\omega)$, then*

$$\beta(\omega^*) \equiv \frac{\omega^*}{S(\omega^*)} \geq \frac{\pi}{2E}. \tag{2.10.1}$$

ACKNOWLEDGEMENTS

Support for this work has been provided by grants from the Natural Sciences and Engineering Research Council (Canada) [OGP-0008806 to JB and OGP-0036920 to MCM], MITACS (Canada) [JB, MCM], the Alexander von Humboldt Stiftung [MCM] and Le Fonds pour la Formation de Chercheurs et l'Aide à la Recherche (Québec) [98ER1057 to MCM, JB]. SB is supported by a studentship from MITACS.

Chapter 3

OSCILLATIONS IN CYCLICAL NEUTROPENIA: NEW EVIDENCE BASED ON MATHEMATICAL MODELING

AUTEURS : SAMUEL BERNARD, JACQUES BÉLAIR ET MICHAEL C. MACKEY

3.1. CONTRIBUTION DE L'AUTEUR À L'ARTICLE

Cet article présente un système novateur d'équations différentielles à retard modélisant la production de globules blancs. Tous les résultats originaux sont de moi, soit : le développement du modèle, l'évaluation des paramètres physiologiques, l'analyse de stabilité et les simulations numériques. Les coauteurs ont révisé le manuscrit et ont apporté des suggestions quant à la mise en place du contenu.

3.2. OSCILLATIONS DANS LA NEUTROPÉNIE CYCLIQUE : NOUVELLES PREUVES BASÉES SUR UNE MODÉLISATION MATHÉMATIQUE

Dans le Chapitre 2, nous avons étudié la stabilité locale d'une équation différentielle scalaire à retard et en avons conclu que la distribution des retards ne pouvait être à l'origine des oscillations observées dans le nombre de globules blancs chez les patients atteints de neutropénie cyclique. Ce résultat nous permet de négliger, dans un premier temps, les distributions de retards induites par les divisions et la maturation des précurseurs des cellules sanguines dans la modélisation de la production des cellules sanguines. Le présent Chapitre traite donc d'équations différentielles avec retards

discrets. Le Chapitre 5 introduit un modèle pouvant servir de base pour une description physiologiquement réaliste de la distribution des temps de maturation/division des cellules sanguines.

Nous présentons un modèle dynamique de production/régulation des neutrophiles en circulation. Ce modèle, dérivé de caractéristiques physiologiques pertinentes du système hématopoïétique, est analysé en utilisant des méthodes tant analytiques que numériques. Nous montrons l'existence de bifurcations de Hopf et de bifurcations col-noeud de cycles limites. Nous estimons les paramètres cinétiques canins et appliquons ensuite le modèle à la neutropénie cyclique. La neutropénie cyclique est une maladie rare dans laquelle on observe une oscillation dans le nombre de la plupart des cellules sanguines. Le nombre de neutrophiles, quant à lui, oscille entre des valeurs normales et à peine détectables. Nous concluons que la cause majeure des oscillations dans la neutropénie cyclique est une hausse du taux d'apoptose des précurseurs des neutrophiles qui mène à une déstabilisation du compartiment des cellules souches hématopoïétiques. Le modèle se définit comme suit,

$$\frac{dN}{dt} = -\alpha N + AF(N_{\tau_N})S_{\tau_N}, \tag{3.2.1}$$

et

$$\frac{dS}{dt} = -F(N)S - K(S)S + 2e^{-\gamma_S \tau_S} K(S_{\tau_S})S_{\tau_S}. \tag{3.2.2}$$

Les variables N et S représentent respectivement le nombre de neutrophiles mûrs et de cellules souches hématopoïétiques par kg de masse corporelle. Les boucles de feedback F et K sont respectivement les taux de différenciation des cellules souches vers la lignée des neutrophiles et le taux de réintroduction des cellules souches en prolifération. Les deux retards τ_N et τ_S modélisent les temps de transit des précurseurs des neutrophiles et la durée du cycle cellulaire des cellules souches. Le paramètre A, qui correspond à l'amplification due aux divisions successives des précurseurs des neutrophiles, joue un rôle primordial dans l'apparition des oscillations. L'amplification A tient compte de l'apoptose des précurseurs et la hausse observée cliniquement de l'apoptose chez ces cellules entraîne la baisse de A et une bifurcation de Hopf surcritique se produit alors.

3.3. ABSTRACT

We present a dynamical model of the production and regulation of circulating blood neutrophil number. This model is derived from physiologically relevant features of the hematopoietic system, and is analyzed using both analytic and numerical methods. Supercritical Hopf bifurcations and saddle-node bifurcations of limit cycles are shown to exist. We make the estimation of kinetic parameters for dogs and then apply the model to cyclical neutropenia in the grey collie, a rare disorder in which oscillations in all blood cell counts are found. We conclude that the major cause of the oscillations in cyclical neutropenia is an increased rate of apoptosis of neutrophil precursors which leads to a destabilization of the hematopoietic stem cell compartment.

3.4. INTRODUCTION

Hematopoiesis is the term used to describe the production of blood cells. Even though all blood cells come from a unique source, the hematopoietic stem cells (HSC), the mechanisms regulating this production are still obscure. Nevertheless, it seems clear that the production of erythrocytes and platelets is controlled by feedback mechanisms involving specific cytokines such as erythropoietin (Epo) and thrombopoietin (Tpo) (Haurie et al., 1998; Mahaffy et al., 1998; Santillan et al., 2000). However, the regulation of leukopoiesis (production of white blood cells) is not as well understood and the local HSC regulation mechanisms are even less clear (Rubinow et Lebowitz, 1975; MacDonald, 1978; Hearn et al., 1998; Haurie et al., 1998, 1999a,b, 2000; Mackey, 2001). Because of their dynamical character, cyclical neutropenia and other periodic hematological disorders offer us opportunities to better comprehend the nature of these regulatory processes (von Schulthess et Mazer, 1982).

Cyclical neutropenia (CN) is a rare hematological disorder characterized by oscillations in the circulating neutrophil count. These levels fall from normal to barely detectable levels with a period of 19 to 21 days in humans (Guerry et al., 1973; Dale et Hammond, 1988; Haurie et al., 1998), and periods up to 40 days have been observed (Haurie et al., 1998). These oscillations in the neutrophil count about a subnormal level are generally accompanied by oscillations around normal levels in other blood cell lineages such as platelets, lymphocytes and reticulocytes (Haurie et al., 1998, 2000).

Many mathematical models have been proposed to explain the origin of these oscillations as well as to understand the control of neutrophil production in nonpathological cases. For a discussion of previous models that have been developed see, (Hearn et al., 1998). In most of them, the production is controlled by a feedback loop located at the level of the neutrophil precursors. Many authors have suggested a destabilization of this feedback loop as a source of oscillations in the neutrophil count seen in cyclical neutropenia (Morley et al., 1969; Morley et Stohlman, 1970; Morley, 1970; King-Smith et Morley, 1970; Reeve, 1973; MacDonald, 1978; Kazarinoff et van den Driessche, 1979; von Schulthess et Mazer, 1982; Shvitra et al., 1983; Wichmann et al., 1988; Schmitz et al., 1990, 1995). However, it has also been shown to be unlikely that such a destabilization could account for oscillations in CN (Hearn et al., 1998), further suggesting that the origin of the oscillations is due to destabilization of the HSC regulation mechanisms. This would also explain the fact that other cell lineages oscillate with the same period as the neutrophils (Haurie et al., 1998, 2000).

Fortunately, cyclical neutropenia is found in an animal model. All grey collies (Lund et al., 1967) are born with this congenital disease with an oscillation period on the order of 11 to 16 days (Haurie et al., 1998, 1999b, 2000). This canine model has provided extensive experimental data on the nature of CN. The challenge is to transfer to humans the knowledge derived from dogs.

In this paper, our primary goal is to model cyclical neutropenia in the grey collie and understand its dynamic behavior. A variety of experimental data show that CN is associated with an elevated rate of apoptosis in neutrophil precursors (Dale et al., 2000; Aprikyan et al., 2001). The model developed in this paper is used to explore the possibility that the oscillations characteristic of CN are actually a consequence of this increased rate of apoptosis.

The paper is organized as follow. In Section 3.5 we develop the model, which is a simple two compartment production system. In Section 3.6, we use the experimental and clinical literature to estimate the model parameters, mainly using data from mice and dogs. In Section 3.7 we analyze the model using a combination of analytical and numerical continuation methods. A local supercritical Hopf bifurcation and a saddle-node bifurcation of limit cycles are found as critical parameters are varied. Numerical

simulations are presented in Section 3.8 and in Section 3.9 we present a new hypothesis for the origin of the oscillations characteristic of cyclical neutropenia. We propose this oscillation mechanism as a generic way to introduce oscillations in hematopoiesis. In Section 3.10 we discuss some of the difficulties in estimating the system parameters for dogs and the important issues in adapting such a model for humans.

3.5. A MODEL OF WHITE BLOOD CELL PRODUCTION

3.5.1. The model equations

Figure 3.1 illustrates the two components of this model: the hematopoietic stem cell (HSC) compartment (denoted S) and the maturing neutrophil compartment (denoted N). The HSCs are self-renewing and pluripotential (can differentiate into any blood cell type), and the rate at which they differentiate into the neutrophil line is assumed to be determined by the level of circulating neutrophils. As these neutrophil precursors differentiate, their numbers are amplified by successive divisions. After a certain maturation time τ_N they become mature neutrophils and are released into blood. The transit time through the neutrophil precursor compartment is not fixed but follows a distribution of times resembling a gamma distribution (Guerry et al., 1973; Deubelbeiss et al., 1975; Price et al., 1996; Basu et al., 2002). In the present paper however, the single fixed transit time τ_N will be used since it simplifies the model without compromising essential features (Bernard et al., 2001).

As shown in Fig. 3.1, there are two feedback loops. The first is between the mature neutrophil compartment and the *rate* ($F(N)$) of HSC differentiation into the neutrophil line. $F(N)$ operates with a delay τ_N that accounts for the time required for neutrophil division and maturation so the flux of cells from the resting phase of the HSC compartment is $F(N_{\tau_N})S_{\tau_N}$. Here, as elsewhere, the notation x_τ means $x(t-\tau)$.

The second loop regulates the *rate* ($K(S)$) at which HSCs reenter the proliferative cycle from G_0 state, and it operates with a delay τ_S that accounts for the length of time required to produce two daughter HSCs from one mother cell. $K(S)$ is a monotone decreasing function of S (and therefore acts like a negative feedback). The flux of cells out of the resting phase of the HSC compartment is given by $K(S)S$. $K(S)$ regulates the level of hematopoietic stem cells (S), while F(N) controls the number of neutrophils.

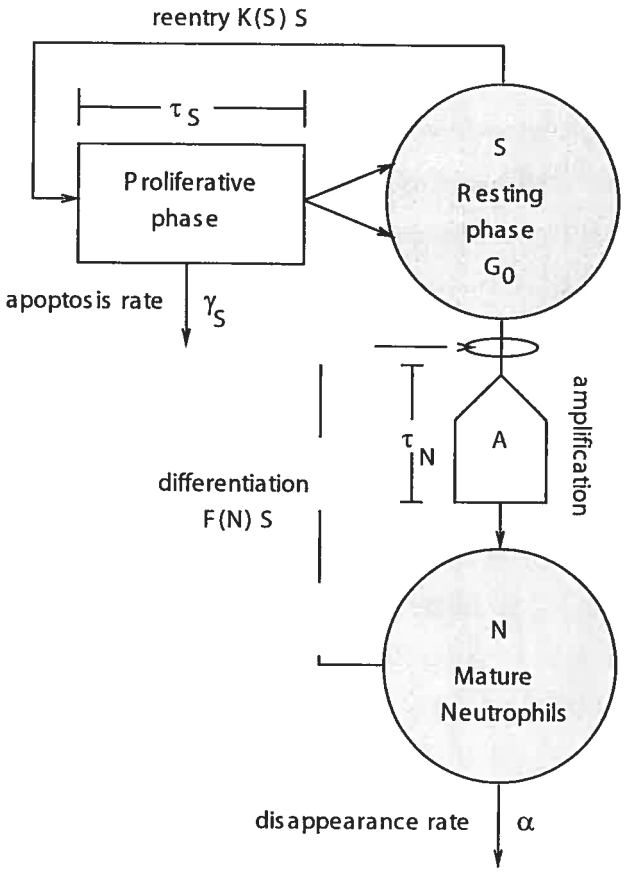

FIGURE 3.1. Model of neutrophil production. The variable S represents the number of hematopoietic stem cells in the resting (G_0) phase. Cells in the resting phase can either enter the proliferative phase at a rate $K(S)$ or differentiate at a rate $F(N)$ to ultimately give rise to mature neutrophils N, the second variable. Cells in the HSC proliferative phase undergo apoptosis at a rate γ_S and the cell cycle duration is τ_S. Cells in the differentiation pathway are amplified by successive divisions by a factor A which is also used to account for cell loss due to apoptosis. After a time τ_N, differentiated cells become mature neutrophils N and are released into the blood. It is assumed that mature neutrophils die at a fixed rate α. Two feedback loops control the entire process through the proliferation rate $K(S)$ and the differentiation rate $F(N)$.

The main agent controlling the peripheral neutrophil regulatory system through $F(N)$ is granulocyte colony stimulating factor (G-CSF), which acts in two ways. First, it decreases the apoptosis rate of neutrophil precursors (leading to an increase of the amplification number A in the model (Basu et al., 2002)) and, second, it increases the rate of HSC differentiation into the neutrophil precursor compartment. The clearance of G-CSF decreases as the number of neutrophils decreases (Kearns et al., 1993; Terashi et al., 1999) and the neutrophil count increases when the level of G-CSF is increased (Petros, 1992; Chatta et al., 1994; Price et al., 1996). This type of regulation suggests a negative feedback: an increase of neutrophil count is followed by a decrease in G-CSF concentration, leading to a decrease in neutrophil count. The effect of G-CSF is analyzed in Appendix 3.11. Other effects of elevated G-CSF concentration are to decrease both the mean and variance of the maturation time τ_N (Chatta et al., 1994; Schmitz et al., 1994; Price et al., 1996; Haurie et al., 1999b) and to decrease the rate of apoptosis of stem cells.

In the present model, we have implicitly included the effect of G-CSF through the feedback $F(N)$. We have not included the effect of G-CSF on the amplification A. Rather, the parameter A is used as a bifurcation parameter. A recent study indicates that cyclical neutropenia is associated, in part, with an increased rate of apoptosis (Aprikyan et al., 2001) and the model developed and analyzed in this paper is used to determine whether this effect is sufficient to induce the dynamical behavior of the neutrophil count observed in cyclical neutropenia.

From Fig. 3.1 we can write down the model equations. The production of N is equal to the influx $F(N)S$ in the precursor compartment times the amplification A, delayed by the transit time τ_N, for a total production of $AF(N_{\tau_N})S_{\tau_N}$. The loss from the compartment N is the efflux to death αN, so that the total variation of N is

$$\frac{dN}{dt} = -\alpha N + AF(N_{\tau_N})S_{\tau_N}. \tag{3.5.1}$$

The production of S is equal to the flux of cells reentering the proliferative phase, $K(S)S$, times the fraction of surviving cells $\exp(-\gamma_S\tau_S)$ times the cell division factor 2, delayed by the cell cycle time τ_S, for a total production of $2\exp(-\gamma_S\tau_S)K(S_{\tau_S})S_{\tau_S}$. The loss from compartment S is the flux reentering the proliferating phase, $K(S)S$, plus the

efflux into differentiation $F(N)S$. The total variation of S is then

$$\frac{dS}{dt} = -F(N)S - K(S)S + 2e^{-\gamma_S \tau_S} K(S_{\tau_S}) S_{\tau_S}. \tag{3.5.2}$$

The model parameters are the circulating neutrophil death rate α, the neutrophil pathway amplification A, the maturation delay of neutrophil precursors τ_N, the HSC proliferative phase duration τ_S and the apoptotic rate of proliferating HSC, γ_S. As noted above, the function F is the differentiation rate from the HSC compartment into the neutrophil lineage and the function K is the HSC self-renewal (proliferation) rate. These functions are made more precise in Appendix 3.11.

3.6. PARAMETER ESTIMATION

Estimation of the parameters is one of the most critical aspects of our work since it is crucial to establish the cause for the onset of oscillations in CN. Parameters that are outside the feedback functions can be retrieved or easily derived from experimental data found in literature.

In humans and dogs, circulating neutrophils disappear at a rate of $\alpha = 2.4$ day^{-1} (Deubelbeiss et al., 1975; Haurie et al., 2000). A number of these parameters depend on the number of stem cells S at steady state. Estimates of this number can vary dramatically, depending on what kind of cells are classified as stem cells. Here a stem cell is defined as a non-differentiated, pluripotential and self-renewing cell. Data from the literature (Boggs et al., 1982; Micklem et al., 1987; Harrison et al., 1988; McCarthy, 1997) give a value of between 1 and 50 stem cells per 10^5 nucleated bone marrow cells in mice with a value of 8 stem cells per 10^5 nucleated bone marrow cells in cats (Abkowitz et al., 2000). (Novak et Nečas, 1994) give a mean count of 1.4×10^{10} nucleated bone marrow cells per kg in mice. This leads to an estimate of 1.12×10^6 HSC/kg [1]. We assume a number of stem cells of $S_* = 1.1 \times 10^6$ cell/kg of body weight. The daily neutrophil production in dogs has been evaluated to 1.65×10^9 cell/kg/day (Deubelbeiss et al., 1975). The average circulating neutrophil count N_* is therefore 6.9×10^8 cells/kg. The proliferation rate K has been evaluated for mice in (Abkowitz

[1] The actual density of HSC in the bone marrow is almost immaterial. Indeed, changing the HSC level by a factor 10 together with the amplification A will result in the same values. Therefore, we will use the value 1.12×10^6 HSC/kg for the normal HSC number.

et al., 2000) to be about 20 to 25 times per year and once each 19 days in (Bradford et al., 1997), giving a value of $K_* = 0.06$ day^{-1}. Under steady state assumption, with an apoptosis rate into the HSC proliferative phase $\gamma_S = 0.07$ day^{-1} (Mackey, 2001), and a cell cycle duration $\tau_S = 2.8$ days (Mackey, 2001; Cheshier et al., 1999; Abkowitz et al., 2000), we find

$$F_* = \frac{K_*}{2e^{-\gamma_S \tau_S} - 1} = 0.04 \text{ day}^{-1}. \tag{3.6.1}$$

Then, we can give an estimation of the normal amplification factor between HSCs and the mature neutrophil pool,

$$A = \frac{\alpha N_*}{F_* S_*} = 2^{15.2}. \tag{3.6.2}$$

This is the effective amplification, and without apoptosis in the proliferative compartment of neutrophil precursors, the number of divisions performed by precursors would be around 15. The ratio between the steady state granulocyte turnover rate and the maximal turnover rate (when there is no apoptosis) has been estimated as between 8 and 16 (Hearn et al., 1998; Haurie et al., 2000), implying that 3 or 4 more divisions than the effective number of division is required to produce enough neutrophil under steady state. The maximum total number of divisions between the stem cell and mature neutrophils is then around 18 (15 effective plus 3 to compensate apoptosis).

The parameters within the feedback functions $K(S)$ and $F(N)$ are much more difficult to estimate. Under steady state conditions, these functions are constant, so we must rely on the dynamics of cyclical neutropenia to guide these estimations. Since the dynamics found in cyclical neutropenia are varied (Haurie et al., 1998, 1999b), we may expect an equally large variation in these parameters.

The two feedback functions include six parameters: f_0, k_0, θ_1, θ_2, n and s. These parameters have been fitted by visual inspection of the dynamics of the model compared to experimental data on circulating neutrophil counts in CN. However, some of these parameters can be related to other experimental data or modeling. The maximal reentry rate k_0 can be evaluated from cell division tracking experiments (Lyons, 1999). In a recent study (Bernard et al., 2003c), a model based on physiologically relevant properties was used to evaluate kinetic parameters from primitive murine bone marrow cells stimulated *in vitro* (Oostendorp et al., 2000). Values of 2.0 to 2.5 day^{-1} were found for the reentry rate into the cell cycle, suggesting a value of $k_0 \geq 2.5$ day^{-1}. A

value of $k_0 = 8.0$ day^{-1} gave a good fit to experimental data. The parameter s controls the steepness of the feedback function K, and is associated with the number of cytokines involved in the division signaling (see Appendix 3.11). It not clear what this value should be but there is evidence that at least two different cytokines are needed to trigger HSC proliferation *in vitro* (McKinstry et al., 1997). In (Pujo-Menjouet and Mackey, to appear), a study is carried out when s takes large values, but traditionally small values have been used in modeling (Andersen et Mackey, 2001). We will therefore assume a value of $s = 2$. The two parameters k_0 and s, with the steady state value K_* allow us to compute the value of $\theta_2 = 0.095 \times 10^6$ cell/kg. With the same argument, we will choose $n = 1$, since we are primarily concerned with the effect of G-CSF alone.

The parameters of F, f_0 and θ_1, are more difficult to estimate since cellular differentiation dynamics are not well characterized. Some experiments report a 20-fold increase in differentiation activity under administration of G-CSF (Lotem et Sachs, 1988; Ward et al., 1999; Akbarzadeh et al., 2002) suggesting a value of f_0 of the order of $20 \times 0.04 = 0.8$ day^{-1}. This value, along with F_* and n, gives a value of $\theta_1 = 0.36 \times 10^8$ cell/kg.

Table 3.1 shows the ranges for which the parameters are in agreement with experimental data.

3.7. Analysis of the model

3.7.1. Two mechanisms for the onset of oscillations

In this section we study the linear stability of the model eqns (3.5.1) and (3.5.2). First note that there exists one and only one positive steady state for N and S if

$$f_0 < \frac{1}{2}(2\exp(-\gamma_S \tau_S) - 1)k_0. \tag{3.7.1}$$

(See Appendix 3.12 for a proof of this claim). The right-hand side of this equation is half the output of the HSC proliferative phase minus one i.e., half the net increase due to one cell division times the proliferative rate k_0. The condition states that the rate of differentiation must be smaller than this output rate. Condition (3.7.1) is always satisfied for the range of parameters used here. Let N_* and S_* denote the unique positive steady state values of N and S respectively when it exists. Then in the neighborhood of

parameter	unit	range	value used	reference
A	100	0∼1000	380	1, 2
f_0	day^{-1}	0.4∼1.5	0.8	3, m
θ_1	10^8 cell/kg	0.1∼2.0	0.36	m
k_0	day^{-1}	2.0∼10.0	8.0	m
θ_2	10^6 cell/kg	0.0001∼0.10	0.095	m
n	—	—	1	4
s	—	2∼3	2	4
τ_N	day	3.0∼10	3.5	5
τ_S	day	1.4∼4.2	2.8	1, 6
γ_S	day^{-1}	0.01∼0.20	0.07	1
α	day^{-1}	2.2∼2.5	2.4	7
S_*	10^6 cell/kg	0.001∼1.1	1.1	1, 8
N_*	10^8 cell/kg	5.0∼10	6.9	1, 9
F_*	day^{-1}	0.01∼0.04	0.04	1
K_*	day^{-1}	0.02∼0.06	0.06	1

TABLE 3.1. Estimated model parameters. The "range" column shows values found in literature or values which are consistent with numerical simulation. The column "value used" shows the value used here in the numerical analysis and simulations. For the references, 1 = (Mackey, 2001), 2 = (Novak et Nečas, 1994; Hearn et al., 1998), 3 = (Haurie et al., 2000), 4 = (Andersen et Mackey, 2001; Niu et al., 1999; Bagley et al., 1997), 5 = (Lebowitz et Rubinow, 1969; Nakamura, 1999; Burthem et al., 2002), 6 = (Cheshier et al., 1999), 7 = (Haurie et al., 2000, 1999b; Hearn et al., 1998), 8 = (Edelstein-Keshet et al., 2001), 9 = (Haurie et al., 2000). The "m" in reference means that the parameter has been chosen to make the model fit available data. All HSC data come from mice, cats, or dogs.

this unique nontrivial stationary solution, we can linearize eqns (3.5.1, 3.5.2) to obtain the characteristic equation.

$$\begin{aligned}\lambda^2-(A_1+B_2)\lambda-A_2\lambda e^{-\lambda\tau_N}-B_3\lambda e^{-\lambda\tau_S}+B_2A_1\\ +(A_2B_2+B_1A_3)e^{-\lambda\tau_N}+A_1B_3e^{-\lambda\tau_S}+A_2B_3e^{-\lambda(\tau_N+\tau_S)}=0.\end{aligned} \tag{3.7.2}$$

This characteristic equations is derived in Appendix 3.13. Equation (3.7.2) is a transcendental equation and it is not possible to study the roots of this equation by means of analytical tools alone. A simpler equation is obtained, however, if we assume that the function F is a constant. In that case, eqn (3.5.2) is uncoupled from eqn (3.5.1) and an analytical stability study can be performed on eqn (3.5.2) alone. The mechanisms leading to oscillations found in this simpler reduction of the model have been also found numerically in the full nonlinear model i.e., when F is a function of the number of neutrophils N. These mechanisms are explained below and numerical methods have been used to plot the bifurcation diagrams for the full model Fig. (3.2 and 3.3).

Based on our model analysis, there are two physiologically plausible mechanisms that can lead to oscillation in the model described by eqns (3.5.1, 3.5.2). Both involve the stem cell compartment:

Mechanism 1. In the first, we assume that the stem cell parameters are at their normal values (cf. Table 3.1), and we mimic an increase in the rate of apoptosis in the neutrophil compartment by decreasing the parameter A. This leads to an increase in the stem cell differentiation rate $F(N)$ that may destabilize the stem cell compartment.

Mechanism 2. The other mechanism is an increase in the apoptosis rate γ_S in the stem cell compartment. This leads to an increased rate of replication $K(S)$ that may also destabilize the system. The second mechanism has been studied in (Mackey, 1978a; Fowler et Mackey, 2002), and can lead to long period oscillations (from 20 to 40 days, as shown in Fig. 3.4, bottom panel). This destabilization can only occur when the differentiation rate F is sufficiently small [2].

[2]Considerations of telomere loss during stem cell replication (Vickers et al., 2000) indicate that the differentiation rate F could be very small in humans compared to those in mice or dogs. This may explain why long period oscillations are sometimes observed in humans and not in grey collies. This also suggests that, in some cases, the source of oscillation in cyclical neutropenia may be different in humans and grey collies (although the differences in parameter values between the two species may also account for a difference in the period).

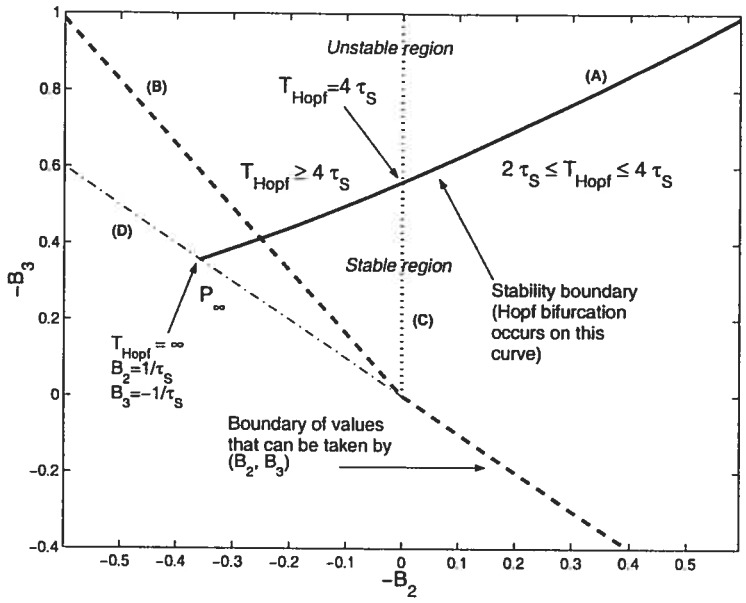

FIGURE 3.2. Stability region in the B_2B_3-plane when F is a constant. The stability region is below the thick curve (A) and to the right of the dashed line (B). The system becomes unstable through a Hopf bifurcation when (B_2, B_3) crosses the stability boundary (A). The period of oscillation at the bifurcation depends on the position of the bifurcation point relative to the dotted line (C). If the bifurcation occurs to the right of the dotted line, then $2\tau_S \leq T_{Hopf} < 4\tau_S$. If the bifurcation occurs to the left of the dotted line, then $T_{Hopf} \geq 4\tau_S$. The period increases when the bifurcation point goes to the left of the figure (B_2 more positive) and tends to infinity when the stability curve (A) meets the dashed-dotted curve (D) at point P_∞. The dashed curve (B) delimits the values that can be taken by (B_2, B_3). The upper part of line (B) has a slope of $2\exp -\gamma_S\tau_S > 1$ and approaches 1 when γ_S is increased. The only way for a bifurcation to occur near P_∞ is by either increasing τ_S or γ_S. The parameters used to plot this figure are $\gamma_S = 0.07$ day^{-1} and $\tau_S = 2.8$ days.

To distinguish between the two mechanisms, we have to look at the sign of B_2 in eqn (3.7.2). If B_2 is positive, then a long period (greater than $4\tau_S$) bifurcation can occur. A high value of F in B_2 will make it negative and in this case an increase in γ_S will give the same effect as Mechanism 1. Let $F \equiv F_*$ be constant, so that A_2 and B_1

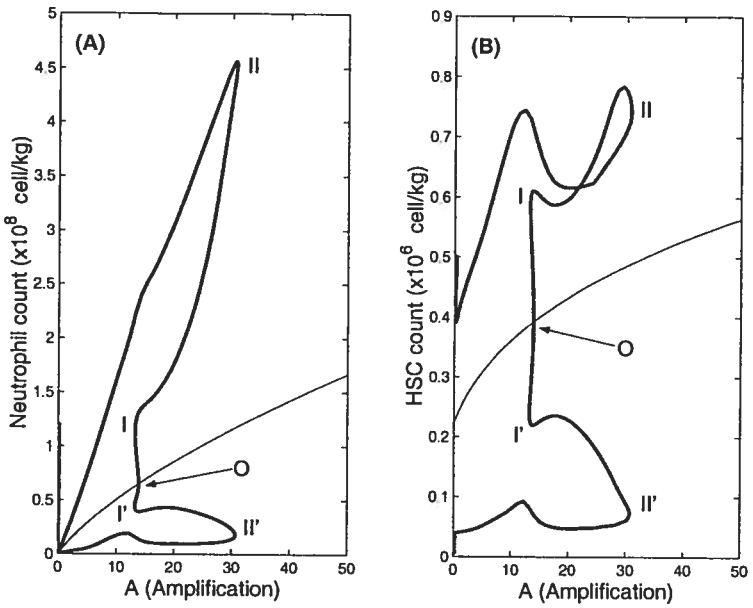

FIGURE 3.3. Bifurcation diagrams for N *(panel A)* and S *(panel B)* with respect to the parameter A. In each panel, the thin line represents the steady state (N_*, S_*) and the thick lines represents the envelope of the periodic solution around that steady state (the envelope is defined by the maximum and the minimum oscillation values for each value of the parameter A). In both panels, the point O is a supercritical Hopf bifurcation, and when A is decreasing, the steady state is destabilized. At this point O ($A = 13.87$), a small stable limit cycle appears with increasing amplitude until its envelope reaches the point I and I' (at $A = 13.24$). At this point the limit cycle disappears through a reverse saddle-node bifurcation of limit cycles (point I), together with an unstable limit cycle between points I and II ($A = 30.73$). This unstable limit cycle, with envelope defined by curves between points I and II and between I' and II', appears at a larger value of A (point II) through another saddle-node bifurcation of limit cycles together with a stable limit cycle of large amplitude. The large amplitude limit cycle exists from point II to $A = 0$, and coexists with a locally stable steady state up to point O, with a stable limit cycle between points O and I, and is the only attractor for A values to the left of point I. The steady state for N ranges from 0 to 1.7 $\times 10^8$ cell/kg whereas S ranges from 0.22 to 0.56 $\times 10^6$ cell/kg. Parameters used for this simulation as in Table 3.1.

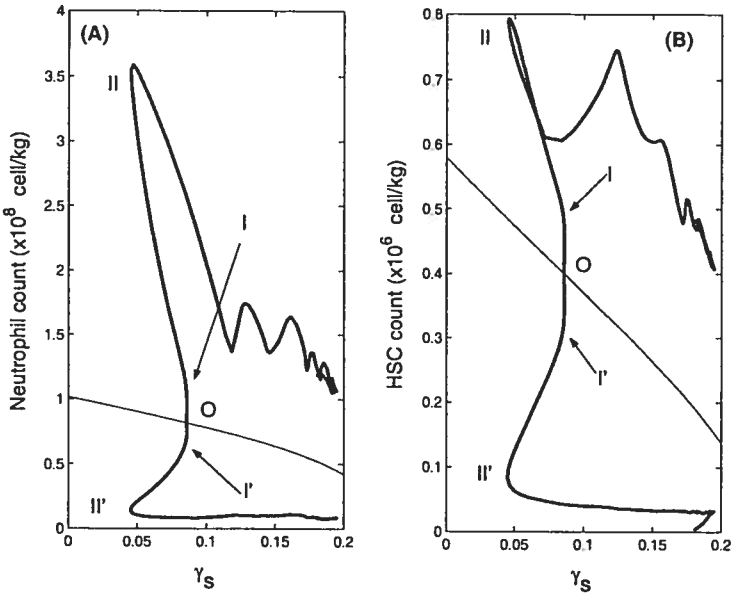

FIGURE 3.4. Bifurcation diagrams for N *(panel A)* and S *(panel B)* with respect to parameter γ_S. In each panel, the thin line represents the steady state (N_*, S_*) and the thick line represents the envelope of the periodic solution around that steady state. In both panels, the point O corresponds to a supercritical Hopf bifurcation, and when γ_S is increasing, the steady state is destabilized. At this point O ($\gamma_S = 0.08589$ day^{-1}), a small stable limit cycle appears with increasing amplitude until its envelope reaches the point I and I' (at $\gamma_S = 0.08606$ day^{-1}). At this point the limit cycle disappears through a reverse saddle-node bifurcation of limit cycles (point I), together with an unstable limit cycle between points I and II ($\gamma_S = 0.045$ day^{-1}). This unstable limit cycle, with envelope defined by curves between points I and II and between I' and II', appears at a larger value of A (point II) through another saddle-node bifurcation of limit cycles together with a stable limit cycle of large amplitude. The large amplitude limit cycle exists from point II to γ_S near 0.20, and coexists with a locally stable steady state up to point O, with a stable limit cycle between points O and I, and is the only attractor for γ_S values to the right of point I. What happens when γ_S approaches is not clear numerically. Note the scale for each panel, the steady state for N ranges from 0.45 to 1.0 $\times 10^8$ cell/kg whereas S ranges from 0.14 to 0.58 $\times 10^6$ cell/kg. Parameters used are as in Table 3.1 except $A = 20$.

are zero. This is the quasi-steady state assumption. The characteristic equation (3.7.2) reduces to

$$(\lambda - A_1)(\lambda - B_2 - B_3 \exp(-\lambda \tau_S)) = 0. \tag{3.7.3}$$

As long as $A_1 < 0$, the stability only depends on the second factor in eqn (3.7.3). The location of the roots of eqn (3.7.3) will determine the stability of eqns (3.5.1, 3.5.2) under the quasi-steady state assumption. This characteristic eqn (3.7.3) has been studied in many papers and recently in (Bernard et al., 2001). The stability space (B_1, B_2) can be divided in three regions.

(1) If $-B_2 \geq |B_3|$, then the steady state of system (3.5.1, 3.5.2) is locally stable;

(2) if $B_3 > -B_2$, then the unique positive steady state condition is violated, and we will not consider this case further;

(3) if $B_3 \leq -|B_2|$, then the local stability of system (3.5.1, 3.5.2) is dependent on the following condition (Hayes, 1950):

$$\tau_S < \frac{\arccos\left(\frac{-B_2}{B_3}\right)}{\sqrt{B_3^2 - B_2^2}}. \tag{3.7.4}$$

This condition states that the cell cycle duration τ_S of the stem cells must be small enough for the solutions to be locally stable.

Only case 3 is of interest since it is the only one potentially leading to a loss of stability of the steady state and giving rise to oscillations. In the following analysis, case 3 will be assumed: $B_3 \leq -|B_2|$. When Inequality (3.7.4) becomes an equality, a Hopf bifurcation occurs (Bernard et al., 2001) with period

$$T_{Hopf} = \frac{2\pi}{\sqrt{B_3^2 - B_2^2}}. \tag{3.7.5}$$

When B_2 is negative, the arccos in inequality (3.7.4) is bounded below by $\pi/2$ and above by π. Thus, from eqns (3.7.4) and (3.7.5), it is easy to show that the period T_{Hopf} is restricted to the interval $[2\tau_S, 4\tau_S]$ for B_2 negative. In this case no long period oscillations can occur. However, if B_2 is positive and close to B_3, a Hopf bifurcation will have a Hopf period $T_{Hopf} \geq 4\tau_S$ and thus a long period bifurcation can occur if the denominator of eqn (3.7.5) becomes small. We can even give an upper bound for the

value T_{Hopf}. From the definition of B_2 and B_3 in eqn (3.13.3), we have

$$B_3 < -2\exp(-\gamma_S\tau_S)B_2, \tag{3.7.6}$$

and as we are in case 3,

$$B_3^2 > 4\exp(-2\gamma_S\tau_S)B_2^2. \tag{3.7.7}$$

Inserting eqn (3.7.7) into eqn (3.7.5) leads to

$$T_{Hopf} < \frac{2\pi}{|B_2|\sqrt{4\exp(-2\gamma_S\tau_S)-1}}. \tag{3.7.8}$$

Refer to Fig. 3.2 to see what happens for each value of (B_2, B_3) in term of stability and bifurcation period. From eqn (3.7.8) we see that it is necessary to have a large value of $\gamma_S\tau_S$ for a long Hopf period at the bifurcation point. Another requirement from eqn (3.7.5) is that $B_3 \sim -B_2$, which can only happen when the differentiation rate F is small and $2\exp(-\gamma_S\tau_S)$ is near 1.

3.7.2. Numerical analysis of the model

The numerical analysis described in this section does not take the form of traditional numerical simulations since we used a `Matlab` package, `DDE-BIFTOOLS` (Engelborghs et al., 2001), which is based on continuation methods that are in widespread use for ordinary differential equations through the software `AUTO` (Doedel, 1981).

First assume that for a given value of A (large enough), the unique positive steady state is locally stable. When A is decreased, corresponding to an increased level of neutrophil precursor apoptosis, this steady state is destabilized (Mechanism 1). A second way to destabilize the system is by increasing the apoptosis rate γ_S in the HSC compartment (Mechanism 2). Figures 3 and 4 show the bifurcation diagrams for the full model for changes in either the amplification A or the HSC apoptosis rate γ_S respectively. From the numerical analysis, the destabilization of the fixed point in both cases occurs via a supercritical Hopf bifurcation (point O in Figs. 3 and 4). Before this bifurcation can be observed, the system undergoes a saddle-node bifurcation of limit cycles: a stable and an unstable limit cycle appear at points II in Figs. 3 and 4. This happens either when A decreases or when γ_S increases.

In Fig. 3.3, the bifurcation diagram is plotted for N_* and S_* with respect to A, and represents Mechanism 1. Four types of solutions can be found in the figure: stable

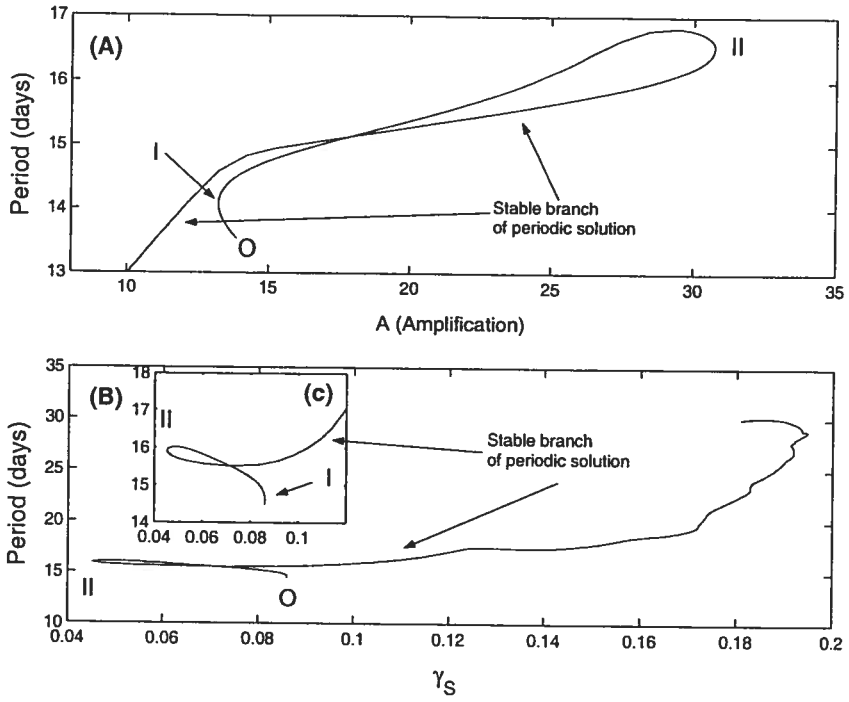

FIGURE 3.5. Period of oscillation of the system with respect to bifurcation parameters A *(panel A)* and γ_S *(panel B)*. In each panel, the period of each existing limit cycle is plotted. The numbering O, I and II refers to Figs. 3 and 4 where the corresponding points are shown. In panel (A), the period of oscillation shows a plateau for the stable branch for values of A between 12 and 30. In panel (B), a large increase is seen when γ_S approaches 0.20 day^{-1}. In panel (c) is a enlargement of the left part of the curve to show details of the intersection and turning points I and II.

steady-states, unstable steady-states, stable limit cycles and unstable limit cycles. The steady states (plotted in thin lines) range from 0 to 1.7 $\times 10^8$ cell/kg for N_* and from 0.22 to 0.56 $\times 10^6$ cell/kg for S_* when A goes from 0 to 50. These values of S_* are close to the normal steady state of 1.1 $\times 10^6$ cell/kg, and can be explained by a robust adaptivity, a necessary condition for a system such as the hematopoietic system. Experimental data shows that in neutropenic patients, the neutrophil count is around 0.12 of the normal value (Mackey et al., 2003a), whereas other cell lines do not show significant decreases in their level (Wright et al., 1981; Haurie et al., 1998). The relative independence of S_* with respect to A shows that the model presented here reproduces

well this robustness of the HSC compartment and explains why other cell lineages show oscillations around their normal values in CN without depletion in their level.

However, the effect differs when we look at Fig. 3.4. Indeed, when γ_S is taken as the bifurcation parameter, the diagrams look similar to Fig. 3.3 qualitatively but things are different quantitatively. From a dynamical point of view, we can see that in both panels of Fig. 3.4, a supercritical Hopf bifurcation occurs at point O, and there is a small stable limit cycle as in the bifurcation diagram of A. The stable limit cycle disappears at point I through a saddle-node bifurcation of limit cycles and an unstable limit cycle joints points I and II. At point II, a large limit cycle appears and stays until $\gamma_S = 0.20$ day^{-1}, after which the numerical continuation method failed to follow the periodic solution. If we look at the steady-states, we note that N_* goes from 0.45 to 1.0 $\times 10^8$ cell/kg and S_* from 0.14 to 0.58 $\times 10^6$ cell/kg when the HSC apoptosis rate γ_S goes from 0 to 0.20 day^{-1}. The situation is reversed from the bifurcation diagram with A. Now the HSC steady-state level S_* is decreased by a factor 4 while the neutrophil count decreases by a factor 2. The HSC apoptotic rate γ_S is a sensitive parameter, and small changes can have deleterious effects in the HSC level. In fact, if the apoptotic rate is high enough, less than one daughter cell will come out of the proliferative phase for each mother cell entering the cell cycle. If

$$\gamma_S > \frac{\ln 2}{\tau_S}, \tag{3.7.9}$$

then the HSC count will decrease to zero, meaning that the hematopoietic system can no longer produce blood cells (note that condition (3.7.1) holds this case). This situation is never encountered when A is changed; even when $A = 0$ the steady state $S_* > 0$. For that reason, we hypothesize that the most important source for the onset of oscillations in CN is an elevated apoptotic rate in the recognizable and committed neutrophil precursors (Mechanism 1).

Another piece of evidence supporting the hypothesis that CN in grey collies is due to a higher than normal apoptosis rate in the neutrophil precursors is given by looking at the period of oscillation with respect to A and γ_S in Fig. 3.5. In panel (A) the period is plotted as a function of A. For values of A between 12 and 30, the period of the stable limit cycle is almost constant, ranging from 14 to 16 days. These values corresponds to the ones seen in grey collies with CN. This range from 12 to 30 is also an acceptable

range for A when the model is fitted to experimental data. The rapidly falling period as A becomes smaller than 15 occurs at the same time than the disappearance of the stable limit cycle (point I in Figs. 3 and 5, panels (A)).

In Fig. 3.5 (B), the period of oscillation is plotted as a function of γ_S. As we can see, for a short range ($\gamma_S = 0.05$ to 0.12 day^{-1}), the period is almost constant around 16–17 days. For larger apoptosis rates, the period increases rapidly and reaches nearly 30 days when $\gamma_S = 0.20$ day^{-1}. These long period oscillations have been observed in humans with CN (Haurie et al., 1998), and an increase in HSC apoptosis could, in some cases, play a role.

3.8. Model simulations of neutrophil oscillation

3.8.1. Periodic solutions behavior

We performed numerical simulations on the full model (3.5.1, 3.5.2) using the software `xppaut` (Ermentrout, 2001, 2002).

Figure 3.6 shows two types of periodic solutions that can exist in CN. In panel (A) is shown a small amplitude periodic solution, which had appeared through the Hopf bifurcation (point O in Fig. 3.3). This periodic solution does not exist for a large window of A values, thus it is not likely to be experimentally observable. However, in Fig. 3.6 (B), the periodic solution, which appeared through the saddle-node bifurcation, is representative of the behavior of neutrophil counts in grey collies. The neutrophil count goes from nearly zero to a normal level with a characteristic secondary bump on the falling phases. This second mode in the neutrophil oscillation in grey collies has been shown to be due to the interaction of the delay τ_N and the periodic input of HSC into the neutrophil lineage (Bernard et al., 2001).

3.8.2. Effect of G-CSF administration

In Fig. 3.7 we have simulated the effect of administrating G-CSF to a neutropenic dog. Five effects of G-CSF were considered,

- Decrease of apoptosis in neutrophil precursors, leading to an increase in A,
- Increase in the HSC differentiation rate F, by increasing θ_1. The parameter θ_1 is proportional to the production of G-CSF,

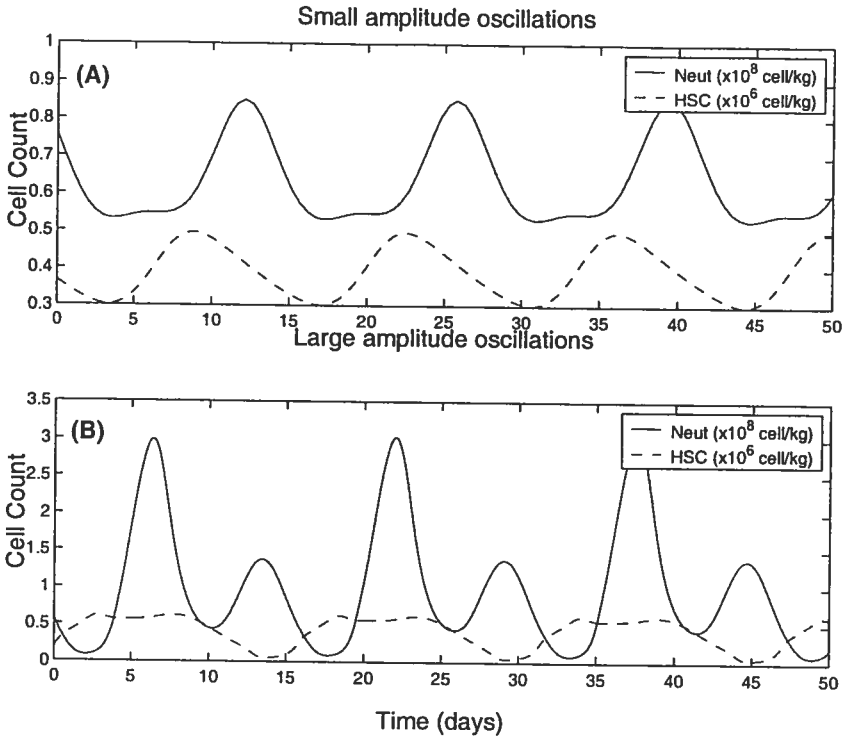

FIGURE 3.6. Small and large oscillations in the neutrophil and HSC count. Parameters as in Table 3.1 except $A = 13.50$ in panel (A) and $A = 20.0$ in panel (B).

- Decrease of apoptosis γ_S of HSC,
- Decrease of the proliferative phase duration τ_S of HSC,
- Decrease of the neutrophil precursors transit time τ_N.

Clinical studies have shown that administrating G-CSF to patients with CN usually results in a net increase of the mean neutrophil count, in the amplitude of oscillation and in the minimum neutrophil count, and a decrease in the period of oscillation (Hammond et al., 1989). The same effects have been observed in grey collies following G-CSF treatment (Haurie et al., 2000). Figure 3.7 shows all of these changes when G-CSF administration is simulated with the above mentioned changes in the model parameters.

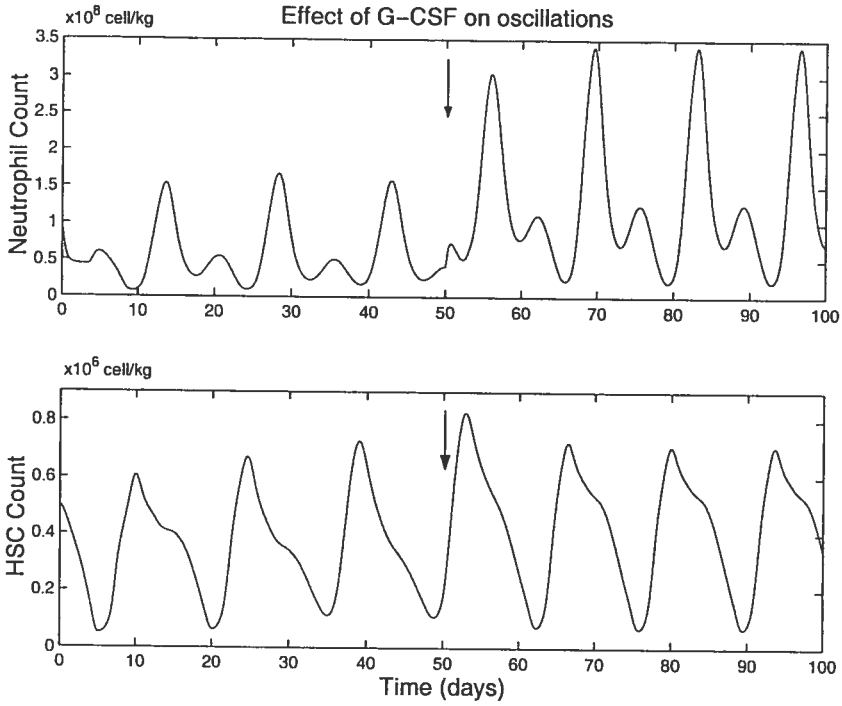

FIGURE 3.7. Effect of G-CSF administration on the circulating neutrophil and HSC counts. Beginning on day 50 (*vertical arrow*), continuous G-CSF administration was simulated by changing five parameters in the following way: A from 10 to 20, θ_1 from 0.36 to 0.80 $\times 10^8$ cell/kg, γ_S from 0.07 to 0.05 day^{-1}, τ_S from 2.8 to 2.6 days and τ_N from 3.5 to 3.0 days.

3.9. A NEW HYPOTHESIS FOR THE ORIGIN OF OSCILLATIONS IN CYCLICAL NEUTROPENIA

The results of Sections 3.7.1 and 3.7.2 suggest a new hypothesis concerning the onset of oscillations seen in cyclical neutropenia. Namely:

We hypothesize that the cause of the oscillations in cyclical neutropenia is a destabilization in the hematopoietic stem cell regulatory system due to an elevated apoptotic rate in the recognizable and committed neutrophil precursors.

This elevation has been observed experimentally (Aprikyan et al., 2001) but a link between elevated apoptosis in committed neutrophil precursors and oscillations in the stem cell compartment has not been clear until now.

Oscillations seen in other cell lineages—reticulocytes, monocytes, platelets, lymphocytes —(Haurie et al., 1999a) further support the idea that the origin of this disorder lies in the primitive bone marrow cell population. In Fig. 3.2, the mean HSC level is about 50 percent normal, whereas the neutrophil level undergoes a ten-fold decrease from normal values in CN. This small decrease in HSC level compared to the neutrophil level explains why the mean level of other blood cell lines are relatively unaffected by CN. The regulation mechanisms in these lines are robust enough to compensate for a periodic decrease in HSC level (this is confirmed by numerical simulations, not shown here). We propose this oscillation mechanism as a generic way to introduce oscillations in hematopoiesis. It could, for instance, explain oscillations of period between 16 and 19 days seen in erythrocyte levels after marrow irradiation in mice (Gurney et al., 1981; Gibson et al., 1984, 1985).

3.10. Discussion

Cyclical neutropenia (CN) is a rare disorder characterized by oscillatory production of blood cells in the bone marrow. The oscillations are most prominent in the neutrophil count, but are also present in other cell lineages (lymphocytes, reticulocytes, monocytes and platelets). In this study, we have developed a physiologically realistic mathematical model for neutrophil production from the hematopoietic stem cells. We tested the hypothesis that the oscillations of CN originate from the hematopoietic stem cells (HSC) (Haurie et al., 2000; Hearn et al., 1998) as a secondary response to a primary increased rate of apoptosis (mimicked by a decrease in the value of the parameter A) in the recognizable neutrophil precursors (Aprikyan et al., 2001). Our numerical simulations show that increasing the apoptosis rate in the neutrophil regulatory system leads to an increased demand on the HSC with a consequent destabilization of the steady-state number of stem cells and the appearance of oscillations through a Hopf bifurcation

Discrepancies between experimental data or indirect measurements of parameters make the parameter estimation procedure difficult. One of the most difficult parameters to estimate is the HSC level in normal dogs. (Abkowitz et al., 2002) hypothesized that

the absolute number of HSC is approximately constant among all mammals. Implications of this claim are numerous, one of them being that in larger mammals, like dogs or humans, the hematopoietic system must work differently than in small mammals in order to meet their blood cell production requirements. As many parameters depend on S_*, a judicious choice must be made.

Another problem raised by stem cell kinetic parameter estimation is translating to humans the model presented here, as few kinetic data for human stem cells *in vivo* are available. To obtain a better understanding of the dynamical features of hematological disorders, kinetic data for humans have to be determined. Existing technologies, such as cell markers, could help to attain this goal. These kinetic data would be of great potential to help in designing more efficient protocols for bone marrow transplants.

Despite the parameter estimation problems, the model presented here captures the essentials of the white blood cell regulatory system in CN. Both experimental data and numerical simulations indicate that regulated apoptosis may be a powerful control mechanism for the production of blood cells and that the loss of control over apoptosis can have significant and negative effects on the dynamical properties of hematopoiesis. Thus, with a decrease in apoptotic rate the hematopoietic system can respond rapidly to an increased demand for circulating blood cells. To make this comment clearer, as pointed out by (Mackey et al., 2003a) the normal input to the post-mitotic neutrophil compartment is about 2.3 times the granulocyte turnover rate (GTR) and thus a reduction of the rate of apoptosis to zero would more than double the GTR. This means, for example, that a substantial fall in neutrophil numbers would lead to an increased level of circulating G-CSF. This would, in turn, lead to a decreased level of apoptosis and consequent increase in the GTR. This elevated effective production of neutrophils would also be felt rapidly since the increased levels of G-CSF would not only decrease the level of apoptosis but also decrease the time spent in the post-mitotic compartment as has been documented by (Chatta et al., 1994) and (Price et al., 1996).

Analytical examination of the model also showed that an increase in the rate of stem cell apoptosis can lead to long period oscillations in the neutrophil count. This could be a factor in the difference between periods observed in dogs and in humans

(14 vs 21 days). However, there is no evidence at this time that the rate of stem cell apoptosis is higher than normal in cyclical neutropenia.

The clinical effects of G-CSF administration have been successfully simulated by varying parameters known to be affected by G-CSF. The amplitude, mean level and nadir of the oscillation increased, while the period decreased following G-CSF administration.

Our results are thus consistent with the hypothesis that CN originates from an elevation of apoptosis rates in the peripheral neutrophil regulatory system that destabilizes the HSC dynamics leading to the oscillatory pattern observed clinically.

Another hematological disease in which oscillations in leukocytes, platelets and erythrocyte precursors can be seen is periodic chronic myelogenous leukemia (PCML) (Fortin et Mackey, 1999). This form of leukemia is characterized by oscillations from normal to high levels in leukocyte count with periods ranging from 35 to 80 days. A relationship exists between some kinds of neutropenia and leukemia since it has been established that some neutropenic patients will eventually develop leukemia (Lensink et al., 1986; Weinblatt et al., 1995; Freedman et al., 2000; Jeha et al., 2000; Dinauer et al., 2000). An interesting question which we are now exploring is whether there exists a causal link between CN and PCML in terms of the dynamics of hematopoietic regulation.

3.11. Formulation of the feedback functions F and K

Recent studies show that a significant degree of G-CSF clearance is performed by the binding of G-CSF by G-CSF receptors located on the surface of neutrophils (Layton et al., 1989; Kato et al., 1997; Stefanich et al., 1997). This binding allows the activation of mechanisms leading to enhanced cell survival (Williams et al., 1990; Borge et al., 1997), increased proliferation and an increased differentiation rate (Haurie et al., 1998; Kanayasu-Toyoda et al., 1999). Even if the exact activation pathway is poorly understood, one can assume that the cellular response is proportional to the number of activated (bound) G-CSF receptors per cell. Assuming that G-CSF binds to the receptor following the law of mass action, we can determine the dependence of the differentiation rate on G-CSF.

Let $[G]$ denote the G-CSF concentration, $[R]$ the density of free receptors, $[L]$ the density of activated receptors and $[N]$ the concentration of neutrophils and their precursors. The total number of receptors is

$$[R]+[L]=m[N] \tag{3.11.1}$$

where m is average number of G-CSF receptors per cell. R can represent dimer or oligomer receptors. If n G-CSF molecules are required to activate one receptor, then from the law of mass action

$$[R]+n[G] \rightleftharpoons [L]. \tag{3.11.2}$$

At equilibrium we have

$$[R][G]^n = k[L], \tag{3.11.3}$$

where k is a reaction coefficient. We assume that the differentiation rate F is proportional to the fraction of bound receptors on a cell,

$$F = f_0 \frac{[L]}{m[N]}. \tag{3.11.4}$$

From eqns (3.11.1) and (3.11.3) we obtain

$$[L] = \frac{m[N][G]^n}{k+[G]^n}. \tag{3.11.5}$$

Using eqn (3.11.4), and dropping the brackets, we arrive at

$$F(G) = f_0 \frac{G^n}{k+G^n}. \tag{3.11.6}$$

G is mainly regulated by the number N of neutrophils such that the clearance of G by N is linear with proportionality constant σ (Terashi et al., 1999; Takatani et al., 1996) and the production P is constant. Thus, the concentration of G-CSF is represented by the equation

$$\dot{G} = P - \sigma NG. \tag{3.11.7}$$

The G-CSF clearance becomes saturated when the level of G-CSF increases (Hayashi et al., 2001) but in this study we assume that this effect is unimportant. This will keep the formulation in the following as simple as possible. Then the steady state is

$$G_* = \frac{P}{\sigma N}. \tag{3.11.8}$$

Replacing G in eqn (3.11.6) by its steady state value G_* gives

$$F(G) = F(G(N)) = \tilde{F}(N) = f_0 \frac{(P/\sigma N)^n}{k + (P/\sigma N)^n} = f_0 \frac{\tilde{k}}{\tilde{k} + N^n}, \tag{3.11.9}$$

where

$$\tilde{k} = \frac{P^n}{k\sigma^n}. \tag{3.11.10}$$

From these considerations, we take F to be of the form

$$F(N) = f_0 \frac{\theta_1^n}{\theta_1^n + N^n} \tag{3.11.11}$$

with $\theta_1^n = \tilde{k}$. Notice that θ_1 depends on the production of G-CSF; this parameter will be affected by administration of exogenous G-CSF. Function F is a Hill function and the exponent n is often referred as a Hill coefficient or a cooperativity coefficient. We can perform much the same derivation for the feedback function K to obtain the same form as in (Mackey, 2001) and (Andersen et Mackey, 2001):

$$K(S) = k_0 \frac{\theta_2^s}{\theta_2^s + S^s} \tag{3.11.12}$$

3.12. EXISTENCE AND UNIQUENESS OF THE STEADY STATE

We present here the details of computations carried out in Section 3.7. In this section we present the proof of the existence and uniqueness of the positive steady state under condition (3.7.1). First write the equations for the steady states.

$$\alpha N_* = AF(N_*)S_*, \tag{3.12.1}$$

and

$$F(N_*) = rK(S_*), \tag{3.12.2}$$

where $r = 2\exp(-\gamma_S \tau_S) - 1$. From the definition of $K(S)$, eqn (3.11.12), and eqn (3.12.2) we can find the steady state S_* in term of N_*,

$$S_* = \theta_2 \sqrt{\left(\frac{rk_0}{F(N_*)} - 1\right)}. \tag{3.12.3}$$

From eqn (3.12.1) and (3.12.3), we can eliminate S_*,

$$N_* = \frac{A\theta_2}{\alpha} \sqrt{\left(\frac{rk_0}{F(N_*)} - 1\right)} F(N_*). \tag{3.12.4}$$

Let the right hand side of eqn (3.12.4) be $G(N_*)$. Then the derivative of G with respect to N_* is,

$$G'(N_*) = \frac{A\theta_2}{2\alpha}\sqrt{\left(\frac{rk_0}{F(N_*)} - 1\right)}\, F'(N_*)\left[2 - \frac{1}{1 - F(N_*)(rk_0)^{-1}}\right]. \tag{3.12.5}$$

If we can prove that $G'(N_*)$ is always negative, then by using the fixed point theorem it is easy to show that there exists one and only one positive steady state N_*, and from that value the uniqueness of the steady state S_* follows naturally. To show that $G'(N_*)$ is negative, we have only to make sure that the factor in the brackets in eqn (3.12.5) is positive since the rest is negative (from the definition of $F(N)$ in eqn (3.11.11), it is obvious that $F'(N) < 0$). So we need to find conditions for which

$$2 - \frac{1}{1 - F(N_*)(rk_0)^{-1}} > 0. \tag{3.12.6}$$

This is equivalent to showing that

$$F(N_*) < \frac{1}{2}rk_0. \tag{3.12.7}$$

We know that $F(N_*) < f_0$, so a sufficient condition for $G'(N_*)$ to be negative is

$$f_0 < \frac{1}{2}rk_0 = \frac{1}{2}(2\exp(-\gamma_S\tau) - 1)k_0, \tag{3.12.8}$$

which completes the proof of the existence and uniqueness of the steady state (N_*, S_*) under condition (3.7.1).

3.13. Linearization and Characteristic Equation

The linearization of eqns (3.5.1, 3.5.2) around the unique positive steady state (N_*, S_*) is performed as follow. First define new variables $x = N - N_*$ and $y = S - S_*$ so that $x = 0$ and $y = 0$ are fixed points. Then by linearizing around the steady state (N_*, S_*), we obtain,

$$\frac{dx}{dt} = A_1 x + A_2 x_{\tau_N} + A_3 y_{\tau_N}, \tag{3.13.1}$$

and

$$\frac{dy}{dt} = B_1 x + B_2 y + B_3 y_{\tau_S}, \tag{3.13.2}$$

where the linearization coefficients are,

$$\begin{aligned} A_1 &= -\alpha & &= (-\alpha N)_N \\ A_2 &= AF'_*S_* & &= (AF(N)S)_N \\ A_3 &= AF_* & &= (AF(N)S)_S \\ B_1 &= -F'_*S_* & &= (-F(N)S)_N \\ B_2 &= -[F_* + K'_*S_* + K_*] & &= (-[F(N)+K(S)]S)_S \\ B_3 &= 2\exp(-\gamma_S\tau_S)(K'_*S_* + K_*) & &= 2\exp(-\gamma_S\tau_S)(K(S)S)_S. \end{aligned} \tag{3.13.3}$$

The subscripts in the right-hand side equalities denote the partial derivative with respect to the variable. The star subscript $(_*)$ in the middle equality means that the function is evaluated at the steady state and the prime stands for the derivative with respect to the argument. These equations can be formulated in a vector equation,

$$\frac{dX}{dt} = LX + R_N X_{\tau_N} + R_S X_{\tau_S}, \tag{3.13.4}$$

where,

$$X = \begin{pmatrix} x \\ y \end{pmatrix}, \tag{3.13.5}$$

and

$$L = \begin{pmatrix} A_1 & 0 \\ B_1 & B_2 \end{pmatrix}, R_N = \begin{pmatrix} A_2 & A_3 \\ 0 & 0 \end{pmatrix}, R_S = \begin{pmatrix} 0 & 0 \\ 0 & B_3 \end{pmatrix}. \tag{3.13.6}$$

The characteristic equation of eqn (3.13.4) is defined as,

$$\det[\lambda I - L - R_N \exp(-\lambda\tau_N) - R_S \exp(\lambda\tau_S)] = 0, \tag{3.13.7}$$

with I the 2x2 identity matrix. The characteristic equation can then be explicitly written as eqn 3.7.2.

ACKNOWLEDGMENTS

We thank Prof. David Dale and Ms. Caroline Haurie for the grey collie data and an anonymous referee for detailed suggestions. This work was supported by MITACS (Canada), the Natural Sciences and Engineering Research Council (NSERC grant OGP-0036920, Canada), the Alexander von Humboldt Stiftung, Le Fonds pour la Formation de Chercheurs et l'Aide à la Recherche (FCAR grant 98ER1057, Québec), the Leverhulme Trust (U.K.) and the Institut des sciences mathématiques (ISM, Québec).

Chapter 4

BIFURCATIONS IN A MODEL OF BLOOD CELL PRODUCTION

AUTEURS : SAMUEL BERNARD, JACQUES BÉLAIR ET MICHAEL C. MACKEY

4.1. CONTRIBUTION DE L'AUTEUR À L'ARTICLE

Cet article est le compte rendu d'une conférence donnée à Będlewo en Pologne en juin 2002. Les résultats, qui sont entièrement de moi, portent sur l'analyse de stabilité et de bifurcations du modèle présenté dans l'article du Chapitre 3. J'ai rédigé l'article et les coauteurs ont révisé le manuscrit et apporté des suggestions quant à la forme et au contenu.

4.2. BIFURCATIONS DANS UN MODÈLE DE PRODUCTION DE GLOBULES BLANCS

Dans le Chapitre 3, un modèle de production de neutrophiles a été introduit puis analysé et appliqué à la neutropénie cyclique. Il est repris ici dans un contexte plus général de production de globules blancs. Une analyse la plus complète possible est effectuée de façon à déterminer une variété des dynamiques (mathématiquement) possibles contenues dans ce modèle.

On étudie la dynamique d'un modèle de production de globules blancs (GB). Le modèle, de nature compartimentale, prend la forme de deux équations différentielles avec deux retards discrets. Nous montrons que la transition de valeurs normales de paramètres à des valeurs pathologiques mène à des bifurcations de Hopf surcritiques

ainsi qu'à des bifurcations col-nœud de cycles limites. Nous caractérisons les points fixes du système et procédons à l'analyse de bifurcation. Nos résultats indiquent qu'une augmentation du taux d'apoptose, soit des cellules hématopoïétiques, soit des précurseurs des GB, induit une bifurcation de Hopf et qu'un régime oscillatoire apparaît. Ces oscillations sont observées dans certains désordres hématologiques.

4.3. ABSTRACT

We study the dynamics of a model of white blood cell (WBC) production. The model consists of two compartmental differential equations with two discrete delays. We show that from normal to pathological parameter values, the system undergoes supercritical Hopf bifurcations and saddle-node bifurcations of limit cycles. We characterize the steady states of the system and perform a bifurcation analysis. Our results indicate that an increase in apoptosis rate of either haematopoietic stem cells or WBC precursors induces a Hopf bifurcation and an oscillatory regime takes place. These oscillations are seen in some haematological diseases.

4.4. INTRODUCTION

Hematopoiesis is the term used to describe the production of blood cells. All blood cells come from a unique source, the hematopoietic stem cells (HSC), but mechanisms regulating this production are not completely understood. Particularly, the regulation of leukopoiesis (production of white blood cells) is not well understood and the local HSC regulation mechanisms are even less clear (Rubinow et Lebowitz, 1975; MacDonald, 1978; Hearn et al., 1998; Haurie et al., 1998, 1999a,b, 2000; Mackey, 2001). Because of their dynamical character, cyclical neutropenia and other periodic hematological disorders offer us opportunities to better comprehend the nature of these regulatory processes (von Schulthess et Mazer, 1982).

Cyclical neutropenia (CN) is a rare hematological disorder characterized by oscillations in the circulating white blood cell (WBC) count. Levels of neutrophils, a type of white blood cell, fall from normal to barely detectable levels with a period of 19 to 21 days in humans (Haurie et al., 1998; Guerry et al., 1973; Dale et Hammond, 1988) and around 14 in grey collies (Haurie et al., 1998). These oscillations in the WBC

count about a subnormal level are generally accompanied by oscillations around normal levels in other blood cell lineages such as platelets, lymphocytes and reticulocytes (Haurie et al., 1998, 2000).

The goal of this paper is to study a simple model of WBC production. We look for mechanisms leading to oscillations in the WBC count and relate these mechanisms to physiological features of the hematopoietic system. We use cyclical neutropenia data from a canine model, the grey collie, which is born with this hematological disorder (Lund et al., 1967).

The paper is organized as follow. In Section 4.5 we present the model, which is a simple two compartment production system. In Section 4.6 we analyze the model using a combination of analytical and numerical continuation methods. It is shown that the positive steady state can be destabilized by a supercritical Hopf bifurcation and that saddle-node bifurcations of limit cycles exist. In Section 4.7, we discuss the implications for the physiological system of such instabilities.

4.5. MODEL

Fig. 4.1 illustrates the two cell types of this model represented in the two compartments outlined in bold: the hematopoietic stem cells (HSC) and the maturing WBCs. The HSCs are self-renewing and pluripotential (can differentiate into any blood cell type), and the rate at which they differentiate into the WBC line is assumed to be determined by the level of circulating WBCs. As these WBC precursors differentiate, their numbers are amplified by successive divisions. After a certain maturation time τ_M they become mature WBCs and are released into the blood.

As shown in Fig. 4.1, there are two feedback loops. The first loop is between the mature WBC compartment and the rate ($F(M)$) of HSC differentiation into the WBC line. $F(M)$ operates with a delay τ_M that accounts for the time required for WBC division and maturation so the flux of cells from the resting phase of the HSC compartment is $S_{\tau_M}F(M_{\tau_M})$. Here, as elsewhere, the notation x_τ means $x(t-\tau)$.

The second feedback loop regulates the rate ($K(S)$) at which HSCs reenter the proliferative cycle from G_0 state, and it operates with a delay τ_S that accounts for the length of time required to produce two daughter HSCs from one mother cell. $K(S)$ is

a monotone decreasing function of S and therefore acts as a negative feedback. The flux of cells out of the resting phase of the HSC compartment is given by $SK(S)$. $K(S)$ regulates the level of hematopoietic stem cells (S), while F(M) controls the number of WBCs.

The main agents controlling the peripheral WBC regulatory system through $F(M)$ are the colony stimulating factors (CSFs) such as granulocyte CSF (G-CSF) or granulocyte-monocyte CSF (GM-CSF). The main effect of CSF is stimulating the production of WBCs. As WBCs are a factor in the clearance of CSF, the type of regulation meditated by these cytokines is a negative feedback. An increase of WBC count is followed by a decrease in CSF concentration, leading to a decrease in WBC count, which in turn leads to an increase in CSF concentration, stimulating WBC production.

From Fig. 4.1 we can write down by inspection the model equations:

$$\frac{dM}{dt} = -\alpha M + AS_{\tau_M}F(M_{\tau_M}), \tag{4.5.1}$$

and

$$\frac{dS}{dt} = -SF(M) - SK(S) + 2e^{-\gamma_S\tau_S}S_{\tau_S}K(S_{\tau_S}). \tag{4.5.2}$$

The model parameters are the circulating WBC death rate α, the WBC pathway amplification A, the maturation delay of WBC precursors τ_M, the HSC proliferative phase duration τ_S and the apoptotic rate of proliferating HSC, γ_S. The feedback functions F and K are taken as Hill functions:

$$F(M) = f_0\frac{\theta_1}{\theta_1 + M} \tag{4.5.3}$$

and

$$K(S) = k_0\frac{\theta_2^s}{\theta_2^s + S^s}. \tag{4.5.4}$$

All parameters describe physiological quantities and are *de facto* assumed to be positive. Table 4.1 shows the parameter values used in this study. Some of them can be evaluated from experimental data found in literature, and references are indicated in Table 4.1. However, the values of parameters such as S_*, τ_M and parameters inside the feedback loops are less clear. A recent study (Abkowitz et al., 2002) indicates that the absolute stem cell population would be conserved in mammals. This implies that the frequency S_* would be much lower in dogs (our model) than in mice (where the data

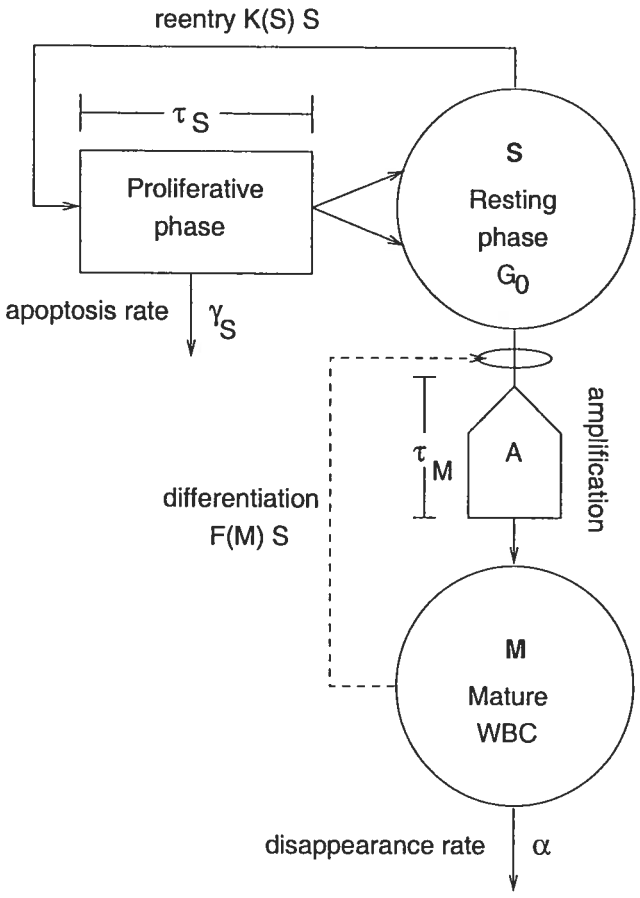

FIGURE 4.1. Model of WBC production. The variable S represents the number of hematopoietic stem cells in the resting (G_0) phase. Cells in the resting phase can either enter the proliferative phase at a rate $K(S)$ or differentiate at a rate $F(M)$ to ultimately give rise to mature WBCs M, the second variable. Cells in the HSC proliferative phase undergo apoptosis at a rate γ_S and the cell cycle duration is τ_S. Cells in the differentiation pathway are amplified by successive divisions by a factor A which is also used to account for cell loss due to apoptosis. After a time τ_M, differentiated cells become mature WBCs M and are released into the blood. It is assumed that mature WBCs die at a fixed rate α. Two feedback loops control the entire process through the proliferation rate $K(S)$ and the differentiation rate $F(M)$.

come from). Moreover, many parameters depends on S_* such as A and τ_M. Nevertheless, numerical simulations have shown that changing the value of S_* (along with A and τ_M) does not change the dynamics qualitatively, and not much quantitatively. For these reasons, we will take the steady state stem cell count S_* found in mice.

In normal condition, the duration of WBC transit time from the most primitive precursor cells to fully mature cells has been evaluated to approximately 12 days (Lebowitz et Rubinow, 1969), the post-mitotic maturation phase to about 3.0 days in dogs (Haurie et al., 2000). Some authors even report a transit time of 42 days or more (to appear). However, clinical data show that the transit time is shortened in CN patients or after granulocyte colony stimulating factor (G-CSF) administration. Considering that the hematopoietic regulatory system acts thorough the maturation cell line, we will take the feedback delay $\tau_M = 3.5$ days (in a recent study (Oostendorp et al., 2000), primitive murine blood cells have been shown to divide up to 8 times in a 3 days *in vitro* culture.) Numerical simulations show that large changes in τ_M (up to 42 days) does not affect significantly the behavior of the solution, although the solution may become apparently quasi-periodic in some ranges of τ_M values.

4.6. ANALYSIS

In this section, we study the stability of steady states and their bifurcations. As the parameter space is vast, we have to choose the most relevant ones to be examined. A key parameter in the onset of hematopoietic disorders such as CN and PCML seems to be the apoptosis rate of blood cell precursors. In the present model, two parameters control this apoptotic rate, the HSC apoptosis rate γ_S and the precursor amplification A, which can be expressed as

$$A = 2^q \exp(-\gamma_P T). \tag{4.6.1}$$

The parameter A is composed of an absolute amplification term 2^q representing q successive divisions, and of a term representing the surviving fraction from apoptosis, $\exp(-\gamma_P T)$, where γ_P is the precursor apoptosis rate and T the time during which the apoptosis occurs. Therefore, our two main bifurcation parameters will be γ_S and A. Other parameters will be fixed as in Table 4.1 unless otherwise noted.

parameter	unit	value	reference
A	100	20.0	1
f_0	day^{-1}	0.8	2
θ_1	10^8cell/kg	0.36	model
k_0	day^{-1}	8.0	model
θ_2	10^6cell/kg	0.095	model
s	—	$2 \sim 3$	3
τ_M	day	3.5	4
τ_S	day	2.8	5
γ_S	day^{-1}	0.07	6
α	day^{-1}	2.4	7
S_*	10^6cell/kg	1.1	8
M_*	10^8cell/kg	6.9	9
F_*	day^{-1}	0.04	2
K_*	day^{-1}	0.06	2

TABLE 4.1. List of parameters used in the model. The references are: 1=(Mackey, 2001; Novak et Nečas, 1994), 2=(Haurie et al., 2000), 3=(Andersen et Mackey, 2001; Niu et al., 1999; Bagley et al., 1997), 4=(Lebowitz et Rubinow, 1969; Nakamura, 1999; Burthem et al., 2002), 5=(Mackey, 2001; Cheshier et al., 1999), 6=(Mackey, 2001), 7=(Deubelbeiss et al., 1975), 8=(Mackey, 2001; Edelstein-Keshet et al., 2001), 9=(Mackey, 2001; Haurie et al., 2000).

4.6.1. Linear stability - Quasi steady state assumption

In this section, we consider a simpler model by assuming the function F to be constant. This uncouples eqns (4.5.1) and (4.5.2) and allow a complete stability analysis of the stem cell compartment. In that case, it is easy to show that a single positive steady state exists for the system if $F < k_0 r$, where $r = 2\exp(-\gamma_S \tau_S) - 1$. The nonzero

steady states are defined by the following relation,

$$S_*^s = \theta_2^s \left[\frac{k_0 r}{F} - 1 \right]. \tag{4.6.2}$$

When the apoptosis rate is increased to

$$\gamma_S = \frac{1}{\tau_S} \ln \left[\frac{2}{\frac{F}{k_0} + 1} \right], \tag{4.6.3}$$

the positive steady state reaches, and collapses with, the null steady state. The linearization around the positive steady state of eqn (4.5.2) allows us to understand the nature of this bifurcation. Let $y = S - S_*$, so the linearized equation from eqn (4.5.2) is

$$\dot{y} = -A_+ y - B_+ y_{\tau_S}, \tag{4.6.4}$$

where the parameters A_+ and B_+ are defined by

$$A_+ = F + \left[(1-s)\frac{F}{r} + s\frac{F^2}{k_0 r^2} \right] \text{ and } B_+ = -(r+1)\left[(1-s)\frac{F}{r} + s\frac{F^2}{k_0 r^2} \right]. \tag{4.6.5}$$

and

$$B_+ = -(r+1)\left[(1-s)\frac{F}{r} + s\frac{F^2}{k_0 r^2} \right]. \tag{4.6.6}$$

The characteristic equation associated with eqn (4.6.4) is

$$\lambda + A_+ + B_+ \exp(-\lambda \tau_S) = 0. \tag{4.6.7}$$

Let us recall a well known theorem (Hayes, 1950; Bernard et al., 2001) on linear delay differential equations. The steady state leading to the characteristic equation (4.6.7) is locally stable if and only if

$$|B_+| < A_+, \tag{4.6.8}$$

or

$$B_+ > |A_+| \text{ and } \tau_S < \frac{\arccos(-A_+/B_+)}{\sqrt{B_+^2 - A_+^2}}. \tag{4.6.9}$$

When $F = k_0 r$, the only steady state is zero. If the apoptosis rate γ_S is decreased by a small amount, we can assume that, for small ε,

$$\frac{F}{k_0 r} = 1 - \varepsilon. \tag{4.6.10}$$

In that case, we can show that

$$\begin{aligned} |B_+| &= \tfrac{F}{r}(1-s\varepsilon)+F(1-s\varepsilon) \\ &< \tfrac{F}{r}(1-s\varepsilon)+F = A_+. \end{aligned} \tag{4.6.11}$$

and thus the positive steady state is locally stable when it is close to zero.

Now if we linearize around the trivial steady state, we find a linearized equation (with $z = S$)

$$\dot{z} = -A_0 z - B_0 z_{\tau_S}, \tag{4.6.12}$$

with

$$A_0 = F + k_0 \text{ and } B_0 = -(r+1)k_0. \tag{4.6.13}$$

Two cases have to be considered. First, if $F \geq k_0 r$, then

$$A_0 \geq k_0 r + k_0 = |B_0| \tag{4.6.14}$$

implies that the null steady state is stable. The other case is $F < k_0 r$: then

$$A_0 < k_0 r + k_0 = -B_0, \tag{4.6.15}$$

and the trivial steady state is unstable.

We have shown so far that when γ_S takes the value given by eqn (4.6.3), the unique positive steady state collapses with the trivial steady state, leading to a bifurcation point. In order to distinguish between the different possible bifurcations, we have to look at the value of the exponent s in the feedback function K. If s is even, then the s-root in eqn (4.6.2) is not real when $F > k_0 r$ so only the trivial steady state exists. When γ_S decreases, leading to a increase of r, a pair of nonzero steady states appear around zero, giving a pitchfork bifurcation. If s is odd, then the s-root always exists. When γ_S decreases, the steady state S_* goes from negative to positive, and there is an exchange stability at zero: this is a transcritical bifurcation.

4.6.1.1. *Oscillation around the positive steady state*

There exists a range of γ_S for which the positive steady state S_* is unstable. Figure 4.2 shows the bifurcation diagram of S with respect to γ_S.

Many authors have speculated about the consequences of such oscillations. There might be a causal link between oscillation in the HSC compartment and oscillations

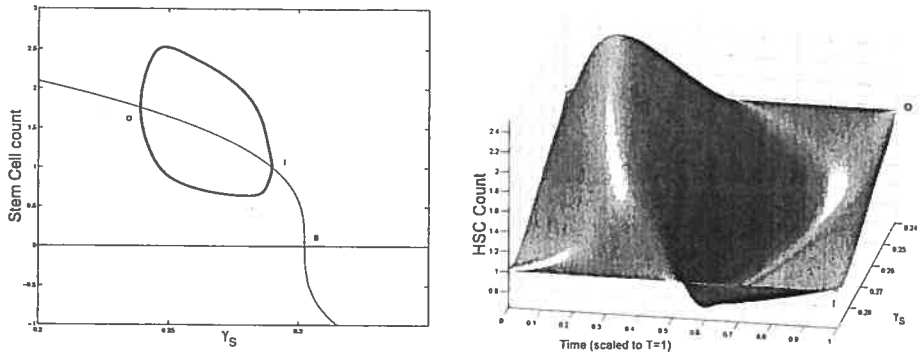

FIGURE 4.2. *Left panel*: bifurcation diagram with apoptosis rate γ_S as a parameter. The positive steady state is represented by the thin line and the envelope of the periodic solution by the thick line. The other parameter values are $F = 0.05$, $\theta_1 = 1.0$, $k_0 = 1.77$, $\tau_S = 2.2$ and $s = 3$. In this case a transcritical bifurcation occurs at point II. At point O, a supercritical Hopf bifurcation occurs and a stable limit cycle appears. This limit cycle eventually disappears through a reverse supercritical Hopf bifurcation at point I. *Right panel*: profiles of periodic solutions for values of γ_S between 0.24 and 0.28 (points O and I in *right panel*). The periodic solutions have been rescaled on a time t' so that each solution has a period $T = 1$. For a given value of γ_S, the vertical axis is the HSC count as a function of t' over one period.

seen in hematological disorders such as periodic chronic myelogenous leukemia or cyclical neutropenia.

4.6.2. Analysis of the full model

In this section, we focus on the behavior of the solution of the full model as the parameter A is varied. It is shown that a supercritical Hopf bifurcation destabilizes the positive fixed point and that for an interval of A, there is bistability. When A approaches 0, the steady state value M_* approaches 0 while S_* stays positive, and a limit cycle coexists with the steady state.

4.6.2.1. *Existence and uniqueness of the positive steady state*

The full model described by eqns (4.5.1, 4.5.2) cannot be easily analyzed. However, by restricting the parameter space, we can give a condition for a single positive steady state to exist. In particular, we take

$$f_0 < \left(1-\frac{1}{s}\right) rk_0 = \left(1-\frac{1}{s}\right)(2\exp(-\gamma_S\tau)-1)k_0, \tag{4.6.16}$$

and show that there exists a single positive steady state for eqns (4.5.1, 4.5.2), denoted (M_*, S_*) through the rest of the paper. In this section, we present a proof for the existence and uniqueness of the positive steady state under condition (4.6.16). First write the equation for the steady state of M. From eqn (4.5.1) we have M_* defined by

$$\alpha M_* = AS_*F(M_*) \tag{4.6.17}$$

From eqn (4.6.17) and the steady state equation for S_*, (4.6.2), we can eliminate S_*, and obtain

$$M_* = \frac{A\theta_2}{\alpha}\sqrt[s]{\left(\frac{rk_0}{F(M_*)}-1\right)}\,F(M_*). \tag{4.6.18}$$

Let the right hand side of eqn (4.6.18) be denoted $G(M_*)$. Then the derivative of G with respect to M_* is,

$$G'(M_*) = \frac{A\theta_2}{s\alpha}\sqrt[s]{\frac{rk_0}{F(M_*)}-1}\,F'(M_*)\left[s-\frac{1}{1-F(M_*)(rk_0)^{-1}}\right]. \tag{4.6.19}$$

If we can prove that $G'(M_*)$ is always negative, then by using the fixed point theorem it is easy to show that there exists a unique positive steady state M_*, and from that value the uniqueness of the steady state S_* follows naturally. To show that $G'(M_*)$ is negative, we must verify that the factor in the brackets in eqn (4.6.19) is positive since the others factors are negative (from the definition of $F(M)$ in eqn (4.5.3), it is obvious that $F'(M) < 0$). So we need to find conditions for which

$$s-\frac{1}{1-F(M_*)(rk_0)^{-1}} > 0, \tag{4.6.20}$$

which is equivalent to showing that

$$F(M_*) < \left(1-\frac{1}{s}\right) rk_0. \tag{4.6.21}$$

We know that $F(M_*) < f_0$, so a sufficient condition for $G'(M_*)$ to be negative is

$$f_0 < \left(1 - \frac{1}{s}\right) rk_0 = \left(1 - \frac{1}{s}\right)(2\exp(-\gamma_S \tau) - 1)k_0, \tag{4.6.22}$$

which completes the proof of the existence and uniqueness of the steady state (M_*, S_*) under condition (4.6.16).

4.6.2.2. *Characteristic equation of the model*

The linearization of eqns (4.5.1, 4.5.2) around the unique positive steady state (M_*, S_*) is performed along the same lines as above. First define new variables $x = M - M_*$ and $y = S - S_*$ so that $x = 0$ and $y = 0$ are te coordinate of the fixed point. Then by linearizing around the steady state (M_*, S_*), we obtain,

$$\frac{dx}{dt} = A_1 x + A_2 x_{\tau_M} + A_3 y_{\tau_M}, \tag{4.6.23}$$

and

$$\frac{dy}{dt} = B_1 x + B_2 y + B_3 y_{\tau_S}, \tag{4.6.24}$$

where the linearization coefficients are,

$$\begin{array}{lllll} A_1 & = & -\alpha & = & (-\alpha M)_M \\ A_2 & = & AF'_* S_* & = & (ASF(M))_M \\ A_3 & = & AF_* & = & (ASF(M))_S \\ B_1 & = & -F'_* S_* & = & (-F(M)S)_M \\ B_2 & = & -[F_* + K'_* S_* + K_*] & = & (-[F(M) + K(S)]S)_S \\ B_3 & = & 2\exp(-\gamma_S \tau_S)(K'_* S_* + K_*) & = & 2\exp(-\gamma_S \tau_S)(K(S)S)_S. \end{array} \tag{4.6.25}$$

The subscripts in the right-hand side equalities denote the partial derivative with respect to the variable. The star subscript $(_*)$ in the middle equality means that the function is evaluated at the steady state, and the prime stands for the derivative with respect to the argument. These equations can be formulated in vector form,

$$\frac{dX}{dt} = LX + R_M X_{\tau_M} + R_S X_{\tau_S}, \tag{4.6.26}$$

where,

$$X = \begin{pmatrix} x \\ y \end{pmatrix}, L = \begin{pmatrix} A_1 & 0 \\ B_1 & B_2 \end{pmatrix},$$

$$L = \begin{pmatrix} A_1 & 0 \\ B_1 & B_2 \end{pmatrix}, R_M = \begin{pmatrix} A_2 & A_3 \\ 0 & 0 \end{pmatrix}, R_S = \begin{pmatrix} 0 & 0 \\ 0 & B_3 \end{pmatrix}.$$

The characteristic equation of eqn (4.6.26) is defined as,

$$\det[\lambda I - L - R_M \exp(-\lambda\tau_M) - R_S \exp(\lambda\tau_S)] = 0, \tag{4.6.27}$$

with I the 2x2 identity matrix. The characteristic equation can then be explicitly written,

$$\begin{aligned} &\lambda^2 - (A_1 + B_2)\lambda - A_2\lambda e^{-\lambda\tau_M} - B_3\lambda e^{-\lambda\tau_S} \\ &+B_2A_1 + (A_2B_2 + B_1A_3)e^{-\lambda\tau_M} + A_1B_3e^{-\lambda\tau_S} \\ &+A_2B_3e^{-\lambda(\tau_M+\tau_S)} = 0. \end{aligned} \tag{4.6.28}$$

The locations of the roots of eqn (4.6.28) will give information about the local stability of the steady state (M_*, S_*). In Section 4.6.2.3, numerical methods are used to study the location of the roots of eqn (4.6.28).

4.6.2.3. *Bifurcation analysis of the full model*

The condition defined by eqn (4.6.16) restricts the values taken by γ_S. Indeed, from eqn (4.6.16), we find

$$\gamma_S < \frac{1}{\tau_S} \ln\left[\frac{2(1-s)k_0}{sf_0 + (s-1)k_0/2}\right]. \tag{4.6.29}$$

This inequality is a little bit more restrictive than the right hand side of eqn (4.6.3). Moreover, numerical simulations when γ_S approaches this value show that the behavior of the solution is highly irregular. For that reason, we concentrate our analysis on the behavior of solutions as the amplification parameter A is varied and keep γ_S well below the critical value defined by eqn (4.6.29).

The fixed point equations are defined by setting the left hand sides of eqns (4.5.1, 4.5.2) equal to zero. Solving for the nonzero steady states leads to

$$M_* = \frac{A}{\alpha} S_* F(M_*) \tag{4.6.30}$$

and

$$S_*^s = \theta_2^s \left[\frac{k_0 r}{F(M)} - 1\right]. \tag{4.6.31}$$

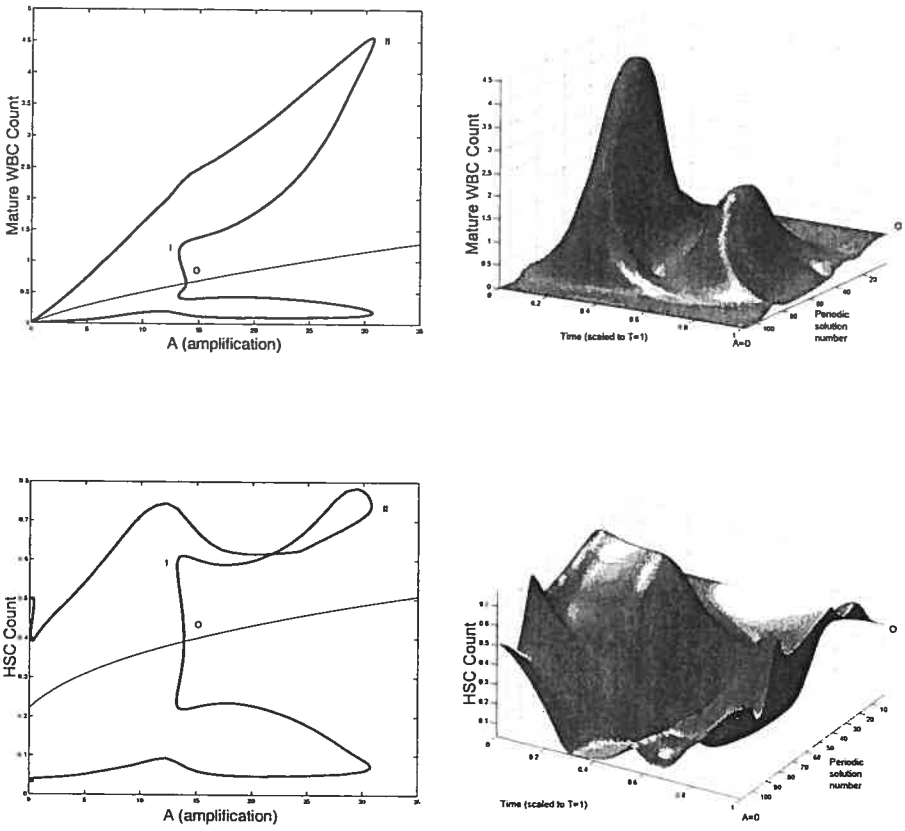

FIGURE 4.3. Bifurcation diagram of the full model (eqns (4.5.1, 4.5.2)) as a function of A. On *left panels* the bifurcation diagrams of mature WBC M_* (*upper panel*) and HSC S_* (*lower panel*) are shown. In each panel the *thin line* is the corresponding steady state and the *thick lines* are the envelope of periodic solutions. Between points O and I is a small amplitude stable periodic solution. Between points I and II there is an unstable period solution and from point II to $A = 0$ there is a large amplitude stable periodic solution. *Right panels*: surface representation of periodic solutions when the amplification A is varied. The periodic solutions in M are represented in *upper right panel* and the periodic solutions in S are represented in *lower right panel*. Periodic solution number 0 corresponds to points O in left panels, and numbers 108 to $A = 0$. To plot this surface, the bifurcation curves in left panels have been "unfolded" so there is only one periodic solution represented at a time. See the caption of Fig. 4.2 for more details.

Equation (4.6.30) can expressed as a $2s$-th order polynomial by replacing S_* by its steady state value. Generally,

$$(M_*^2+\theta_1 M_*)^s = \left(\frac{A}{\alpha} f_0\theta_1\theta_2\right)^s \left(\frac{k_0 r}{f_0\theta_1}(\theta_1+M_*)-1\right). \tag{4.6.32}$$

In the particular case where $s=2$, the steady state equation becomes a fourth order polynomial,

$$\begin{aligned}\alpha^2 M_*^4 + 2\alpha^2\theta_1 M_*^3 + \alpha^2\theta_1^2 M_*^2 - A^2 f_0\theta_1\theta_2^2 r k_0 M_* \\ -A^2 f_0^2\theta_1^2\theta_2^2\left(\tfrac{rk_0}{f_0}-1\right)=0.\end{aligned} \tag{4.6.33}$$

This equation can be solved analytically using symbolic computation software such as `Maple`. At $A=0$, eqn (4.6.33) simplifies and it is easy to show that there exists a double zero root and a double negative root. For $A>0$, as shown above, only one root is positive. With parameter values as in Table 4.1, it is easy to show that the system (4.5.1, 4.5.2) is unstable since the characteristic equation reduces to eqn (4.6.7) and the values of the coefficients are $A_+ = -0.056$ and $B_+ = 1.41$. As $B_+ > |A_+|$, the condition for stability of the nonzero steady state when $A=0$ is then, from condition (4.6.9), $\tau_S < 1.09$. Thus condition is not satisfied since τ_S takes larger values. When $0<A\ll 1$, by continuity, the stability of system (4.5.1, 4.5.2) does not change. At $A=0$, there is an unstable steady state ($M_*\equiv 0, S_*>0$) along with a stable limit cycle in the S variable only and of zero amplitude in M. When A is increased, the unstable steady state becomes positive ($M_*>0, S_*>0$) and the amplitude of the limit cycle becomes nonzero in both M and S. As A is further increased, the analysis becomes much more difficult and the bifurcation study can not be carried out with symbolic tools only.

At this point, one must use numerical methods in order to understand the complexity of the system. To perform the numerical analysis, we used a `Matlab` package, `DDE-BIFTOOLS` (Engelborghs et al., 2001), which is based on continuation methods that are in widespread use for ordinary differential equations through the software `AUTO` (Doedel, 1981). This package is well suited for analysis of delay differential equations.

In Fig. 4.3 we show bifurcation diagrams of M and S as well as their periodic solution profiles. If we follow the evolution of the steady state (M_*, S_*) as the parameter A is decreased, a supercritical Hopf bifurcation occurs (points O in Fig. 4.3, left panels). At this point a small amplitude stable limit cycle appears, and disappears in a

saddle-node bifurcation (points I) together with an unstable limit cycle. This unstable limit cycle had appeared previously in another saddle-node bifurcation (points II), with a large amplitude stable limit cycle. The large amplitude limit cycle exists from point II to $A = 0$. In the right panels of Fig. 4.3, the limit cycle profiles are shown. The time axis in right panels of Fig. 4.3 are rescaled so that the period $T = 1$. It should be noted that when the amplification A ranges in typical CN values (10 to 30), the period of oscillation is between 13 and 17 days, which is in the average for CN in grey collies.

4.7. Discussion

We have analyzed a simple model of white blood cell production. Oscillations in blood cell count have been observed in many hematological diseases such as cyclical neutropenia (CN) or periodic myelogenous leukemia (PCML) (Fortin et Mackey, 1999). In both diseases, an alteration in the apoptotic rate of white blood cell precursors has been observed. The goal of the present paper was to establish, using a simple model, if these changes in apoptosis rates could explain the onset of oscillations. It has been shown in Section 4.6 that the elevation of the apoptosis rate is a sufficient condition for the onset of oscillations in the WBC count. This elevation has been observed in neutrophil precursors in CN patients. We make the hypothesis that this elevation in neutrophil precursors apoptosis rate is the cause of oscillation seen in CN.

The case of PCML is less clear. This form of leukemia is characterized by oscillations from normal to high levels of WBC with periods ranging from 35 to 80 days. A relationship exists between CN and certain forms of leukemia, since some CN patients eventually develop these leukemias. (Lensink et al., 1986; Weinblatt et al., 1995; Freedman et al., 2000; Jeha et al., 2000; Dinauer et al., 2000). However, experimental data show that leukemic cells have a decreased rate of apoptosis. The model presented here does not display any oscillatory behavior when apoptosis rate is decreased below normal. Further investigations will have to be carried out to establish a link between dynamics seen in CN and PCML.

ACKNOWLEDGEMENTS

MCM is supported by the Natural Sciences and Engineering Research Council (NSERC Grant No. OGP-0036920, Canada), MITACS (Canada), and Le Fonds pour la Formation de Chercheurs et l'Aide à la Recherche (FCAR Grant No. 98ER1057, Québec), and the Leverhulme Trust (U.K.). JB is supported by the Natural Sciences and Engineering Research Council (NSERC Grant No. OGP-0008806, Canada), MITACS (Canada), and Le Fonds pour la Formation de Chercheurs et l'Aide à la Recherche (FCAR Grant No. 98ER1057, Québec). SB is supported by MITACS (Canada) and the Institut des sciences mathématiques (ISM, Québec).

Chapter 5

ANALYSIS OF CELL KINETICS USING A CELL DIVISION MARKER: MATHEMATICAL MODELING OF EXPERIMENTAL DATA

AUTEURS : SAMUEL BERNARD, LAURENT PUJO-MENJOUET ET MICHAEL C. MACKEY

5.1. CONTRIBUTION DE L'AUTEUR À L'ARTICLE

Le manuscrit de cet article a été rédigé avec Laurent Pujo-Menjouet. Le modèle hybride de prolifération et maturation cellulaire présenté dans l'article a été développé aussi avec L. P.-M. Je suis responsable des solutions analytiques du modèle avec conditions initiales générales, ainsi que des procédures pour `Matlab`, les simulations numériques, l'évaluation des paramètres et les figures.

5.2. ANALYSE DE LA CINÉTIQUE CELLULAIRE AU MOYEN D'UN MARQUEUR DE DIVISION CELLULAIRE : MODÉLISATION MATHÉMATIQUE DE DONNÉES EXPÉRIMENTALES

Ce dernier article contraste avec les précédents dans la mesure où nous ne considérons pas un modèle comportant des retards. Nous revenons plutôt aux sources et introduisons un système d'équations aux dérivées partielles décrivant et traquant des cellules en prolifération. Ce modèle, en plus d'avoir des applications concrètes décrites

ci-dessous, peut servir de support à une modélisation plus élaborée du système hématopoïétique en incorporant une distribution des temps de maturation/division des cellules précurseurs.

Nous présentons un modèle de prolifération cellulaire capable de traquer les divisions cellulaires. Le modèle, constitué d'un système d'EDP linéaires structurées en âge et en maturation, est hybride, c.-à-d. que les variables de temps et d'âge sont continues et la variable de maturité est discrète. Nous appliquons ce modèle à des données d'expériences de traquage cellulaire, ce qui permet d'estimer les paramètres cinétiques de cellules proliférantes. Le modèle s'écrit comme suit,

$$\frac{\partial p_k(t,a)}{\partial t} + \frac{\partial p_k(t,a)}{\partial a} = -\gamma p_k(t,a), \tag{5.2.1}$$

$$\frac{\partial n_k(t,a)}{\partial t} + \frac{\partial n_k(t,a)}{\partial a} = -(\mu+\beta) n_k(t,a). \tag{5.2.2}$$

Les variables dépendantes sont les densités de cellules en prolifération p_k et au repos n_k s'étant divisées k fois. Les paramètres sont β le taux de réintroduction en prolifération, γ le taux d'apoptose des cellules proliférantes, μ le taux de mortalité/différenciation des cellules au repos et τ la durée de la phase proliférative. Les conditions aux frontières sont

$$\begin{cases} p_k(t,0) &= \beta \int_0^{+\infty} n_k(t,a)da = \beta N_k(t), \\ \\ n_k(t,0) &= 2p_{k-1}(t,\tau). \end{cases} \tag{5.2.3}$$

Avec des conditions initiales bien choisies, le système a une solution explicite, et la solution peut être exprimée de la façon suivante,

$$p_k(t,a) = \frac{(t-a-k\tau)^{k-1}}{(k-1)!} 2^k e^{-k\gamma\tau} \beta^k e^{-\gamma a} e^{-(\mu+\beta)(t-a-k\tau)}, \tag{5.2.4}$$

pour $k \geq 1$ et $t-a \geq k\tau$,

$$n_k(t,a) = \frac{(t-a-k\tau)^{k-2}}{(k-2)!} 2^k e^{-k\gamma\tau} \beta^{k-1} e^{-(\mu+\beta)(t-k\tau)}, \tag{5.2.5}$$

pour $k \geq 2$ et $t-a \geq k\tau$. Pour $k = 0$ et 1, nous avons

$$p_0(t,a) = \delta(a-t)e^{-\gamma a}, \text{ pour } a \leq t \leq \tau, \tag{5.2.6}$$

et

$$n_1(t,a) = 2\delta(a-t+\tau)e^{-\gamma\tau} e^{-(\mu+\beta)a}, \text{ pour } 0 \leq a \leq t-\tau. \tag{5.2.7}$$

Les données expérimentales provenant de cellules primitives murines permettent d'estimer les paramètres à $\beta = 2.2\ d^{-1}$, $\tau = 0.3$ d, $\gamma = 0.3\ d^{-1}$ et $\mu = 0.05\ d^{-1}$. Ces données sont d'une importance notable lorsqu'on considère la capacité des cellules souches à repeupler une moelle osseuse appauvrie.

5.3. ABSTRACT

We consider an age-maturity structured model arising from a blood cell proliferation problem. This model is "hybrid", i.e., continuous in time and age but the maturity variable is discrete. This is due to the fact that we include the cell division marker CarboxyFluorescein diacetate Succinimidyl Ester (CFSE). We use our mathematical analysis in conjunction with experimental data taken from the division analysis of primitive murine bone marrow cells to characterize the maturation/proliferation process. Cell cycle parameters such as proliferative rate β, cell cycle duration τ, apoptosis rate γ and loss rate μ can be evaluated from CFSE+ cell tracking experiments. Our results indicate that after three days in vitro, primitive murine bone marrow cells have parameters $\beta = 2.2\ day^{-1}$, $\tau = 0.3$ day, $\gamma = 0.3\ day^{-1}$ and $\mu = 0.05\ day^{-1}$.

5.4. INTRODUCTION

The problem of trying to determine the connection between cellular proliferation and maturation in vitro and in vivo has intrigued cell biologists for decades. An obvious method of dealing with this is to use a biological marker that is incorporated into the cell and partitioned between daughter cells on division. Thus, one of the most common post World War II techniques for studying cell division in vitro and in vivo was to use tritiated thymidine (^{3}H-Tdr) which is incorporated in the DNA of dividing cells. Mathematical analyses of data from (^{3}H-Tdr) labeling have been carried out by (Takahashi, 1966) and (Lebowitz et Rubinow, 1969). Unfortunately, this approach can not easily give an indication of the total amount of the division history of individual cells. Furthermore it is known that ^{3}H-Tdr can induce apoptosis (Yanokur et al., 2000), and thus the use of this marker may significantly perturb the experimental preparation.

Similarly, the diMethylthiaxol (MTT) reduction assay is able to quantify proliferation at a gross level, but has the complication of being sensitive to the activation state of

cells (Mosmann, 1983). Bromodeoxyuridine (BrdU or BrdUrd) has been extensively used to quantify in vitro and in vivo cell division, (Bertuzzi et al., 2002; Forster et al., 1989; Gratzner, 1982; Houck et Loken, 1985; Bonhoeffer et al., 2000). However, this method is generally unable to distinguish the progeny of cells which have undergone several divisions from those which have undergone a single division.

Recently a new marker, the CarboxyFluorescein diacetate Succinimidyl Ester (CSFE), has made its appearance as an intracellular fluorescent label for lymphocytes. CFSE labels both resting and proliferating cells and divides equally between daughter cells upon cytokinesis in vitro as well as in vivo (Hodgkin et al., 1996; Lyons et Parish, 1994). CFSE shows remarkable fidelity in the distribution of label between daughter cells during division (Fazekas de St Groth et al., 1999; Fulcher et Wong, 1999; Hasbold et al., 1998, 1999; Hasbold et Hodgkin, 2000; Lyons et Parish, 1994; Lyons, 1999; Mintern et al., 1999; Nordon et al., 1999; Parish, 1999; Sheehy et al., 2001; Warren, 1999). Moreover, changes in cell surface phenotype associated with differentiation are unaffected by CFSE labeling indicating that the relationship between cell division cycle number and differentiation can be determined. The main problem with using CFSE to track cellular division is that its fluorescence can only be detected up to and through seven or eight divisions due to label dilution (Oostendorp et al., 2000). Despite this defect, CFSE is of great interest as a tool for tracking cell proliferation and differentiation.

In this paper we develop techniques to analyze CFSE+ cell tracking data to obtain information about cell kinetics. We do this within the context of an extension of the G_0 model of the cell cycle originally developed by (Burns et Tannock, 1970), which is equivalent to the model of (Smith et Martin, 1973). The cells in the population we consider are capable of both simultaneous proliferation and maturation (Mackey et Dörmer, 1982) where the cell maturity is related to the level of CFSE fluorescence. As illustrated in Fig. 5.1, these cells can be located in two different functional states. The cells can either be actively proliferating or in a resting G_0 phase. Consequently, our model is structured with respect to both cellular age and maturity. The main difference between this and previous time-age-maturity models (Pujo-Menjouet et Rudnicki, 2000; Dyson et al., 1996a; Mackey et Dörmer, 1982; Mackey et Rudnicki, 1994, 1999;

Pujo-Menjouet et Rudnicki, 2000) and Dyson at al. (submitted) is that our model is hybrid in the sense that the age variable is continuous but the maturity variable represented by the number of cell divisions tracked through the CFSE fluorescence level is discrete.

This paper is organized as follows. In Section 5.5 we formulate our model and present the results of the model analysis carried out in Appendix A. Section 5.6 gives numerical illustrations of the fit of the model predictions to a set of previously published data taken from in vitro primitive murine bone marrow cells culture. The discussion and conclusions are in Section 5.7.

5.5. Description of the model

We consider a population of cells that can both divide and mature and we follow a cell cohort during successive divisions. Our model is then naturally described by an age-maturity structured model not too dissimilar from those considered by others (Crabb et al., 1996a,b; Dyson et al., 1998, 2000a,b; Henry, 1976; Keyfitz, 1968; Mackey et Dörmer, 1982; Pujo-Menjouet, 2001). The novel part of the model presented here is related to the fact that the cellular population is continuously structured with respect to age, but the maturity variable (represented by the CFSE fluorescence) is discrete. A word of caution is in order here concerning the relation between division number and maturity. We suppose that at each division, cells reach a certain level of maturity where the maturity represents the concentration of what composes a cell such as proteins or other elements one can measure experimentally like the phenotypic under morphotypic or biochemical processes. A given cell population labeled at time $t = 0$ may initially contains cells with different maturity levels, thus the number of divisions that a cell underwent can not be related to any particular maturity traits. Nevertheless, the term maturity is used to denote the number of divisions in order to keep the mathematical modeling carried out here within a general age-maturity structured model framework.

The proliferating phase cells are those in the cycle that are committed to DNA replication and cytokinesis (cell division) with the production of two daughter cells. The position of a cell in the proliferating phase is given by an age a which is assumed

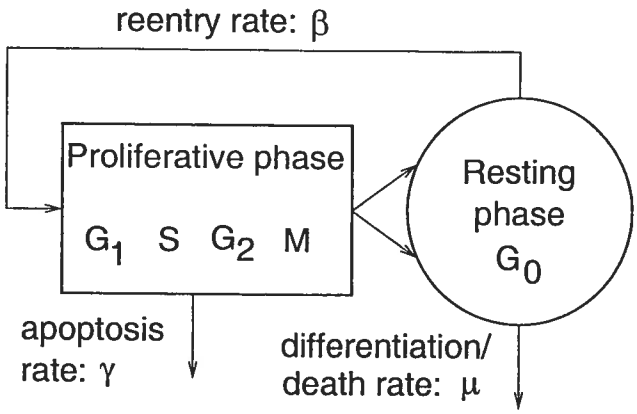

FIGURE 5.1. A schematic representation of the G_0 stem cell model. Proliferating phase cells include those cells in G_1 (the first gap), S (DNA synthesis), G_2 (the second gap), and M (mitosis) while the resting phase cells are in the G_0 phase. μ is the loss rate of resting phase (G_0) cells due to death or differentiation, while γ represents a loss of proliferating phase cells due to apoptosis. β is the rate of cell reentry from G_0 into the proliferative phase, and τ is the duration of the proliferative phase see (Burns et Tannock, 1970; Mackey, 1978b, 1979a,b, 1997) for further details.

to range from $a = 0$ (the point of commitment through entry into the G_1 phase) to $a = \tau$ (the point of cytokinesis). The cells in this phase may also be lost randomly due to apoptosis at a constant rate $\gamma \geq 0$. Immediately after cytokinesis, both daughter cells are assumed to enter the resting G_0 phase. The age in this population ranges from $a = 0$, when cells enter, to $a = +\infty$. We consider two sources of loss in this G_0 phase:

(1) The first loss is random at a rate $\mu \geq 0$,

(2) The second one is the reintroduction of the cell into the proliferating phase with a rate $\beta \geq 0$.

Let $p_k(t,a)$ be the density of the proliferating phase cell population and $n_k(t,a)$ be the density of the resting (G_0) phase cells, where t is time, a is cellular age, and k represents the k^{th} generation of a cell (after k divisions). Note that k is directly related to the average CFSE fluorescence per cell. Indeed, if we denote M the initial average CFSE fluorescence per cell, $M/2$ is the average fluorescence of the daughter cells after the first division and $M/2^k$ the fluorescence after k^{th} divisions. The equations

describing the model are then,

$$\frac{\partial p_k(t,a)}{\partial t} + \frac{\partial p_k(t,a)}{\partial a} = -\gamma p_k(t,a), \tag{5.5.1}$$

$$\frac{\partial n_k(t,a)}{\partial t} + \frac{\partial n_k(t,a)}{\partial a} = -(\mu+\beta) n_k(t,a). \tag{5.5.2}$$

Each of these equations is a conservation equation stating that the total rate of change of either the proliferative or resting phase cells at a given maturation level k is equal to the rate of cellular loss from the respective compartment.

To reflect the biology of cellular division we take the boundary conditions to be

$$\begin{cases} p_k(t,0) &= \beta \int_0^{+\infty} n_k(t,a)da = \beta N_k(t), \\ \\ n_k(t,0) &= 2p_{k-1}(t,\tau). \end{cases} \tag{5.5.3}$$

The first of these boundary conditions simply says that the flux of cells into the proliferative phase at age $a = 0$ in the k^{th} generation is equal to the flux out of the resting phase due to the reentry rate β in the same generation. The second condition says that the flux of cells into the resting phase of the cell cycle at the k^{th} generation is twice the flux of cells of the previous ($(k-1)^{th}$, the mother cell) generation out of the proliferative phase and into cytokinesis (at age $a = \tau$).

Finally, we will consider as initial conditions a mixture of cells in the resting and proliferating phases. These initial conditions represent the distribution of age a of the cells at time $t = 0$, the moment where the CFSE+ cells are isolated after having been CFSE-labeled, see Figure 1 in (Oostendorp et al., 2000) . We need to give the initial distribution of cells in the proliferative and the resting phase i.e., $p_0(0,a)$ and $n_0(0,a)$. From the formulation of the problem, the solution of the model defined by Eqs. 5.5.1 and 5.5.2 does not depend explicitly on $n_0(0,a)$ because only the total quantity of resting cells is required in the boundary conditions (Eq. 5.5.3). Note that the total resting cell number $N_k(t)$ can be described by an ordinary differential equation, and the age structure is not strictly necessary as long as β and μ are age independent. We can therefore take any arbitrary initial distribution for the resting G_0 phase.

On the other hand, the solution of Eqs. 5.5.1 and 5.5.2 does depend on the initial distribution of the proliferating cells, because older cells are obviously more advanced

in the cell cycle and will reenter the resting phase sooner than the younger ones. However, to be able to compute the model solutions explicitly, we have decided, with some loss of generality, to take the initial distribution in both compartments as shown below. This simplification will be of course more visible within the first few generations. In Appendix 5.8.3, a generalization for any arbitrary initial condition is shown, but then the solution is not as tractable.

For clarity, we will divide the initial conditions into two parts: initial condition I (IC^I) and initial condition II (IC^{II}). IC^I is the initial condition when all the cells at time 0 are in proliferative phase and IC^{II} is the initial condition when all cells are in resting phase. As solutions with either IC are particular solutions of Eqs. 5.5.1 and 5.5.2, we can take any linear combination of these solutions to get a solution of the full model for any arbitrary initial condition.

The initial condition IC^I is

$$IC^I \begin{cases} p_0(0,a) = C_0\delta(a), & \text{for } 0 \le a \le \tau, \\ n_0(0,a) = 0, & \text{for all } a \ge 0, \end{cases} \tag{5.5.4}$$

The initial condition IC^{II} is:

$$IC^{II} \begin{cases} p_0(0,a) = 0, & \text{for } 0 \le a \le \tau, \\ n_0(0,a) = C_0\delta(a), & \text{for all } a \ge 0, \end{cases} \tag{5.5.5}$$

In the initial conditions (Eqs. 5.5.4 and 5.5.5), C_0 represents the initial number of cells. The function $\delta(a)$ is the standard Dirac delta function which represents the fact that all cells have initially an age $a = 0$ and is defined by the following properties

$$\begin{aligned} \delta(a) &= 0, \quad \text{for } a \neq 0, \\ \int_{-\infty}^{\infty} \delta(a)\, da &= 1. \end{aligned} \tag{5.5.6}$$

It should be noted that the unit of p_k and n_k is cells/day. The model developed here is focused on fitting experimental data, and as the CFSE fluorescence profile figures usually do not give much information about absolute number of cells, the real value of C_0 is irrelevant for the study. Therefore, we will use $C_0 = 1$ as the initial CFSE+

cell number. This will give a relative cell count with respect to the initial number of CFSE+ cells in simulations.

As we have derived in Appendix 5.8, the solution for the maturation-age problem defined by Eqs. 5.5.1 and 5.5.2 at the k^{th} division of a cell cohort with IC^I (Eq. 5.5.4) is

$$p_k(t,a) = \frac{(t-a-k\tau)^{k-1}}{(k-1)!} 2^k e^{-k\gamma\tau} \beta^k e^{-\gamma a} e^{-(\mu+\beta)(t-a-k\tau)}, \tag{5.5.7}$$

for $k \geq 1$ and $t-a \geq k\tau$,

$$n_k(t,a) = \frac{(t-a-k\tau)^{k-2}}{(k-2)!} 2^k e^{-k\gamma\tau} \beta^{k-1} e^{-(\mu+\beta)(t-k\tau)}, \tag{5.5.8}$$

for $k \geq 2$ and $t-a \geq k\tau$. For $k = 0$ and 1, we have

$$p_0(t,a) = \delta(a-t)e^{-\gamma a}, \text{ for } a \leq t \leq \tau, \tag{5.5.9}$$

and

$$n_1(t,a) = 2\delta(a-t+\tau)e^{-\gamma\tau} e^{-(\mu+\beta)a}, \text{ for } 0 \leq a \leq t-\tau. \tag{5.5.10}$$

Appendix 5.8.1 gives the derivation of this result and Appendix 5.8.2 gives the solution of the model with IC^{II}.

Note that for a given age a, the densities p and n have the functional form of a shifted gamma distribution (up to a multiplicative factor). The gamma distribution has been widely used in the population dynamics literature and is often related to a distribution of maturation times (Haurie et al., 1998; Hearn et al., 1998; Bernard et al., 2001). Therefore, the time required for a single cell to perform a fixed number of divisions follows a gamma distribution. Not only is this distribution easy to handle mathematically, but it also offers a good fit to experimental data. The model presented here gives an analytical explanation, based on physiologically relevant features, for the occurrence of the gamma distribution seen in many cell labeling experiments (Guerry et al., 1973; Deubelbeiss et al., 1975; Price et al., 1996; Basu et al., 2002).

5.6. NUMERICAL ILLUSTRATIONS

A quantitative analysis of lymphocyte proliferation using CFSE has been carried out by (Hasbold et al., 1999). The authors approximate the distribution of cell cycle

durations by Gaussian distributions to fit the experimental data, assuming that the distribution of time until first division is Gaussian. They consider neither the resting G_0 compartment, nor apoptosis. This model is simple and the results are consistent with the data. However, this method does not give any further information such as the proportion of proliferating and resting cells, the loss rate (due to death or differentiation) in each compartment, the reentry rate from the resting phase to the proliferating one, or the time τ required for each cell to divide. Another model by (Zhang et al., 2001) uses discrete time steps to model the proportion of apoptotic, dividing and quiescent cells in a hematopoietic cell population. However, this model does not allow evaluation of kinetic parameters such as the reentry rate into proliferative phase.

Our model is more complicated, but the numerical fit of the model solutions to data allows us to give estimates of these parameters. The objective of this section is to present different aspects of our results. The section is divided into three subsections. In Section 5.6.1, we compare our theoretical results with some existing experimental data on hematopoietic stem cell division in vitro. In Section 5.6.2, we compare the predicted proportion of proliferating and resting cells and their evolution with respect to the total population. Section 5.6.3 is focused on the description of the temporal dynamics of the cell population during a period of time (8h to 72h).

It is important to note that, in the model presented in Section 5.5, we assume that the proliferating cells that are labeled by CFSE are only labeled at age $a = 0$ (IC^I, Eq. 5.5.4), which is not the case in reality. Indeed, CFSE molecules are incorporated by all proliferating cells (Hodgkin et al., 1996; Lyons et Parish, 1994). In Appendix 5.8.3, we present a generalization to take into account an arbitrary initial condition. Thus, for the numerical simulations done here, we will use a combination of IC^I and IC^{II} as initial condition to make the computations as clear as possible so that the role of each parameter can be understood in a better way. The program used to make these numerical simulations is written with the software `Matlab`. It is publicly available and can be downloaded from `http//www.cnd.mcgill.ca/~sberna/cfse/cfse.html`.

5.6.1. Comparison with experimental data

The data we have compared our results to come from the work of (Oostendorp et al., 2000), (Figs. 1 and 2 therein). Data were obtained from primitive murine bone marrow cells. The cells were cultured in vitro with a combination of growth factors: Steel factor (SF), fetal liver tyrosine kinase ligand 3 (FL), and interleukin-11 (IL-11) or hyper-IL-6. Cells were first labeled with CFSE and then incubated overnight before isolating CFSE+ cells. Cells were then cultured for 2 or 3 days more (3 or 4 days in total). Data were obtained by digitizing CFSE profiles from the original figures using the software CurveUnscan (SquarePoint Software, Gentilly, France). The parameters were estimated by fitting the model visually to experimental data.

The results in Fig. 5.2 show a consistent approximation of the experimental data by our solutions with the parameters: $\beta = 2.24$ day^{-1}, $\tau = 0.307$ day, $\gamma = 0.30$ day^{-1} and $\mu = 0.05$ day^{-1}. Cells have been sorted according to their CFSE fluorescence profile after 3 days of culture (2 days after isolating CFSE+ cells). Parameters γ and μ both represent cell loss, and their individual values can not be based solely on CFSE tracking experiments. For this reason, we assumed that the loss rate μ in the resting phase is very small (order of 0.05 day^{-1}) and took γ as the parameter to be fitted. The reentry rate β is similar to the estimations given in (Mackey, 1978b, 1997). It is interesting to observe that after 2 days, some cells have reached the sixth division as shown in the experimental data on Fig. 5.2.

This example of a fit of the data with the model is relatively successful. However, there is a gap between the model predicted result and the experimental data for the cells of generation 0 (at the left hand side of Fig. 5.2). We believe that this difference is primarily due to the fact that in our model, we assumed that the reentry rate β is a constant independent of any factors such as time, generation k or heterogeneity in cell population. In Fig. 5.3, we have plotted two populations of cells predicted by the model with the same parameters $\tau = 0.25$ day, $\gamma = 0.90$ day^{-1}, $\mu = 0.05$ day^{-1} but a different reentry rate β. In the top panel, $\beta = 0.08$ day^{-1} which corresponds to a slowly cycling population and in the bottom panel, $\beta = 2.30$ day^{-1} which corresponds to a rapidly cycling one. It is clear that the data from the first generations are best represented by a slowly cycling population and the later generations with a faster cycling one.

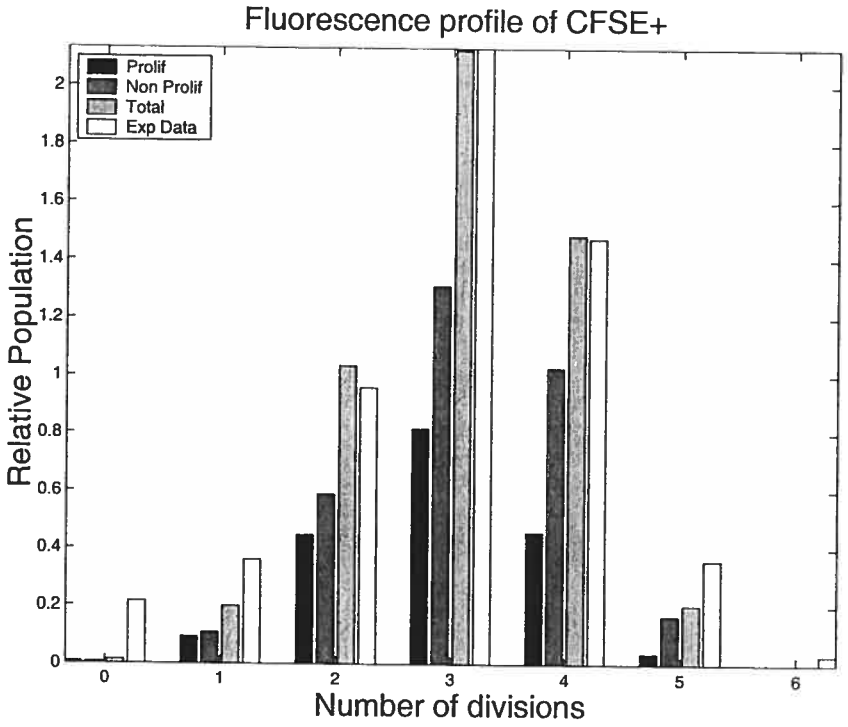

FIGURE 5.2. Comparison of CFSE fluorescence between the experimental data and theoretical results. This figure represents the CFSE profile after 3 days of culture (2 days after isolating CFSE+ cells). The first bar (*black*) represents the model predicted number of proliferating cells, the second one (*dark*) is for the predicted resting phase cells, the third bar (*light*) is the total cell population in the cell compartment and the fourth bar (*white*) is the experimental data. For comparison between the data and the model one should concentrate on the total population. Parameters: $\beta = 2.24$ day^{-1}, $\tau = 0.307$ day, $\gamma = 0.30$ day^{-1} and $\mu = 0.05$ day^{-1}. The initial proportion of cells in resting phase is 0.65. Experimental data taken from (Oostendorp et al., 2000) (Fig. 1, panel 3).

If we sum the two subpopulations of Fig. 5.3 with a proportion of 0.40 for the slow cycling population and 0.60 for the fast cycling, the result presented in Fig. 5.4 is a very good approximation to the experimental data.

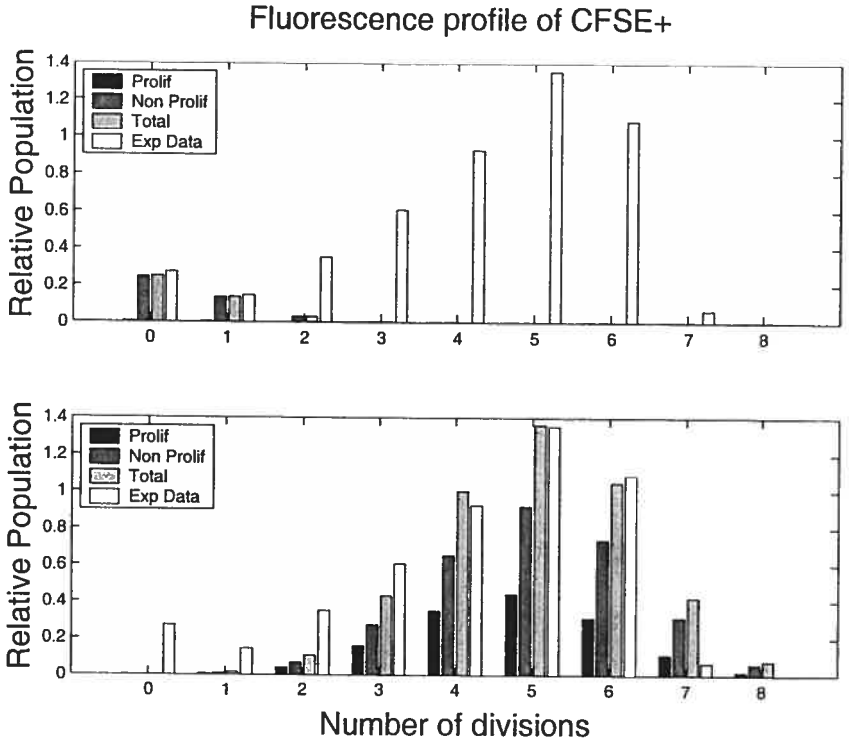

FIGURE 5.3. Representation of two subpopulations with the same parameters: $\tau = 0.25$ day, $\gamma = 0.90$ day^{-1}, $\mu = 0.05$ day^{-1} but a different reentry rate β. *Top panel*: $\beta = 0.08$ day^{-1}, which corresponds to a slowly cycling population of cells. *Bottom panel*: $\beta = 2.30$ day^{-1} which corresponds to a rapidly cycling population. The experimental data come from (Oostendorp et al., 2000) (Fig. 2, bottom panel). Bars as in Fig. 5.2.

5.6.2. Relation between proliferating cells and resting cells

In all the figures representing the simulations, our grey scale coding shows both the proliferating and resting cells for each generation. It is clear from these figures that a change of the proportion of cells in each phase occurs with time. It is interesting not only to compute numerically the proportion of cells in the resting and proliferating phases with respect to cell generation at a fixed time (Fig. 5.5), but also to simulate the evolution of these proportions over time for all generations together (Fig. 5.6).

In Fig. 5.5, we observe an increase in the fraction of cells in the resting cell population and a decrease of the proliferating fraction with respect to division number.

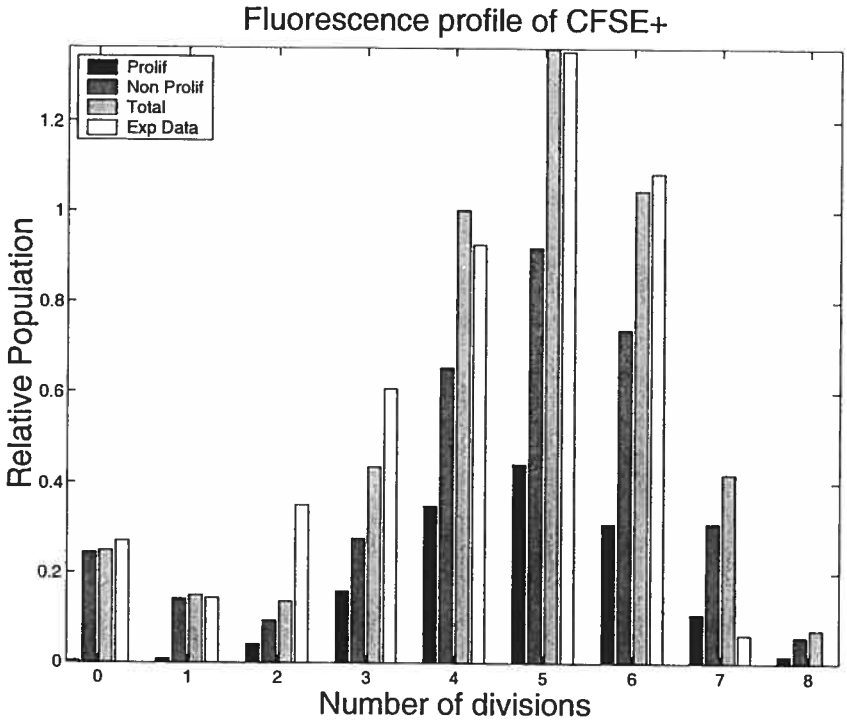

FIGURE 5.4. Approximation of the experimental data after 4 days in culture (3 days after isolating CFSE+ cells) from (Oostendorp et al., 2000) (Fig. 2, bottom panel). Two subpopulations are represented in the present figure: one corresponding to the slowly cycling population ($\beta = 0.08$ day^{-1}) and the other one corresponding to the rapidly cycling population ($\beta = 2.30$ day^{-1}). Parameters: $\beta = 0.08$ and 2.30 day^{-1}, $\tau = 0.25$ day, $\gamma = 0.90$ day^{-1}, $\mu = 0.05$ day^{-1}. The initial proportion of cells in resting phase was 0.90; the slowly cycling population constituting 0.40 of the total and the rapidly cycling one 0.60 of the total initial population. This figure represents the weighted sum of subpanels in Fig. 5.3. Bars as in Fig. 5.2.

The proportion of resting phase cells after several generations becomes larger than the proliferating cells. This would imply that in our model the resting phase plays a role of a cellular "reservoir".

Without the structure of generations, the population model has the property of asynchronous exponential growth, i.e., the cell densities n and p converge to an invariant distribution in time (after multiplication by an exponential factor in time) (Webb, 1985;

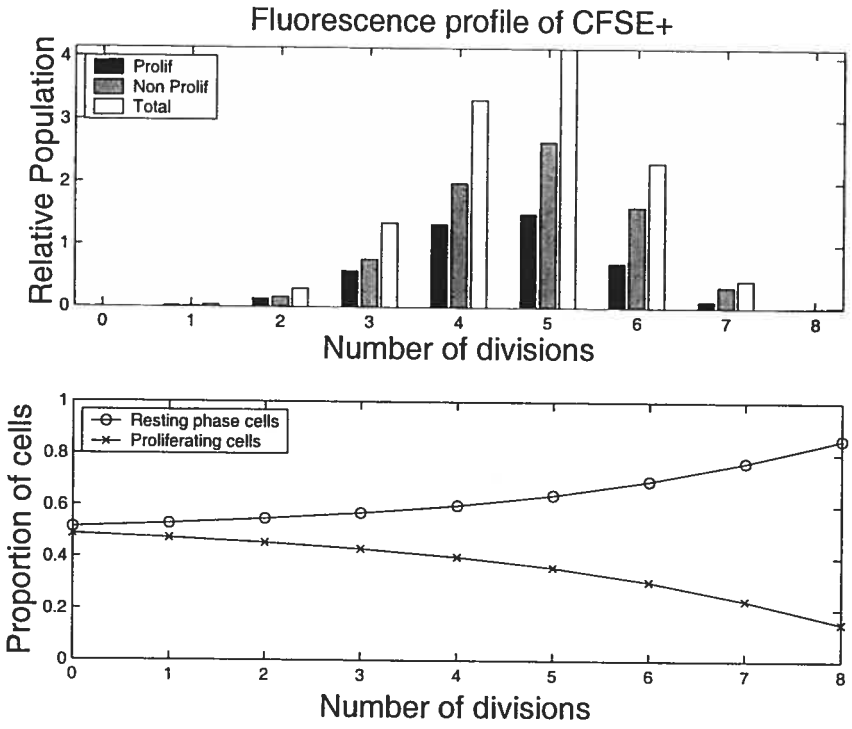

FIGURE 5.5. Model predicted numbers of proliferating and resting phase cells with respect to division number at $t = 3$ days based on the same parameter as in Fig. 5.2: $\beta = 2.24\ \mathrm{d}^{-1}$, $\tau = 0.307$ d, $\gamma = 0.30\ \mathrm{d}^{-1}$, $\mu = 0.05\ \mathrm{d}^{-1}$ and an initial proportion of resting cells of 0.65. The CFSE fluorescence profile is shown in the top panel. In the lower panel, the proportion of cells in the two different compartments for each generation is given.

Arino et al., 1997; Sánchez et Webb, 2001). This property is reflected in Fig. 5.6, where it is shown that the proportion of proliferating and resting phase cells with respect to the total population clearly stabilizes over time. This behavior is expected because, in our simulations, the damped oscillations can be compared to the exchange of two fluids separated into two different boxes. Cells start proliferating very quickly, but then the resting compartment acts as a "reservoir" compartment where a majority of cells will remain after a certain time. However, when the model with the structure of generation is considered, the number of generations with nonzero populations is increasing over time, thus there is no asynchronous exponential growth with respect to the generation structure as we can see in Fig. 5.7.

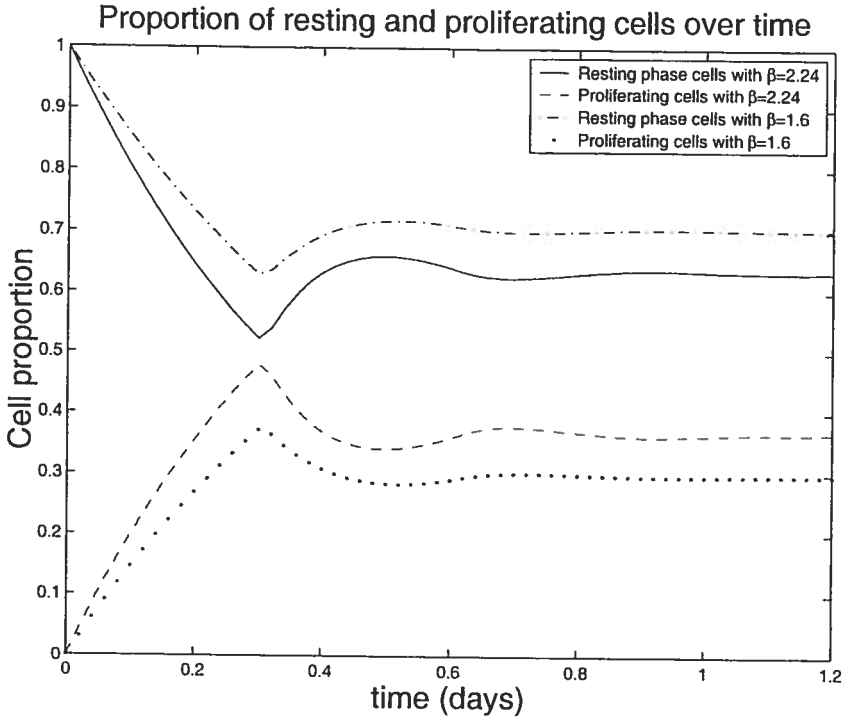

FIGURE 5.6. Model predicted total number of proliferating and resting phase cells as a function of time for the same parameters as in Fig. 5.2, $\beta = 2.24$ day^{-1}, $\tau = 0.307$ day, $\gamma = 0.30$ day^{-1}, $\mu = 0.05$ day^{-1} and an initial proportion of resting cells of 1. The evolution curves are compared to other ones with a smaller reentry rate $\beta = 1.6$ day^{-1}. As expected the proportion of resting phase cells gets larger as β decreases. The transient is due to the fact that proliferating cells take a time τ to divide and reenter in the resting phase. After time $t = \tau$ the curves stabilize rapidly.

5.6.3. Asynchronous evolution of divided and undivided cells

Because our model is able to describe the evolution of a cohort of cells over time, we simulated this situation in Fig. 5.7 for time between 8h and 72h. The result shows the standard CFSE profile usually observed in vitro as well as in vivo (Lyons et Parish, 1994). This profile is sometimes refered to as the "asynchronous division shape" (Hasbold et al., 1999; Hodgkin et al., 1996): after several days, some cells remain undivided whereas some have divided several times. The term "asynchronous" here has a different meaning from the one of "asynchronous exponential growth" in Section 5.6.2. This

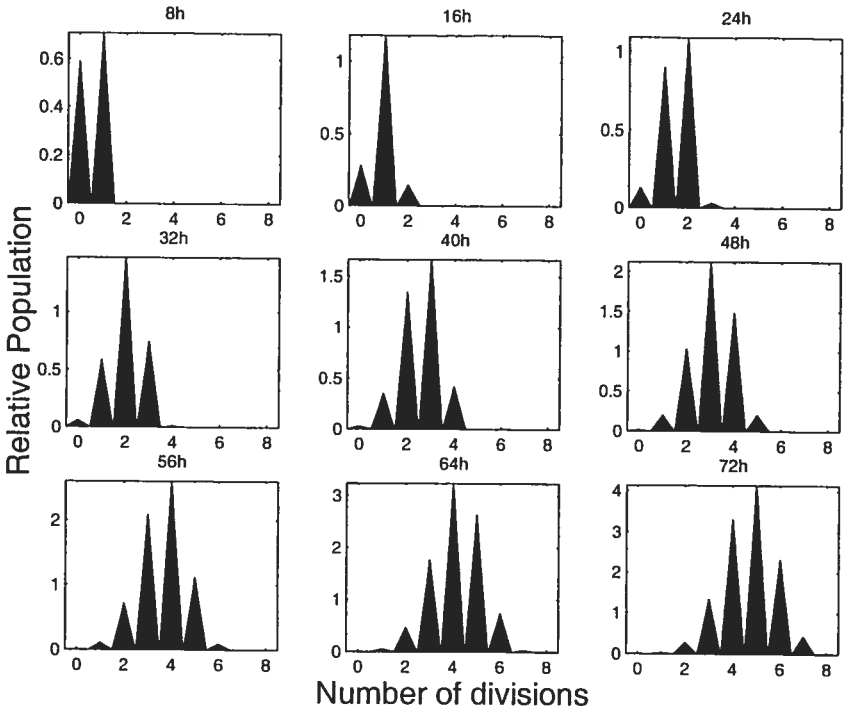

FIGURE 5.7. Predicted CFSE fluorescence of labeled cells between 8h and 72h based on our analysis with $\beta = 2.24\ d^{-1}$, $\tau = 0.307$ d, $\gamma = 0.30\ d^{-1}$, $\mu = 0.05\ d^{-1}$ and initial proportion of resting cells of 0.65. The peaks in each panel represents the total relative number of cells of each generation for different times. After 2 days (48h) the CFSE profile correspond to the one of Fig. 5.2.

asynchrony is due to the fact that within a same generation, some cells remain in the resting phase G_0 and some keep on proliferating. The progressive cell divisions can be tracked during several days (72h in our simulation) giving rise to this typical asynchronous CFSE profile. As time goes on, the division profile takes a slightly asymmetric, left skewed shape.

5.7. CONCLUSION

The model we have developed here to describe the tracking of cell division using CFSE has two main advantages. First, our approach is simple and the computations to obtain the solutions are more technical than highly theoretical. This allows us to understand the role of each parameter in shaping the results, and gives a biological

interpretation to our results. Secondly, our simulations are quite satisfactory in the sense that our estimations are consistent with the experimental data. These combine to give an understandable model that is easy to handle with respect to data analysis and which yields results consistent to the experimental results.

As noted in the introduction of Section 5.6, this model is not the first attempt in the literature to describe a quantitative analysis of cell division using CFSE. (Hasbold et al., 1999) and (Zhang et al., 2001), have proposed simple models showing excellent agreement with the experimental data. The model we present here gives a more detailed description of the mechanisms involved in the cell division such as the G_0 resting phase, which is not taken in consideration in (Hasbold et al., 1999), and provides more information about the role of several parameters such as the reentry rate β, which is impossible to evaluate in (Zhang et al., 2001).

Some points remain that could be improved. It is commonly believed that β depends on the total population N of resting cells in vivo (Mackey, 1978b, 1997; Mackey et Rudnicki, 1994, 1999; Pujo-Menjouet et Rudnicki, 2000) and probably on the division history of the cell as well as the population heterogeneity. The usual shape of β is a decreasing function of the total population in the resting phase (a Hill function most of the time). Indeed, regarding our simulations, one can easily notice that the function β should not be considered as a constant. Our "hybrid" model would then be nonlinear and the explicit form of the solutions more difficult to obtain analytically. We believe that β plays a more important role than the one we gave it in our assumptions. The results of the parameters estimations in Fig. 5.3 and 5.4 have shown that β depends on characteristics of two subpopulations, characteristics that may depend on division history and/or population density. This nonlinear model will be the object of future investigations.

Even with these cautionary comments, the results presented here allow estimations on the range of the mean generation time. The mean generation time (MGT) is defined as the average time required for a cell to perform an entire cycle i.e., from the beginning of the resting (G_0) phase at $a = 0$ to the beginning of the next resting phase after cell division. In other words, this is the average time required to go through phases G_0, G_1, S, G_2 and M successively. In term of our parameters, the MGT is $T_g = \tau + 1/\beta$. This

MGT is not affected by the loss rates μ and γ because only cells which survive through the resting and proliferative phases are taken into account. The MGT should not be interpreted as the average time spent by a cell into the resting and proliferating phases. In this case, the average time spent in the resting phase is $< t_n >= (\beta+\mu)^{-1}$ and the average time in the proliferative phase is $< t_p >= (1-\gamma\tau\exp(-\gamma\tau)[1-\exp(-\gamma\tau)]^{-1})/\gamma$. It is interesting to note that in the example of two subpopulations (Figs. 5.3 and 5.4), the value of $\beta = 0.08$ day^{-1} corresponds to a MGT of $T_g = 12.75$ days and for the value $\beta = 2.30$ day^{-1}, it is $T_g = 0.68$ day. The large difference between these two values suggests that the primitive murine bone marrow cell population analyzed here is heterogenous and consists, after 4 days of culture, of a slowly cycling subpopulation and a rapidly cycling one, or perhaps a continuum between these two extremes. The existence of several subpopulations could be explained by the differentiation of some of the primitive cells initially in the culture. This interpretation is consistent with experimental data about the quiescence of primitive hematopoietic stem cells (Bradford et al., 1997) implying that more mature cells cycle more rapidly than primitive ones (Furukawa, 1998).

One of the main issues regarding the analysis of hematopoietic stem cell kinetics is their capability of repopulating a depleted bone marrow and this study provides a new theoretical framework to identify good candidates for cell transplant. The MGT is a critical parameter when the repopulating ability of a cell population is considered. The model presented here allows the characterization of different cell populations by estimating their kinetics properties using CFSE profile analysis.

The kinetics of stem cells is still poorly understood due to the lack of experimental tools and the apparent heterogeneity of stem cell populations. CFSE+ cell tracking experiments along with a mathematical model of proliferation are a good example of the fruitful cooperation between experimental methods and theoretical models to gain insight into the complex behavior of self-renewing cell populations.

5.8. COMPUTATION OF $p_k(t,a)$ AND $n_k(t,a)$

We present here the computation of the solution of Eqs. 5.5.1 and 5.5.2. First we solve Eqs. 5.5.1 and 5.5.2 with initial conditions I. From that solution, we then derive

the solution with initial conditions *II*. In the following, we will denote p^I and n^I the solution associated with IC^I and p^{II}, n^{II} the solution associated with IC^{II}. Then, from those two particular solutions, we can write down a general form of solution associated with an arbitrary initial density distribution at time $t = 0$.

5.8.1. Solution with Initial Conditions I (IC^I)

In this section we present the computation of results presented in Section 5.5.

Using the method of characteristics, we can solve Eqs. 5.5.1 and 5.5.2 to obtain a general implicit solution for p_k and n_k.

$$p_k(t,a) = \begin{cases} p_k(0,a-t)e^{-\gamma t}, & \text{for } 0 \leq t \leq a \leq \tau, \\ \\ p_k(t-a,0)e^{-\gamma a}, & \text{for } a < t, \end{cases} \tag{5.8.1}$$

and

$$n_k(t,a) = \begin{cases} n_k(0,a-t)e^{-(\mu+\beta)t}, & \text{for } 0 \leq t \leq a, \\ \\ n_k(t-a,0)e^{-(\mu+\beta)a}, & \text{for } a < t. \end{cases} \tag{5.8.2}$$

Including the boundary conditions defined by Eq. 5.5.3 and IC^I (Eq. 5.5.4) into these solutions, we have

$$p_0^I(t,a) = \delta(a-t)e^{-\gamma a}, \text{ for } 0 \leq a \leq t \leq \tau, \tag{5.8.3}$$

and

$$n_1^I(t,a) = 2p_0^I(t-a,\tau)e^{-(\mu+\beta)a}, \text{ for } 0 \leq a \leq t, \tag{5.8.4}$$

leading, with Eq. 5.8.3, to

$$n_1^I(t,a) = 2\delta(a-t+\tau)e^{-\gamma\tau}e^{-(\mu+\beta)a}, \text{ for } 0 \leq a \leq t-\tau, \tag{5.8.5}$$

for the first cohort. All these functions are assumed to take a zero value outside the region of definition. To simplify reading, we will not write it explicitly. The function δ is the Dirac delta function as defined in Eq. 5.5.6. Define the total number of cells of maturity k at time $t > 0$ as

$$P_k(t) = \int_0^\tau p_k(t,a)da,$$

and

$$N_k(t) = \int_0^{+\infty} n_k(t,a)da.$$

Then, it is easy to show that $N_1^I(t) = 2e^{-\gamma\tau}e^{-(\mu+\beta)(t-\tau)}$, for $t \geq \tau$, by integrating Eq. 5.8.5. This allows us to compute $p_1^I(t,a)$ as follows

$$\begin{aligned} p_1^I(t,a) &= p_1^I(t-a,0)e^{-\gamma a}, \\ &= \beta N_1^I(t-a)e^{-\gamma a}, \\ &= 2\beta e^{-\gamma\tau}e^{-(\mu+\beta)(t-a-\tau)}e^{-\gamma a}, \end{aligned} \tag{5.8.6}$$

for $0 \leq a \leq t-\tau$. Using the same argument, we find that

$$n_2^I(t,a) = 2^2\beta e^{-2\gamma\tau}e^{-(\mu+\beta)(t-2\tau)}, \text{ for } 0 \leq a \leq t-2\tau. \tag{5.8.7}$$

Note that $n_2^I(t,a)$ does not depend on a and Eq. 5.8.7 is valid only for $a \leq t-2\tau$. Integrating with respect to age, we have

$$N_2^I(t) = \int_0^{t-2\tau} n_2^I(t,a)da = (t-2\tau)2^2\beta e^{-2\gamma\tau}e^{-(\mu+\beta)(t-2\tau)}. \tag{5.8.8}$$

Proceeding the same way as for Eq. 5.8.6 we obtain

$$p_2^I(t,a) = (t-a-2\tau)2^2e^{-2\gamma\tau}\beta^2e^{-\gamma a}e^{-(\mu+\beta)(t-a-2\tau)}. \tag{5.8.9}$$

We can inductively generalize this result for any general division number k. We have shown that Eqs. 5.8.6 and 5.8.7 are solutions of Eqs. 5.5.1 and 5.5.2 respectively for $k=1$ and $k=2$. Suppose that Eqs. 5.5.7 and 5.5.8 are solutions of Eqs. 5.5.1 and 5.5.2 for $k>1$ and $k>2$. Let us prove that Eqs. 5.5.7 and 5.5.8 are valid for $k+1$. Starting with Eq. 5.5.8 we have, using the induction hypothesis on p_k,

$$\begin{aligned} n_{k+1}(t,a) &= n_{k+1}(t-a,0)e^{-(\mu+\beta)a}, \\ &= 2p_k(t-a,\tau)e^{-(\mu+\beta)a}, \\ &= \frac{(t-a-(k+1)\tau)^{k-1}}{(k-1)!}2^{k+1}e^{-k\gamma\tau}\beta^k e^{-\gamma\tau}e^{-(\mu+\beta)(t-a-(k+1)\tau)}e^{-(\mu+\beta)a}, \\ &= \frac{(t-a-(k+1)\tau)^{k-1}}{(k-1)!}2^{k+1}e^{-k\gamma\tau}\beta^k e^{-\gamma\tau}e^{-(\mu+\beta)(t-(k+1)\tau)}. \end{aligned} \tag{5.8.10}$$

This completes the computation for n_{k+1}, so Eq. 5.5.8 is satisfied. Let show now that Eq. 5.5.7 holds. From Eqs. 5.5.3 and 5.8.1, we have

$$p_k^I(t,a) = p_k^I(t-a,0)e^{-\gamma a} = \beta N_k^I(t-a)e^{-\gamma a}. \tag{5.8.11}$$

Moreover, we know that

$$\begin{aligned} N_k^I(t) &= \int_0^{t-k\tau} \frac{(t-a-k\tau)^{k-2}}{(k-2)!} 2^k e^{-k\gamma\tau}\beta^{k-1}e^{-(\mu+\beta)(t-k\tau)}da, \\ &= 2^k e^{-k\gamma\tau}\beta^{k-1}e^{-(\mu+\beta)(t-k\tau)}\int_0^{t-k\tau}\frac{(a)^{k-2}}{(k-2)!}da, \\ &= 2^k e^{-k\gamma\tau}\beta^{k-1}e^{-(\mu+\beta)(t-k\tau)}\frac{(t-k\tau)^{k-1}}{(k-1)!}. \end{aligned} \tag{5.8.12}$$

Replacing $N_k^I(t-a)$ in Eq. 5.8.11, it is clear that Eq. 5.5.7 is satisfied and this completes the computation of p_k^I and n_k^I.

5.8.2. Solution with Initial Conditions II (IC^{II})

The computation of the solutions p^{II} and n^{II} is carried the same way as for p^I and n^I. The IC^{II} is

$$p_k^{II}(0,a) = 0, \ \textit{for all } k \geq 0, \tag{5.8.13}$$

and

$$n_0^{II}(0,a) = C_0\delta(a), \ \textit{for } 0 \leq a, \tag{5.8.14}$$

and 0 for $k \geq 1$. As already discussed, without loss of generality, we can set $C_0 = 1$. Then we have for $k = 0$,

$$n_0^{II}(t,a) = \delta(a-t)e^{-(\beta+\mu)a}, \text{ for } 0 \leq a \leq t, \tag{5.8.15}$$

For $k > 0$, notice that,

$$n_k^{II}(t,a) = \frac{n_{k+1}^I(t+\tau,a)}{2\exp(-\gamma\tau)}. \tag{5.8.16}$$

Eq. 5.8.16 needs explanation. The solution $n_k^{II}(t,a)$ in Eq. 5.8.16 is deduced from the solution $n_k^I(t,a)$ with IC^I in the following way. Let us consider the initial cohort of proliferating cells $p_0^I(0,a)$ starting at time $t = 0$ and age $a = 0$. This cohort will divide at a time $t = \tau$ and will be the initial condition $n_0^{II}(0,a)$. In other words, all these cells

will be at the beginning of the resting phase $n_1^I(\tau,a)$. Because $n_0^{II}(0,a)$ and $n_1^I(\tau,a)$ are equivalent up to a multiplicative constant, we can choose this constant so that

$$n_0^{II}(0,a) = p_0^I(0,a). \tag{5.8.17}$$

Further, since

$$n_1^I(\tau,a) = 2\exp(-\gamma\tau)p_0^I(0,a), \tag{5.8.18}$$

it follows that,

$$n_0^{II}(0,a) = \frac{n_1^I(\tau,a)}{2\exp(-\gamma\tau)}. \tag{5.8.19}$$

Then the general Eq. 5.8.16 follows naturally. So,

$$n_k^{II}(t,a) = \frac{(t-a-k\tau)^{k-1}}{(k-1)!}2^k\beta^k e^{-k\gamma\tau}e^{-(\beta+\mu)(t-k\tau)}, \tag{5.8.20}$$

for $k \geq 1$ and $t-a \geq k\tau$. If we integrate Eq. 5.8.20 with respect to age we find

$$N_k^{II}(t) = \frac{(t-k\tau)^k}{k!}2^k\beta^k e^{-k\gamma\tau}e^{-(\beta+\mu)(t-k\tau)}, \tag{5.8.21}$$

for $k \geq 0$. An equation similar to Eq. 5.8.16 holds for $p_k^{II}(t,a)$,

$$p_k^{II}(t,a) = \frac{p_{k+1}^I(t+\tau,a)}{2\exp(-\gamma\tau)}. \tag{5.8.22}$$

Then

$$p_k^{II}(t,a) = \frac{(t-a-k\tau)^k}{k!}2^k\beta^{k+1}e^{-k\gamma\tau}e^{-(\beta+\mu)(t-a-k\tau)}e^{-\gamma a}, \tag{5.8.23}$$

for $k \geq 0$ and $t-a \geq k\tau$.

5.8.3. Solution with a general initial density distribution

We present here a formula giving the general solution of the model 5.5.1- 5.5.2 using a linear combination of particular solutions with IC^I and IC^{II}. As previously mentioned, the initial age density distribution of the resting cell population will not affect the solution after the first division, so we will only consider an arbitrary function $g(a)$ representing the initial density distribution of cell in the proliferative phase. That is the density of proliferating cells at time $t = 0$ is,

$$p_0(0,a) = g(a), \text{ for } 0 \leq a \leq \tau, \tag{5.8.24}$$

where g is an positive integrable function on the interval $a \in [0,\tau]$. Without loss of generality, we can assume that $\int_0^\tau g(a)da = 1$. The density of proliferating cells with initial distribution $g(a)$ is

$$p_k^g(t,a) = \int_0^\tau p_k^I(t+s,a)e^{\gamma s}g(s)ds, \tag{5.8.25}$$

and the density of resting phase cells is

$$n_k^g(t,a) = \int_0^\tau n_k^I(t+s,a)e^{\gamma s}g(s)ds. \tag{5.8.26}$$

For a complete description of the initial conditions, we only have to give the number of cells in the resting phase at time $t = 0$. Assume that the total number of cells at time $t = 0$ is 1, then the initial number of proliferating cells ρ plus the number of resting phase cells equal 1. The complete general solution p_k, n_k is then

$$p_k(t,a) = \rho p_k^g(t,a) + (1-\rho)p_k^{II}(t,a), \tag{5.8.27}$$

and

$$n_k(t,a) = \rho n_k^g(t,a) + (1-\rho)n_k^{II}(t,a) \tag{5.8.28}$$

for $k \geq 0$. It is worth noting that using different initial distributions g does not significantly influence the behavior of the solution, even for small times t. However, the solution is affected by the initial ratio ρ of proliferating cells.

ACKNOWLEDGEMENTS

SB is supported by Mathematics of Information Technology and complex systems (Canada) and l'Institut des Sciences Mathématiques (Québec). LP-M is supported by Mathematics of Information Technology and complex systems (Canada). MCM is supported by the Natural Sciences and Engineering Research Council (NSERC Grant No. OGP-0036920, Canada), Mathematics of Information Technology and complex systems (Canada), and Le Fonds pour la Formation de Chercheurs et l'Aide à la Recherche (FCAR Grant No. 98ER1057, Québec).

Chapitre 6

SYNTHÈSE ET CONCLUSION

Le système hématopoïétique est vraisemblablement un système physiologique de choix quant à sa modélisation par des modèles structurés en âge, l'impressionnante littérature scientifique sur le sujet en fait foi. La prolifération cellulaire parallèle à la différenciation des progéniteurs des cellules sanguines suggèrent une structure de maturation. Dans les Chapitres 2, 3, 4, la structure de maturation a été abandonnée pour être remplacée par un système avec retards. Cette réduction d'un système d'équations aux dérivées partielles à un système d'équations différentielles à retard a permis une étude des propriétés de stabilité locale, ainsi qu'une étude numérique des dynamiques présentes, notamment des points de bifurcation, des cycles limites et de la multistabilité. Mises à part les applications de ces types de systèmes, les liens entre équations aux dérivées partielles et équations différentielles à retard méritent d'être approfondis. Deux aspects militent en faveurs de la réduction, lorsque possible, des EDP en EDR. D'une part, les coûts de calcul sont parfois moindres pour les EDR. D'autre part, l'étude de l'existence et de la stabilité des solutions d'EDR peut aussi être plus simple.

La modélisation de maladies dynamiques permet de mieux comprendre la nature des mécanismes de contrôle intervenant dans la production de cellules sanguines, tant au niveau pathologique que normal. Les désordres liés à l'hématopoïèse sont nombreux et peuvent être mortels. Une meilleure compréhension des effets de ces désordres sur la dynamique de la production cellulaire est nécessaire pour établir des stratégies efficaces de traitement.

La neutropénie cyclique, maladie rare, exhibant des oscillations dans le compte de différentes lignées de cellules sanguines—globules blancs, plaquettes, réticulocytes—a permis de modéliser le système de production de neutrophiles et jette un éclairage nouveau sur les mécanismes mis en œuvre par le système hématopoïétique pour réguler la production de cellules sanguine. Deux facteurs semblent y être primordiaux : l'apoptose des précurseurs et la différenciation de cellules souches hématopoïétiques. L'apoptose, à première vue, paraît contre-productive, puisque selon certaines données expérimentales (Mackey et al., 2003a), même chez les sujets sains, plus de la moitié des précurseurs est éventuellement éliminée par ce mécanisme. Par contre, l'apoptose alloue une régulation négative presque instantanée, permettant au corps de s'ajuster très rapidement en cas de traumatisme ou d'infection. De plus, la rapidité d'adaptation stabilise le système hématopoïétique (un feedback négatif sans retard est toujours localement stable). Dans le cas de la neutropénie cyclique, les données cliniques montrent que l'apoptose est très élevée et plus ou moins régulée, ce qui pousse les cellules souches à augmenter leur taux de différenciation et entraîne de ce fait une instabilité. La différenciation des cellules souches, bien que nécessaire pour maintenir le bassin de précurseurs, est en fait un mauvais facteur de régulation. Tel que vu dans l'introduction, plusieurs désordres sanguins montrent des oscillations même si le compte des cellules sanguines n'est pas diminué. Il est possible que les symptômes de ces maladies aient en commun un déséquilibre dans le contrôle de l'apoptose.

Bibliographie

ABKOWITZ J.L., CATLIN S.N., MCCALLIE M.T., ET GUTTORP P., 2002. Evidence that the number of hematopoietic stem cells per animal is conserved in mammals. *Blood*, 100, 2665–2667.

ABKOWITZ J.L., GOLINELLI D., HARRISON D.E., ET GUTTORP P., 2000. In vivo kinetics of murine hemopoietic stem cells. *Blood*, 96, 3399–3405.

ADIMY M. ET PUJO-MENJOUET L., 2001. A singular transport model describing cellular division. *C.R. Acad. Sci. I-Math*, 332, 1071–1076.

AKBARZADEH S., WARD A.C., MCPHEE D.O.M., ALEXANDER W.S., LIESCHKE G.J., ET LAYTON J.E., 2002. Tyrosine residues of the granulocyte colony-stimulating factor receptor transmit proliferation and differentiation signals in murine bone marrow cells. *Blood*, 99, 879–887.

ANDERSEN L.K. ET MACKEY M.C., 2001. Resonance in periodic chemotheray : A case study of acute myelogenous leukemia. *J. Theor. Biol.*, 209, 113–130.

ANDERSON R.F.V., 1991. Geometric and probabilistic stability criteria for delay systems. *Math. Biosci.*, 105, 81–96.

ANDERSON R.F.V., 1992. Intrinsic parameters and stability of differential-delay equations. *J. Math. Anal. Appl.*, 163, 184–199.

APRIKYAN A.A.G., LILES W.C., BOXER L.A., ET DALE D.C., 2002. Mutant elastase in pathogenesis of cyclic and severe congenital neutropenia. *J. Pediat. Hematol. Onc.*, 24, 784–786.

APRIKYAN A.A.G., LILES W.C., RODGER E., JONAS M., CHI E.Y., ET DALE D.C., 2001. Impaired survival of bone marrow hematopoietic progenitor cells in cyclic neutropenia. *Blood*, 97, 147–153.

ARINO O., SÁNCHEZ E., ET WEBB G.F., 1997. Necessary and sufficient conditions

for asynchronous exponential growth in age structured cell populations with quiescence. *J. Math. Anal. Appl.*, 215, 499–513.

AVALOS B.R., BROUDY V.C., CESELSKI S.K., DRUKER B.J., GRIFFIN J.D., ET HAMMOND W.P., 1994. Abnormal response to granulocyte colony stimulating factor (G-CSF) in canine cyclic hematopoiesis is not caused by altered G-CSF receptor expression. *Blood*, 84, 789–794.

BAGLEY C.J., WOODCOCK J.M., STOMSKI F.C., ET LOPEZ A.F., 1997. The structural and functional basis of cytokine receptor activation : Lessons from the common subunit of the granulocyte-macrophage colony-stimulating factor, interleukin-3 (il-3), and il-5 receptors. *Blood*, 89, 1471–1482.

BASU S., HODGSON G., KATZ M., ET DUNN A.R., 2002. Evaluation of role of g-csf in the production, survival, and release of neutrophils from bone marrow into circulation. *Blood*, 100, 854–861.

BÉLAIR J. ET CAMPBELL S.A., 1994. Stability and bifurcations of equilibria in a multiple-delayed differential equation. *SIAM J. Appl. Math.*, 54, 1402–1424.

BÉLAIR J., CAMPBELL S.A., ET VAN DEN DRIESSCHE P., 1996. Frustration, stability and delay-induced oscillations in a neural network model. *SIAM J. Appl. Math.*, 56, 245–255.

BÉLAIR J. ET MACKEY M.C., 1987. A model for the regulation of mammalian platelet. *Ann. N.Y. Acad. Sci.*, 504, 280–282.

BÉLAIR J., MACKEY M.C., ET MAHAFFY J.M., 1995. Age-structured and two-delay models for erythropoiesis. *Math. Biosci.*, 128, 317–346.

BENNETT M. ET GRUNWALD A.J., 2001. Hydroxyurea and periodicity in myeloproliferative disease. *Eur. J. Haematol.*, 66, 317–323.

BERNARD S., BÉLAIR J., ET MACKEY M.C., 2001. Sufficient conditions for stability of linear differential equations with distributed delay. *Discrete Contin. Dyn. Syst. Ser. B*, 1, 233–256.

BERNARD S., BÉLAIR J., ET MACKEY M.C., 2003a. Bifurcations in a white blood cell production model. *C. R. Biologies*.

BERNARD S., BÉLAIR J., ET MACKEY M.C., 2003b. Oscillations in cyclical neutropenia : New evidence based on mathematical modeling. *J. Theor. Biol.*, 223,

283–298.

BERNARD S., PUJO-MENJOUET L., ET MACKEY M.C., 2003c. Analysis of cell kinetics using a cell division marker : Mathematical modeling of experimental data. *Biophys. J.*, 84, 3414–3424.

BERTUZZI A., FARETTA M., GANDOLFI A., SINISGALLI C., STARACE G., VALOTI G., ET UBEZIO P., 2002. Kinetic heterogeneity of an experimental tumour revealed by BrdUrd incorporation and mathematical modelling. *B. Math. Biol.*, 64, 355–384.

BIRGENS H.S. ET KARL H., 1993. Reversible adult-onset cyclic haematopoiesis with a cycle length of 100 days. *Brit. J. Haematol.*, 83, 181–186.

BOESE F.G., 1989. The stability chart for the linearized Cushing equation with a discrete delay and with a gamma-distributed delay. *J. Math. Anal. Appl.*, 140, 510–536.

BOGGS D.R., BOGGS S.S., SAXE D.F., GRESS L.A., ET CANFIELD D.R., 1982. Hematopoietic stem cells with high proliferative potential. assay of their concentration in marrow by the frequency and duration of cure of W/Wv mice. *J. Clin. Invest.*, 70, 242–253.

BONHOEFFER S., MOHRI H., HO D., ET PERELSON A.S., 2000. Quantification of cell turnover kinetics using 5-bromo-2'-deoxyuridine1. *J. Immunol.*, 164, 5049–5054.

BORGE O.J., RAMSFJELL V., CUI L., ET JACOBSEN S.E., 1997. Ability of early acting cytokines to directly promote survival and suppress apoptosis of human primitive CD34+CD38- bone marrow cells with multilineage potential at the single cell level : Key role of thrombopoietin. *Blood*, 90, 2282–2292.

BRADFORD G.B., WILLIAMS B., ROSSI R., ET BERTONCELLO I., 1997. Quiescence, cycling, and turnover in the primitive hematopoietic stem cell compartment. *Exp. Hematol.*, 25, 445–453.

BURNS F. ET TANNOCK I., 1970. On the existence of a G_0 phase in the cell cycle. *Cell Tissue Kinet.*, 3, 321–334.

BURTHEM J., MOTTRAM R., LUCAS G.S., ET WHETTON A.D., 2002. Imatinib mesilate (STI571) causes an increased rate of maturation and a reduced expansion of cell number during the granulocytic differentiation of CD34+ cells from CML

patients. *non publié*.

CAMPBELL S.A., BÉLAIR J., OHIRA T., ET MILTON J.G., 1995. Limit cycles, tori and complex dynamics in a second-order differential equation with delayed negative feedback. *J. Dynam. Differential Equations*, 7, 213–236.

CARULLI G., MARINI A., AZZARÀ A., VANACORE R., ET PETRINI M., 2000. Cyclic oscillations of neutrophils, monocytes, and CD8-positive lymphocytes in a healthy subject. *Haematologica*, 85, 447–448.

CHATTA G.S., PRICE T.H., ALLEN R.C., ET DALE D.C., 1994. Effects of *in vivo* recombinant methionyl human granulocyte colony stimulating factor on the neutrophil response and peripheral blood colony forming cells in healthy young and elderly adult volunteers. *Blood*, 84, 2923–2929.

CHESHIER S., MORRISON S., LIAO X., ET WEISSMAN I., 1999. In vivo proliferation and cell cycle kinetics of long term self renewing haematopoietic stem cells. *Proc. Natl. Acad. Sci. USA*, 96, 3120–3125.

COOKE K. ET GROSSMAN Z., 1982. Discrete delay, distributed delay and stability switches. *J. Math. Anal. Appl.*, 86, 592–627.

CRABB R., LOSSON J., ET MACKEY M.C., 1996a. Dependence on initial conditions in nonlocal PDE's and hereditary dynamical systems. *Proc. Inter. Conf. Nonlin. Anal (Tampa Bay)*, 4, 3125–3136.

CRABB R., MACKEY M.C., ET REY A., 1996b. Propagating fronts, chaos and multistability in a cell replication model. *Chaos*, 3, 477–492.

DALE D.C., ALLING D.W., ET WOLFF S.M., 1973. Application of time series analysis to serial blood neutrophil counts in normal individuals and patients receiving cyclophosphamide. *Brit. J. Haematol.*, 24, 57–64.

DALE D.C., BONILLA M.A., DAVIS M.W., NAKANISHI A.M., HAMMOND W.P., KURTZBERG J., WANG W., JAKUBOWSKI A., WINTON E., LALEZARI P., ROBINSON W., GLASPY J.A., EMERSON S., GABRILOVE J., VINCENT M., ET BOXER L.A., 1993. A randomized controlled phase III trial of recombinant human granulocyte colony stimulating factor (filgrastim) for treatment of severe chronic neutropenia. *Blood*, 81, 2496–2502.

DALE D.C. ET HAMMOND W.P., 1988. Cyclic neutropenia : A clinical review. *Blood*

Rev., 2, 178–185.

DALE D.C., PERSON R.E., BOLYARD A.A., APRIKYAN A.A.G., BOS C., BONILLA M.A., BOXER L.A., KANNOURAKIS G., ZEIDLER C., WELTE K., BENSON K.F., ET HORWITZ M., 2000. Mutations in the gene encoding neutrophil elastase in congenital and cyclic neutropenia. *Blood*, 96, 2317–2322.

DEUBELBEISS K.A., DANCEY J.T., HARKER L.A., ET FINCH C.A., 1975. Neutrophil kinetics in the dog. *J. Clin. Invest.*, 55, 833–839.

DINAUER M.C., LEKSTROM-HIMES J.A., ET DALE D.C., 2000. Inherited Neutrophil Disorders : Molecular Basis and New Therapies. *Hematology*, 2000, 303–318.

DOEDEL E.J., 1981. Auto : A program for the automatic bifurcation analysis of autonomous systems. Dans *Proc. 10th Manitoba Conf. on Num. Math. and Comp., Univ. of Manitoba, Winnipeg, Canada*, p. 265–284.

DYSON J., VILLELLA-BRESSAN R., ET WEBB G.F., 1996a. A singular transport equation modelling a proliferating maturity structured cell population. *Can. Appl. Math. Quart.*, p. 65–95.

DYSON J., VILLELLA-BRESSAN R., ET WEBB G.F., 1996b. A singular transport equation with delays. *Proc. Second International Conference on Differential Equations in Marrakesh*.

DYSON J., VILLELLA-BRESSAN R., ET WEBB G.F., 1997. Hypercyclicity of solutions of a transport equation with delays. *J. Nonlinear Anal. : Theory, Methods and Appl.*, p. 1343–1351.

DYSON J., VILLELLA-BRESSAN R., ET WEBB G.F., 1998. An age and maturity structured model of cell population dynamics. Dans M. HORN E.G.W. G. SIMONNETT, réd., *Mathematical Models in Medical and Health Science*, p. 66–116. Vanderbilt University Press, Nashville, TN.

DYSON J., VILLELLA-BRESSAN R., ET WEBB G.F., 2000a. A nonlinear age and maturity structured model of population dynamics. I. Basic theory. *J. Math. Anal. Appl.*, 242, 93–104.

DYSON J., VILLELLA-BRESSAN R., ET WEBB G.F., 2000b. A nonlinear age and maturity structured model of population dynamics. II. Chaos. *J. Math. Anal. Appl.*, 242, 255–270.

EDELSTEIN-KESHET L., ISRAEL A., ET LANSDORP P., 2001. Modelling perspective on aging : Can mathematics help us stay young ? *J. Theor. Biol.*, 213, 509–525.

EL'SGOL'TS, 1966. *Introduction to the theory of differential equations with deviating argument*. Holden-Day.

ENGELBORGHS K., LUZYANINA T., ET SAMAEY G., 2001. DDE-BIFTOOL v. 2.00 : a matlab package for bifurcation analysis of delay differential equations. Katholieke Universiteit Leuven, http ://www.cs.kuleuven.ac.be/ koen/.

ERMENTROUT B., 2001. XPPAUT version 5.4 sofware. http ://www.math.pitt.edu/ bard/xpp/xpp.html.

ERMENTROUT B., 2002. *Simulating, Analyzing, and Animating Dynamical Systems : A Guide to Xppaut for Researchers and Students (Software, Environments, Tools)*. SIAM, 1re éd.

FAZEKAS DE ST GROTH B., SMITH A.L., KOH W.P., GIRGIS L., COOK M.C., ET BERTOLINO P., 1999. Carboxyfluorescein diacetate succinimidyl ester and the virgin lymphocyte : A marriage made in heaven. *Immunol. Cell Biol.*, 77, 530–538.

FOKAS A.S., KELLER J.B., ET CLARKSON B.D., 1991. Mathematical model of granulocytopoiesis and chronic myelogenous leukemia. *Cancer Res.*, 51, 2084–2091.

FORSTER I., VEIRA P., ET RAJEWSKI K., 1989. Flow cytometric analysis of cell proliferation dynamics in the B cell compartment of the mouse. *Int. Immun.*, 1, 321–331.

FORTIN P. ET MACKEY M.C., 1999. Periodic chronic myelogenous leukemia : Spectral analysis of blood cell counts and etiological implications. *Brit. J. Haematol.*, 104, 336–345.

FOWLER A.C. ET MACKEY M.C., 2002. Relaxation oscillations in a class of delay differential equations. *SIAM J. Appl. Math.*, 63, 299–323.

FREEDMAN M.H., BONILLA M.A., FIER C., BOLYARD A.A., SCARLATA D., BOXER L.A., BROWN S., CHAM B., KANNOURAKIS G., KINSEY S.E., MORI P.G., COTTLE T., WELTE K., ET DALE D.C., 2000. Myelodysplasia syndrome and acute myeloid leukemia in patients with congenital neutropenia receiving g-csf therapy. *Blood*, 96, 429–436.

FULCHER D.A. ET WONG S.W.J., 1999. Carboxyfluorescein succinimidyl ester-based proliferative assays for assesment of T cell function in the diagnostic laboratory. *Immunol. Cell Biol.*, 77, 559–564.

FURUKAWA Y., 1998. Cell cycle regulation of hematopoietic stem cells. *Hum. Cell*, 11, 81–92.

GIBSON C.M., GURNEY C.W., GASTON E.O., ET SIMMONS E.L., 1984. Cyclic erythropoiesis in the S1/S1^d mouse. *Exp. Hematol.*, 12, 343–348.

GIBSON C.M., GURNEY C.W., SIMMONS E.L., ET GASTON E.O., 1985. Further studies on cyclic erythropoiesis in mice. *Exp. Hematol.*, 13, 855–860.

GLUMENSON L.E., 1973. A comprehensive modeling procedure for the human granulopoietic system : Over-all view and summary of data. *Blood*, 42, 303–313.

GLUMENSON L.E., 1975. A comprehensive modeling procedure for the human granulopoietic system : Detailed description and application to cancer chemotherapy. *Math. Biosci.*, 26, 217–239.

GOPALSAMY, 1992. *Stability and oscillations in delay differential equations of population dynamics*. MIA. Kluwer Acad. Press.

GRATZNER H.G., 1982. Monoclonal antibody to 5-bromo- and 5-iododeoxyuridine : A new reagent for detection of DNA replication. *Science*, 218, 474–475.

GRIGNANI F., 1985. Chronic myelogenous leukemia. *Crit. Rev. Oncology-Hematol.*, 4, 31–66.

GUERRY D., DALE D.C., OMINE M., PERRY S., ET WOLFF S.M., 1973. Periodic hematopoiesis in human cyclic neutropenia. *J. Clin. Inves.*, 52, 3220–3230.

GURNEY C.W., SIMMONS E.L., ET GASTON E.O., 1981. Cyclic erythropoiesis in W/W^v mice following a single small dose of ^{89}Sr. *Exp. Hematol.*, 9, 118–122.

HALANAY, 1966. *Differential Equation*. Academic Press.

HALE J.K. ET VERDUYN LUNEL S.M., 1991. *Introduction to functional differential equations*, t. 99 de *Applied Mathematical Sciences Series*. Springer-Verlag, New York.

HAMMOND W.P., BOONE T.C., DONAHUE R.E., SOUZA L.M., ET DALE D.C., 1990. Comparison of treatment of canine cyclic, hematopoiesis with recombinant human granulocyte-macrophage colony-stimulating factor (GM-CSF), G-CSF,

Interleukin-3, and canine G-CSF. *Blood*, 76, 523–532.

HAMMOND W.P., PRICE T.H., SOUZA L.M., ET DALE D.C., 1989. Treatment of cyclic neutropenia with granulocyte colony stimulating factor. *New Engl. J. Med.*, 320, 1306–1311.

HARRISON D.E., ASTLE C.M., ET LERNER C., 1988. Number and continuous proliferative pattern of transplanted primitive immunohematopoietic stem cells. *Proc. Natl. Acad. Sci. USA*, 85, 822–826.

HASBOLD J., GETT A.V., RUSH J.S., DEENICK E., AVERY D., JUN J., ET HODGKIN P.D., 1999. Quantitative analysis of lymphocyte differentiation and proliferation in vitro using carboxyfluorescein diacetate succinimidyl ester. *Immunol. Cell Biol.*, 77, 516–522.

HASBOLD J. ET HODGKIN P.D., 2000. Flow cytometric cell division tracking using nuclei. *Cytometry*, 40, 230–237.

HASBOLD J., LYONS A.B., KEHRY M.R., ET HODGKIN P.D., 1998. Cell division number regulates IgG1 and IgE switching of B cells following stimulation by CD40 ligand and IL-4. *Eur. J. Immunol.*, 28, 1040–1051.

HAURIE C., DALE D.C., ET MACKEY M.C., 1998. Cyclical neutropenia and other periodic hematological diseases : A review of mechanisms and mathematical models. *Blood*, 92, 2629–2640.

HAURIE C., DALE D.C., ET MACKEY M.C., 1999a. Occurrence of periodic oscillations in the differential blood counts of congenital, idiopathic and cyclical neutropenic patients before and during treatment with G-CSF. *Exp. Hematol.*, 27, 401–409.

HAURIE C., DALE D.C., RUDNICKI R., ET MACKEY M.C., 2000. Modeling complex neutrophil dynamics in the grey collie. *J. Theor. Biol.*, 204, 505–519.

HAURIE C., PERSON R., DALE D.C., ET MACKEY M.C., 1999b. Haematopoietic dynamics in grey collies. *Exp. Hematol.*, 27, 1139–1148.

HAYASHI N., ASO H., HIGASHIDA M., KINOSHITA H., OHDO S., YUKAWA E., ET HIGUCHI S., 2001. Estimation of rhg-csf absorption kinetics after subcutaneous administration using a modified wagner-nelson method with a nonlinear elimination model. *Eur. J. Pharm. Sci.*, 13, 151–158.

HAYES N.D., 1950. Roots of the transcendental equation associated with a certain

difference-differential equation. *J. Lond. Math. Soc.*, 25, 226–232.

HEARN T., HAURIE C., ET MACKEY M.C., 1998. Cyclical neutropenia and the peripheral control of white blood cell production. *J. Theor. Biol.*, 192, 167–181.

HENRY L.L., 1976. *Population analysis and models*. Edward Arnold, London.

HODGKIN P.D., LEE J.H., ET LYONS A.B., 1996. B cell differentiation and isotype switching is related to division cycle number. *J. Exp. Med.*, 184, 277–281.

HORWITZ M., BENSON K.F., PERSON R.E., APRIKYAN A.A.G., ET DALE D.C., 1999. Mutations in ela2, encoding neutrophil elastase, define a 21-day biological clock in cyclic haematopoiesis. *Nature Genetics*.

HOUCK D.W. ET LOKEN M.R., 1985. Simultaneous analysis of cell surface antigens, bromodeoxyuridine incorporation and DNA content. *Cytometry*, 6, 531–538.

JEHA S., CHAN K.W., APRIKYAN A.A.G., HOOTS W.K., CULBERT S., ZIETZ H., DALE D.C., ET ALBITAR M., 2000. Spontaneous remission of granulocyte colony-stimulating factor-associated leukemia in a child with severe congenital neutropenia. *Blood*, 96, 3647–3649.

KANAYASU-TOYODA T., YAMAGUCHI T., UCHIDA E., ET HAYAKAWA T., 1999. Commitment of neutrophilic differentiation and proliferation of HL-60 cells coincides with expression of transferrin receptor. Effect of granulocyte colony stimulating factor on differentiation and proliferation. *J. Biol. Chem.*, 274, 25 471–25 480.

KATO M., KAMIYAMA H., OKAZAKI A., KUMAKI K., KATO Y., ET SUGIYAMA Y., 1997. Mechanism for the nonlinear pharmacokinetics of erythropoietin in rats. *Rats J. Pharmacol. Exp. Ther.*, 283, 520–527.

KAZARINOFF N.D. ET VAN DEN DRIESSCHE P., 1979. Control of oscillations in hematopoiesis. *Science*, 203, 1348–1350.

KEARNS C.M., WANG W.C., STUTE N., IHLE J.N., ET EVANS W.E., 1993. Disposition of recombinant human granulocyte colony stimulating factor in children with severe chronic neutropenia. *J. Pediatr.*, 123, 471–479.

KENDALL D.G., 1948. On the role of variable generation time in the development of a stochastic birth process. *Biometrika*, 35, 316–330.

KEYFITZ N., 1968. *Introduction to the mathematics of population*. Addison-Wesley, Reading, Mass.

KING-SMITH E.A. ET MORLEY A., 1970. Computer simulation of granulopoiesis : Normal and impaired granulopoiesis. *Blood*, 36, 254–262.

KIRK J., ORR J.S., ET HOP C.S., 1968. A mathematical analysis of red blood cell and bone marrow stem cell control mechanism. *Brit. J. Haematol.*, 15, 35–46.

KUANG Y., 1993. *Delay Differential Equations With Applications In Population Dynamics*, t. 191 de *Math. Science Engineering*. Academic Press.

KUANG Y., 1994. Nonoccurence of stability switching in systems of differential equations with distributed delays. *Quaterly of Applied Mathematics*, LII, 569–578.

LAYTON J.E., HOCKMAN H., SHERIDAN W.P., ET MORSTYN G., 1989. Evidence for a novel *in vivo* control mechanism of granulopoiesis : Mature cell-related control of a regulatory growth factor. *Blood*, 74, 1303–1307.

LEBOWITZ J.L. ET RUBINOW S.I., 1969. Grain count distributions in labeled cell populations. *J. Theor. Biol.*, 23, 99–123.

LENSINK D.B., BARTON A.B., APPELBAUM R.R., ET HAMMOND W.P., 1986. Cyclic neutropenia as a premalignant manifestation of acute lymphoblastic leukemia. *Am. J. Hematol.*, 22, 9–16.

LOEFFLER M. ET PANTEL K., 1990. A mathematical model of erythropoiesis suggests an altered plasma volume control as cause for anemia in aged mice. *Exper. Gerontol*, 25, 483–495.

LOEFFLER M., PANTEL K., WULFF H., ET WICHMANN H.E., 1989. A mathematical model of erythropoiesis in mice and rats. Part I : Structure of the model. *Cell Tissue Kinet.*, 22, 13–20.

LONGTIN A. ET MILTON J.G., 1988. Complex oscillations in the human pupil light reflex with mixed delayed feedback. *Math. Biosci.*, 90, 183–189.

LONGTIN A. ET MILTON J.G., 1989a. Insight into the transfer function, gain, and oscillation onset for the pupil light reflex using nonlinear delay-differential equations. *Biol. Cybern.*, 61, 51–59.

LONGTIN A. ET MILTON J.G., 1989b. Modelling autonomous oscillations in the human pupil light reflex using nonlinear delay-differential equations. *B. Math. Biol.*, 51, 605–624.

LONGTIN A., MILTON J.G., BOS J., ET MACKEY M.C., 1990. Noise and critical

behavior of the pupil light reflex at oscillation onset. *Phys. Rev. A*, 41, 6992–7005.

LOTEM J. ET SACHS L., 1988. In vivo control of differentiation of myeloid leukemic cells by recombinant granulocyte-macrophage colony-stimulating factor and interleukin 3. *Blood*, 71, 375–382.

LUND J.E., PADGETT G.A., ET OTT R.L., 1967. Cyclic neutropenia in grey collie dogs. *Blood*, 29, 452–461.

LYONS A.B., 1999. Divided we stand : Tracking cell proliferation with carboxyfluorescein diacetate succinimidyl ester. *Immunol. Cell Biol.*, 77, 509–515.

LYONS A.B. ET PARISH C.R., 1994. Determination of lymphocyte division by flow cytometry. *J. Immunol. Methods*, 171, 131–137.

MACDONALD N., 1978. Cyclical neutropenia : Models with two cell types and two time lags. Dans VALLERON A. ET MACDONALD P., réds., *Biomathematics and Cell Kinetics*, p. 287–295. Elsevier/North-Holland, Amsterdam.

MACKEY M.C., 1978a. A unified hypothesis for the origin of aplastic anemia and periodic haematopoiesis. *Blood*, 51, 941–956.

MACKEY M.C., 1978b. Unified hypothesis of the origin of aplastic anemia and periodic hematopoiesis. *Blood*, 51, 941–956.

MACKEY M.C., 1979a. Dynamic haematological disorders of stem cell origin. Dans VASSILEVA-POPOVA J.G. ET JENSEN E.V., réds., *Biophysical and Biochemical Information Transfer in Recognition*, p. 373–409. Plenum Publishing Corp., New York.

MACKEY M.C., 1979b. Periodic auto-immune hemolytic anemia : An induced dynamical disease. *B. Math. Biol.*, 41, 829–834.

MACKEY M.C., 1997. Mathematical models of hematopoietic cell replication and control. Dans OTHMER H.G., ADLER F.R., LEWIS M.A., ET DALTON J.C., réds., *The Art of Mathematical Modeling : Case Studies in Ecology, Physiology & Biofluids*, p. 149–178. Prentice Hall.

MACKEY M.C., 2001. Cell kinetic status of hematopoietic stem cells. *Cell Prolif.*, 34, 71–83.

MACKEY M.C. ET AN DER HEIDEN U., 1982. The dynamics of production and destruction : Analytic insight into complex behavior. *J. Math. Biol.*, 16, 75–101.

MACKEY M.C. ET AN DER HEIDEN U., 1984. The dynamics of recurrent inhibition. *J. Math. Biol.*, 19, 211–225.

MACKEY M.C., APRIKYAN A.A.G., ET DALE D.C., 2003a. The rate of apoptosis in post mitotic neutrophil precursors of normal and neutropenic humans. *Cell Prolif.*, 36, 27–34.

MACKEY M.C. ET DÖRMER P., 1982. Continuous maturation of proliferating erythroid precursors. *Cell Tissue Kinet.*, 15, 381–392.

MACKEY M.C. ET GLASS L., 1979. Pathological conditions resulting from instabilities in physiological control systems. *Ann. N.Y. Acad. Sci.*, 316, 214–235.

MACKEY M.C. ET GLASS L., 1988. *From Clock to Chaos*. Princeton University Press.

MACKEY M.C., HAURIE C., ET BÉLAIR J., 2003b. Cell replication and control, chapter 9. Dans BEUTER A., GLASS L., MACKEY M.C., ET TITCOMBE M., réds., *Nonlinear Dynamics in Physiology and Medicine*, p. 1–2. Springer-Verlag, New York.

MACKEY M.C. ET RUDNICKI R., 1994. Global stability in a delayed partial differential equation describing cellular replication. *J. Math. Biol.*, 33, 89–109.

MACKEY M.C. ET RUDNICKI R., 1999. A new criterion for the global stability of simultaneous cell replication and maturation processes. *J. Math. Biol.*, 38, 195–219.

MAHAFFY J.M., BÉLAIR J., ET MACKEY M.C., 1998. Hematopoietic model with moving boundary condition and state dependent delay : Applications in erythropiesis. *J. Theor. Biol.*, 190, 135–146.

MCCARTHY K.F., 1997. Population size and radiosensitivity of murine hematopoietic endogenous long-term repopulating cells. *Blood*, 89, 834–841.

MCKINSTRY W.J., LI C.L., RASKO J.E., NICOLA N.A., JOHNSON G.R., ET METCALF D., 1997. Cytokine receptor expression on hematopoietic stem and progenitor cells. *Blood*, 89, 65–71.

MENSOUR B. ET LONGTIN A., 1995. Controlling chaos to store information in delay-differential equations. *Phys. Lett. A*, 205, 18–24.

MICKLEM H.S., LENNON J.E., ANSELL J.D., ET A. G.R., 1987. Numbers and dispersion of repopulating hematopoietic cell clones in radiation chimeras as functions

of injected cell dose. *Exp. Hematol.*, 15, 251–257.

MILTON J., CAMPBELL S.A., ET BÉLAIR J., 1995. Dynamic feedback and the design of closed-loop drug delivery systems. *J. Biological Systems*, 3, 711–718.

MINTERN J., LI M., DAVEY G.M., BLANAS E., KURTS C., CARBONE F.R., ET HEATH W.R., 1999. The use of carboxyfluorescein diacetate succinimidyl ester to determine the site, duration and cell type responsible for antigen presentation in vivo. *Immunol. Cell Biol.*, 77, 539–543.

MONOT C., NAJEAN Y., DRESCH C., ET MARTIN J., 1975. Models of erythropoiesis and clinical diagnosis. *Math. Biosci.*, 27, 145–154.

MORLEY A., 1969. Blood-cell cycles in polycythaemia vera. *Aust. Ann. Med.*, 18, 124.

MORLEY A., 1970. Periodic diseases, physiological rhythms and feedback control–a hypothesis. *Aust. Ann. Med.*, 3, 244–249.

MORLEY A., 1979. Cyclic hemopoiesis and feedback control. *Blood Cells*, 4, 172–185.

MORLEY A., KING-SMITH E.A., ET STOHLMAN F., 1969. The oscillatory nature of hemopoiesis. Dans STOHLMAN F., réd., *Hemopoietic Cellular Proliferation*, p. 3–14. Grune & Stratton, New York.

MORLEY A. ET STOHLMAN F., 1970. Cyclophosphamide induced cyclical neutropenia. *New Engl. J. Med.*, 282, 643 –646.

MOSMANN T., 1983. Rapid colorimetric assay for cellular growth and survival : Application to proliferation and cytotoxicity assays. *J. Immunol. Methods*, 65, 55–63.

MYLREA K.C. ET ALBRECHT P.H., 1971. Mathematical analysis and digital simulation of the control of erythropoiesis. *J. Theor. Biol.*, 33, 279–297.

NAKAMURA M., 1999. *Estimation of cell cycle parameters from cell division tracking data*. Thèse de maître, U. New South Wales.

NIU L., GOLDE D.W., VERA J.C., ET HEANEY M.L., 1999. Kinetic resolution of two mechanisms for high-affinity granulocyte-macrophage colony-stimulating factor binding to its receptor. *Blood*, 94, 3748–3753.

NORDON R.E., NAKAMURA M., RAMIREZ C., ET ODELL R., 1999. Analysis of growth kinetics by division tracking. *Immunol. Cell Biol.*, 77, 523–529.

NOVAK J.P. ET NEČAS E., 1994. Proliferation differentiation pathways of murine, haematopoiesis : Correlation of lineage fluxes. *Cell Prolif.*, 27, 597–633.

OOSTENDORP R.A., AUDET J., ET EAVES C.J., 2000. High-resolution tracking of cell division suggests similar cell cycle kinetics of hematopoietic stem cells stimulated in vitro and in vivo. *Blood*, 95, 855–862.

PARISH C.R., 1999. Fluorescent dyes for lymphocyte migration and proliferation studies. *Immunol. Cell Biol.*, 77, 499–508.

PETROS W.P., 1992. Pharmacokinetics and administration of colony-stimulating factors. *Pharmacotherapy*, 12, 32S–38S.

PRICE T.H., CHATTA G.S., ET DALE D.C., 1996. Effect of recombinant granulocyte colony stimulating factor on neutrophil kinetics in normal young and elderly humans. *Blood*, 88, 335–340.

PUJO-MENJOUET L., 2001. *Contribution à l'étude d'une équation de transport à retards décrivant une dynamique de population cellulaire.* Thèse de doctorat, Univ. de Pau et des Pays de l'Adour, France.

PUJO-MENJOUET L. ET RUDNICKI R., 2000. Global stability of cellular populations with unequal division. *Can. Appl. Math. Quart.*, 8, 99–102.

REEVE J., 1973. An analogue model of granulopoiesis for the analysis of isotopic and other data obtained in the non-steady state. *Brit. J. Haematol.*, 25, 15–32.

RUBINOW S.I., 1969. A simple model of a steady state differentiating cell system. *J. Cell. Biol.*, 43, 32–39.

RUBINOW S.I. ET LEBOWITZ J.L., 1975. A mathematical model of neutrophil production and control in normal man. *J. Math. Biol.*, 1, 187–225.

RUBINOW S.I. ET LEBOWITZ J.L., 1976a. A mathematical model of the acute myeloblastic leukemia. *Biophys. J.*, 16, 897–91.

RUBINOW S.I. ET LEBOWITZ J.L., 1976b. A mathematical model of the chemotherapeutic treatment of acute myeloblastic leukemia. *Biophys. J.*, 16, 1257–1271.

RUBINOW S.I., LEBOWITZ J.L., ET SAPSE A.M., 1971. Parameterization of *in vivo* leukemic cell populations. *Biophys. J.*, 11, 175–188.

SÁNCHEZ E. ET WEBB G.F., 2001. Semigroup theory for population dynamics. Lecture notes for 2001 Siguenza Summer School.

SANTILLAN M., BÉLAIR J., MAHAFFY J.M., ET MACKEY M.C., 2000. Regulation of platelet production : The normal response to perturbation and cyclical platelet disease. *J. Theor. Biol.*, 206, 585–903.

SCHMITZ S., FRANKE H., LOEFFLER M., WICHMANN H.E., ET DIEHL V., 1994. Reduced variance of bone-marrow transit time of granulopoiesis : A possible pathomechanism of human cyclic neutropenia. *Cell Prolif.*, 27, 655–667.

SCHMITZ S., FRANKE H., WICHMANN H.E., ET DIEHL V., 1995. The effect of continuous G-CSF application in human cyclic neutropenia : A model analysis. *Brit. J. Haematol.*, 90, 41–47.

SCHMITZ S., LOEFFLER M., JONES J.B., LANGE R.D., ET WICHMANN H.E., 1990. Synchrony of bone marrow proliferation and maturation as the origin of cyclic haemopoiesis. *Cell Tissue Kinet.*, 23, 425–441.

SHEEHY M.E., MCDERMITT A.B., FURLAN S.N., KLENERMAN P., ET NIXON D.F., 2001. A novel technique for the fluorometric assesment of T lymphocyte antigen specific lysis. *J. Immunol. Methods*, 249, 99–110.

SHVITRA D., LAUGALYS R., ET KOLESOV Y.S., 1983. Mathematical modeling of the production of white blood cells. Dans MARCHUK G. ET BELYKH L., réds., *Mathematical Modeling in Immunology and Medicine*, p. 211–223. North-Holland, Amsterdam.

SMEBY W. ET BENESTAD H.B., 1980. Simulation of murine granulopoiesis. *Blut*, 41, 47–60.

SMITH J.A. ET MARTIN L., 1973. Do cell cycle ? *Proc. Natl. Acad. Sci. USA*, 70, 1263–1267.

STEENSMA D.P., HARRISON C.N., ET TEFFERI A., 2001. Hydroxyurea-associated platelet count oscillations in polycythemia vera : a report of four new cases and a review. *Leuk. Lymphoma*, 42, 1243–1253.

STEFANICH E., SENN T., WIDMER R., FRATINO C., KELLER G.A., ET FIELDER P.J., 1997. Metabolism of thrombopoietin (TPO) in vivo : Determination of the binding dynamics for TPO in mice. *Blood*, 89, 4063–4070.

STEINBACH K.H., RAFFLER H., PABST G., ET FLIEDNER T.M., 1980. A mathematical model of canine granulocytopoiesis. *J. Math. Biol.*, 10, 1–12.

TAKAHASHI M., 1966. Theoretical basis for cell cycle analysis. I. Labelled mitosis wave method. *J. Theor. Biol.*, 13, 202–211.

TAKATANI H., SODA H., FUKUDA M., WATANABE M., KINOSHITA A., NAKAMURA T., ET OKA M., 1996. Levels of recombinant human granulocyte colony-stimulating factor in serum are inversely correlated with circulating neutrophil counts. *Antimicrob. Agents Ch.*, 40, 988–991.

TERASHI K., OKA M., OHDO S., FURUKUBO T., IKEDA C., FUKUDA M., SODA H., HIGUCHI S., ET KOHNO S., 1999. Close association between clearance of recombinant human granulocyte colony-stimulating factor (G-CSF) and G-CSF receptor on neutrophils in cancer patients. *Antimicrob. Agents Ch.*, 43, 21–24.

VÁCHA J. ET ZNOJIL V., 1975. Application of a mathematical model of erythropoiesis to the process of recovery after acute x-irradiation of mice. *Biofizika*, 20, 872–879.

VICKERS M., BROWN G.C., COLOGNE J.B., ET KYOIZUMI S., 2000. Modelling haemopoietic stem cell division by analysis of mutant red cells. *Brit. J. Haematol.*, 110, 54–62.

VON SCHULTHESS G.K. ET MAZER N.A., 1982. Cyclic neutropenia (CN) : A clue to the control of granulopoiesis. *Blood*, 59, 27–37.

WARD A.C., VAN AESCH Y.M., GITS J., SCHELEN A.M., DE KONING J.P., VAN LEEUWEN D., FREEDMAN M.H., ET TOUW I.P., 1999. Novel Point Mutation in the Extracellular Domain of the Granulocyte Colony-stimulating Factor (G-CSF) Receptor in a Case of Severe Congenital Neutropenia Hyporesponsive to G-CSF Treatment. *J. Exp. Med.*, 190, 497–508.

WARREN H.S., 1999. Using carboxyfluorescein diacetate succinimidyl ester to monitor human NK cell division : Analysis of the effect of activating and inhibitory class I MHC receptors. *Immunol. Cell Biol.*, 77, 544–551.

WEBB G.F., 1985. *Theory of Nonlinear age-dependent population dynamics*, t. 89 de *Monographs and Textbooks in Pure and Appl. Math. Series*. Dekker.

WEINBLATT M.E., SCIMECA P., JAMES-HERRY A., SAHDEV I., ET KOCHEN J., 1995. Transformation of congenital neutropenia into monosomy 7 and acute non-lymphoblastic leukemia in a child treated with granulocyte colony-stimulating factor. *J. Pediatr.*, 126, 263–2655.

WHELDON T.E., 1975. Mathematical models of oscillatory blood cell production. *Math. Biosci.*, 24, 289–305.

WICHMANN H.E., LOEFFLER M., ET SCHMITZ S., 1988. A concept of hemopoietic regulation and its biomathematical realization. *Blood Cells*, 14, 411–429.

WICHMANN H.E. ET LOFFLER M., 1988. *Mathematical Modeling of Cell Proliferation : Stem Cell Regulation in Hemopoiesis*. CRC Press, Boca Raton.

WICHMANN H.E., LOFFLER M., PANTEL K., ET WULFF H., 1989. A mathematical model of erythropoiesis in mice and rats. part 2 : Stimulated erythropoiesis. *Cell Tissue Kinet.*, 22, 31–49.

WICHMANN H.E., SPECHTMEYER H., GERECKE D., ET GROSS R., 1976. A mathematical model of erythropoiesis in man. *Lecture Notes in Biomathematics*, 11, 159–179.

WILLIAMS G.T., SMITH C.A., SPOONCER E., DEXTER T.M., ET TAYLOR D.R., 1990. Haemopoietic colony stimulating factors promote cell survival by suppressing apoptosis. *Nature*, 343, 76–79.

WRIGHT D.G., DALE D.C., FAUCI A.S., ET WOLFF S.M., 1981. Human cyclic neutropenia : clinical review and long term follow up of patients. *Medicine*, 60, 1–13.

WULF H., WICHMANN H.E., PANTEL K., ET LOEFFLER M., 1989. A mathematical model of erythropoiesis in mice and rats. part 3 : Suppressed erythropoiesis. *Cell Tissue Kinet.*, 22, 51–61.

YANOKUR M., TAKASE K., YAMAMOTO K., ET TERAOKA H., 2000. Cell death and cell-cycle arrest induced by incorporation of [3H] thymidine into human haemopoietic cell lines. *Int. J. Radiat. Biol.*, 76, 295–303.

ZHANG X.W., AUDET J., PIRET J.M., ET LI Y.X., 2001. Cell cycle distribution of primitive haematopoietic cells stimulated in vitro and in vivo. *Cell Prolif.*, 34, 321–330.

ZNOJIL V. ET VÁCHA J., 1975. Mathematical model of the cytokinetics of erythropoiesis in the bone marrow and spleen of mice. *Biofizika*, 20, 661–668.

Annexe A

PROCÉDURES MATLAB POUR LES ÉQUATIONS CINÉTIQUES DU CHAPITRE 5

```
function [Total,NonP,Prol]=PlotMixedPop(t,k0,k1,beta,tau,gam,mu,ic,data);
%  PlotDivisionMix plots the histogram of division distribution
%   [T1,N1,P1]=PlotMixedPop(t,k0,k1,beta,tau,gam,mu,ic); plot
%   the histogram of the relative cell population versus the
%   number of cellular divisions performed by a number m
%   subpopulation cohorts of cells
%   initially labeled by CFSE at time t=0.
%
%   The histogram is plotted at time t,from
%   division number k0 to k1 as x-axis, with parameters:
%
%   beta = reentry rate into proliferative phase, represented
%          as a vector beta=[b1 l1; b2 l2; ... ;bm lm] where
%          b1,b2,...,bm are the reentry rate wrt each populations
%          and l1,l2,...,lm are the initial proportion of each populations
%          (the sum of l1 to lm must be 1);
%   tau = cell cycle duration,
%   gam = apoptosis in the proliferative phase,
%   mu = disapearance rate from the resting (G_0) phase
%        (apoptosis, differentiation,...)
%   ic = initial proportion of cells in resting (G_0) phase,
%        must be between 0 and 1.
%   data = vector containing experimental data [f1 fm] where corresponding
%          to fuorescence profile for divisions k0 to k1
%          if no data, enter the null vector []
%
%   Initial condition: IC% of cells in resting phase
%   Condition I:  All cells in proliferating phase at time 0
%                 and age 0.
%   Condition II: All cells in resting phase at time 0 and age 0.
```

```
%   Mixed conditions: (1-ic)*I + ic*II
%   Mixed populations: beta vector representing different pop
%                      beta=[b1 l1; b2 l2; ... bm lm];
%
%  See also PlotDivisionMix
%

% (c) Samuel Bernard, Universite de Montreal and
    %     CND, McGill University, 2002


m=length(beta(:,1));
dl=length(data);

for j=1:m,
    [T,N,P]=...
        PlotDivisionMix(t,k0,k1,beta(j,1),tau,gam,mu,ic,data);
    T1(:,j)=T'*beta(j,2);
    N1(:,j)=N'*beta(j,2);
    P1(:,j)=P'*beta(j,2);
end;


Total=sum(T1,2)';
NonP=sum(N1,2)';
Prol=sum(P1,2)';
X=k0:k1;
if dl==0,
    Y=[Prol' NonP' Total'];
    bar(X,Y)
    legend('Prolif','Non Prolif','Total',2);
else
    if dl<length(X),
        data(dl+1:length(X))=0;
    elseif dl>length(X),
        data=data(1:length(X));
    end;
    Y=[Prol' NonP' Total',data'];
    bar(X,Y)
    legend('Prolif','Non Prolif','Total','Exp Data',2);
end;

yt=1.05*max(Total);
title('Fluorescence prolfile of CFSE+','FontSize',18);
xlabel('Number of divisions','FontSize',18);
ylabel('Relative Population','FontSize',18);
tb=num2str(beta);
```

```
tb2=strcat('\beta=',tb);
tt=num2str(tau);
tt2=strcat('\tau=',tt);
tg=num2str(gam);
tg2=strcat('\gamma=',tg);
td=num2str(mu);
td2=strcat('\mu=',td);
ti=num2str(100*ic);
ti2=strcat('% non prolif=',ti);
text(k1-1,0.9*yt,tb2);
text(k1-1,0.85*yt,tt2);
text(k1-1,0.80*yt,tg2);
text(k1-1,0.75*yt,td2);
text(k1-1,0.70*yt,ti2);
axis tight

function [Total,NonP,Prol]=PlotDivisionMix(t,k0,k1,beta,tau,gam,mu,ic,data);
%  PlotDivisionMix plots the histogram of division distribution
%   [Total,NonP,Prol]=PlotDivisionMix(t,k0,k1,beta,tau,gam,mu,ic); plots
%   the histogram of the relative CFSE fluorescence versus the
%   number of cellular divisions performed by a cohort of cells
%   initially labeled by CFSE at time t=0.
%
%   The histogram is plotted at time t,from
%   division number k0 to k1 as x-axis, with parameters:
%
%   beta = reentry rate into proliferative phase,
%   tau = cell cycle duration,
%   gam = apoptosis in the proliferative phase,
%   mu = disapearance rate from the resting (G_0) phase
%        (apoptosis, differentiation,...)
%   ic = initial proportion of cells in resting (G_0) phase,
%        must be between 0 and 1.
%
%   data = vector containing experimental data [f1 fm] where corresponding
%          to fuorescence profile for divisions k0 to k1
%          if no data, enter the null vector []
%
%   Output:
%   Total is a vector of length (k1-k0+1) containing the relative
%         fluorescence of the total population for division
%         for division number k0 to k1,
%   NonP  is a vector of length (k1-k0+1) containing the relative
%         fluorescence of the resting (G_0) phase population for division
%         for division number k0 to k1,
%   Prol  is a vector of length (k1-k0+1) containing the relative
%         fluorescence of the proliferative population for division
```

```
%         for division number k0 to k1,
%
%   Initial condition: IC% of cells in resting phase
%   Condition I:  All cells in proliferating phase at time 0
%                 and age 0.
%   Condition II: All cells in resting phase at time 0 and age 0.
%   Mixed conditions: (1-ic)*I + ic*II
%
    % (c) Samuel Bernard, Universite de Montreal and
    %     CND, McGill University, 2002

% Needs PDensity, PDensity2.


dl=length(data);

for k=k0:k1,  % Condition I
    if k==0,
        N(k+1)=0;
        P(k+1)=exp(-gam*t)*(t<=tau);
    else
        N(k+1)=2^k*beta^(k-1)*exp(-k*gam*tau).*...
            exp(-(beta+mu)*(t-k*tau)).*(t-k*tau)^(k-1)/factorial(k-1)...
            .*(t>=k*tau);
        P(k+1)=quadl(@PDensity,0,tau,[],[],t,k,beta,tau,gam,mu);
    end;
        T(k+1)=N(k+1)+P(k+1);
end;

for k=k0:k1,  % Condition II
    N2(k+1)=2^k*beta^k*exp(-k*gam*tau).*...
        exp(-(beta+mu)*(t-k*tau)).*(t-k*tau)^k/factorial(k)...
        .*(t>=k*tau);
    P2(k+1)=quadl(@PDensity2,0,tau,[],[],t,k,beta,tau,gam,mu);
    T2(k+1)=N2(k+1)+P2(k+1);
end;

Total=(1-ic).*T+ic.*T2;;
NonP=(1-ic)*N+ic*N2;
Prol=(1-ic)*P+ic*P2;
X=k0:k1;
if dl==0,
    Y=[Prol' NonP' Total'];
    bar(X,Y)
    legend('Prolif','Non Prolif','Total',2);
else
    if dl<length(X),
```

```
        data(dl+1:length(X))=0;
    elseif dl>length(X),
        data=data(1:length(X));
    end;
    Y=[Prol' NonP' Total' data'];
    bar(X,Y)
    legend('Prolif','Non Prolif','Total','Exp Data',2);
end;

yt=1.05*max(Total);
title('Fluorescence profile of CFSE+','FontSize',18);
xlabel('Number of divisions','FontSize',18);
ylabel('Relative Population','FontSize',18);
tb=num2str(beta);
tb2=strcat('\beta=',tb);
tt=num2str(tau);
tt2=strcat('\tau=',tt);
tg=num2str(gam);
tg2=strcat('\gamma=',tg);
td=num2str(mu);
td2=strcat('\mu=',td);
ti=num2str(ic);
ti2=strcat('IC=',ti);
texte=strvcat(tb2,tt2,tg2,td2,ti2);
text(k1-1,0.7*yt,texte);
axis tight


function PlotDensity(t0,t1,a0,a1,k,beta,tau,gam,mu,ng);
% PLOTDENSITY plots densities p(t,a) and n(t,a)
%   PlotDensity(t0,t1,a0,a1,k,beta,tau,gam,mu,ng); plots
%   the densities n_k(t,a) and p_k(t,a) where in a 3D plot
%   with time t ranging from t0 to t1, and age a ranging from
%   a0 to a1 for cells having performed k divisions.  The parameters
%   are:
%   beta = reentry rate into proliferative phase,
%   tau = cell cycle duration,
%   gam = apoptosis in the proliferative phase,
%   mu = disapearance rate from the resting (G_0) phase
%        (apoptosis, differentiation,...)
%   ng is the grid resolution (25 is fine).
%   k is a vector containing generation to be plotted e.g. k=[2 3 4]
%

% (c) Samuel Bernard, Universite de Montreal and
    %     CND, McGill University, 2002
```

```
ht=(t1-t0)/ng;
ha=(a1-a0)/ng;

nk=length(k);

t=t0:ht:t1;
a=a0:ha:a1;
[T,A]=meshgrid(t,a);

for m=1:nk,
  subplot(nk,2,2*m-1)
  N=NDensity(A,T,k(m),beta,tau,gam,mu);
  surf(T,A,N);
  titre='n density when k=';
  ks=num2str(k(m));
  tks=strcat(titre,ks);
  title(tks);
  ylabel('age (days)');
  shading interp;
  axis([ t0 t1 a0 a1 ]);
  colormap cool;
  view(2);
end;
xlabel('time (days)')

for m=1:nk,
  subplot(nk,2,2*m)
  P=PDensity(A,T,k(m),beta,tau,gam,mu);
  surf(T,A,P);
  titre='p density when k=';
  ks=num2str(k(m));
  tks=strcat(titre,ks);
  title(tks);
  shading interp;
  axis([ t0 t1 a0 a1 ]);
  colormap cool;
  view(2);
end;
xlabel('time (days)')

function p=PDensity2(a,t,k,beta,tau,gam,mu);
%  PDensity2 gives the density of k-divided cells
%   p=PDensity2(a,t,k,beta,tau,gam,mu); gives the density of
%   proliferation cells in a time-age structured model
%   of cell proliferation.
%   PDensity2(a,t,k,beta,tau,gam,mu); is the cell density
%   at time t, of age a, which have divided k times, (k>=1).
```

```
%   beta is the reentry rate into the
%   proliferative phase, tau is the duration of the proliferative
%   phase and gam is the rate of apoptosis of cells in proliferative
%   phase.
%   INITIAL CONDITION: DIRAC DELTA FOR N IN T=0 A=0

% (c) Samuel Bernard, Universite de Montreal and
    %     CND, McGill University, 2002

p=(t-a-k*tau).^k/factorial(k)*2^k*beta^(k+1)*exp(-k*gam*tau).*...
      exp(-(beta+mu)*(t-a-k*tau)).*exp(-gam*a).*(t>=a+k*tau).*...
      (a<=tau);



function p=PDensity(a,t,k,beta,tau,gam,mu);
%  PDensity gives the density of k-divided cells
%   p=PDensity(a,t,k,beta,tau,gam,mu); gives the density of
%   proliferating cells in a time-age structured model
%   of cell proliferation.
%   PDensity(a,t,k,beta,tau,gam,mu); is the cell density
%   at time t, of age a, which have divided k times, (k>=1).
%   beta is the reentry rate into the
%   proliferative phase, tau is the duration of the proliferative
%   phase and gam is the rate of apoptosis of cells in proliferative
%   phase.
%   INITIAL CONDITION: DIRAC DELTA FOR P IN T=0 A=0

     % (c) Samuel Bernard, Universite de Montreal and
    %     CND, McGill University, 2002

p=(t-a-k*tau).^(k-1)/factorial(k-1)*2^k*beta^k*exp(-k*gam*tau).*...
      exp(-(beta+mu)*(t-a-k*tau)).*exp(-gam*a).*(k>=1).*(t>=a+k*tau).*...
      (a<=tau)+...
      (t==a).*(k==0).*exp(-gam*a);



function n=NDensity2(a,t,k,beta,tau,gam,mu);
%  NDensity2 gives the density of k-divided cells
%   n=NDensity2(a,t,k,beta,tau,gam,mu); gives the density of
%   resting phase (G_0) cells in a time-age structured model
%   of cell proliferation.
%   NDensity2(a,t,k,beta,tau,gam,mu); is the cell density
%   at time t, of age a, which have divided k times, (k>=1).
%   beta is the reentry rate into the
%   proliferative phase, tau is the duration of the proliferative
```

```
%   phase and gam is the rate of apoptosis of cells in proliferative
%   phase.
%   INITIAL CONDITION: DIRAC DELTA FOR N IN T=0 A=0

 % (c) Samuel Bernard, Universite de Montreal and
    %     CND, McGill University, 2002

n=(t-a-k*tau).^(k-1)./factorial(k-1).*2^k.*beta^k.*exp(-k*gam*tau).*...
     exp(-(beta+mu).*(t-k*tau))*(k>=1).*(t>=a+k*tau)+...
     (t-tau==a).*(k==0).*exp(-(beta+mu).*a);

function n=NDensity(a,t,k,beta,tau,gam,mu);
%  NDensity gives the density of k-divided cells
%   n=NDensity(a,t,k,beta,tau,gam,mu); gives the density of
%   resting phase (G_0) cells in a time-age structured model
%   of cell proliferation.
%   NDensity(a,t,k,beta,tau,gam,mu); is the cell density
%   at time t, of age a, which have divided k times, (k>=1).
%   beta is the reentry rate into the
%   proliferative phase, tau is the duration of the proliferative
%   phase and gam is the rate of apoptosis of cells in proliferative
%   phase.
%   INITIAL CONDITION: DIRAC DELTA FOR P IN T=0 A=0

 % (c) Samuel Bernard, Universite de Montreal and
    %     CND, McGill University, 2002

n=(t-a-k*tau).^(k-2)./factorial(k-2).*2^k.*beta^(k-1).*exp(-k*gam*tau).*...
     exp(-(beta+mu).*(t-k*tau))*(k>=2).*(t>=a+k*tau)+...
     2.*(t-tau==a).*(k==1).*exp(-gam*tau).*exp(-(beta+mu).*a);
```

Annexe B

ACCORD DES AUTEURS ET DES ÉDITEURS

Accord des auteurs pour l'inclusion d'article dans la thèse

1. Identification de l'étudiant

Nom de l'étudiant : [redacted]

Code permanent : [redacted]

Département de mathématiques et de statistique,

Faculté des arts et des sciences,

Université de Montréal.

Programme : Ph.D. Mathématiques appliquées.

2. Description de l'article (auteurs, titre, revue, date)

Bernard, S., Bélair, J., et Mackey, M.C., (2001) Sufficient conditions for stability of linear differential equations with distributed delays. Discrete and Continuous Dynamical Systems-Series B. 1 : 233-256.

3. Déclaration des coauteurs autres que l'étudiant

À titre de coauteur de l'article identifié ci-dessus, je suis d'accord pour que SAMUEL BERNARD inclue cet article dans sa thèse de doctorat qui a pour titre ÉQUATIONS DIFFÉRENTIELLES À RETARD ET LEUR APPLICATION EN HÉMATOPOÏÈSE, AVEC ÉTUDE DU CAS DE LA NEUTROPÉNIE CYCLIQUE.

JACQUES BÉLAIR [redacted]		28 août 03
Coauteur	Signature	Date
MICHAEL C. MACKEY [redacted]		27/08/03
Coauteur	Signature	Date

1. Identification de l'étudiant

Nom de l'étudiant : [redacted]

Code permanent : [redacted]

Département de mathématiques et de statistique,

Faculté des arts et des sciences,

Université de Montréal.

Programme : Ph.D. Mathématiques appliquées.

2. Description de l'article (auteurs, titre, revue, date)

Bernard, S., Bélair, J., Mackey, M.C., (2003) Oscillations in Cyclical Neutropenia : New Evidence Based on Mathematical Modeling, J. Theor. Biol. 223 : 283-298.

3. Déclaration des coauteurs autres que l'étudiant

À titre de coauteur de l'article identifié ci-dessus, je suis d'accord pour que SAMUEL BERNARD inclue cet article dans sa thèse de doctorat qui a pour titre ÉQUATIONS DIFFÉRENTIELLES À RETARD ET LEUR APPLICATION EN HÉMATOPOÏÈSE, AVEC ÉTUDE DU CAS DE LA NEUTROPÉNIE CYCLIQUE.

JACQUES BÉLAIR [redacted]		28 août 03
Coauteur	Signature	Date
MICHAEL C. MACKEY [redacted]		27/08/03
Coauteur	Signature	Date

1. Identification de l'étudiant

Nom de l'étudiant : [redacted]

Code permanent : [redacted]

Département de mathématiques et de statistique,

Faculté des arts et des sciences,

Université de Montréal.

Programme : Ph.D. Mathématiques appliquées.

2. Description de l'article (auteurs, titre, revue, date)

Bernard, S., Bélair, J., Mackey, M.C., Bifurcations in a model of blood cell production, accepté en juin 2003 pour publication dans C. R. Biologies.

3. Déclaration des coauteurs autres que l'étudiant

À titre de coauteur de l'article identifié ci-dessus, je suis d'accord pour que SAMUEL BERNARD inclue cet article dans sa thèse de doctorat qui a pour titre ÉQUATIONS DIFFÉRENTIELLES À RETARD ET LEUR APPLICATION EN HÉMATOPOÏÈSE, AVEC ÉTUDE DU CAS DE LA NEUTROPÉNIE CYCLIQUE.

JACQUES BÉLAIR [redacted] 28 août 03

Coauteur Signature Date

MICHAEL C. MACKEY [redacted] 27/08/03

Coauteur Signature Date

1. Identification de l'étudiant

Nom de l'étudiant : [redacted]

Code permanent : [redacted]

Département de mathématiques et de statistique,
Faculté des arts et des sciences,
Université de Montréal.
Programme : Ph.D. Mathématiques appliquées.

2. Description de l'article (auteurs, titre, revue, date)

Bernard, S., Pujo-Menjouet, L., Mackey M.C., (2003) Analysis of Cell Kinetics Using a Cell Division Marker : Mathematical Modeling of Experimental Data, Biophys. J. 84 : 3414-3424.

3. Déclaration des coauteurs autres que l'étudiant

À titre de coauteur de l'article identifié ci-dessus, je suis d'accord pour que SAMUEL BERNARD inclue cet article dans sa thèse de doctorat qui a pour titre ÉQUATIONS DIFFÉRENTIELLES À RETARD ET LEUR APPLICATION EN HÉMATOPOÏÈSE, AVEC ÉTUDE DU CAS DE LA NEUTROPÉNIE CYCLIQUE.

LAURENT PUJO-MENJOUET [redacted] 25 Août 2003

Coauteur Signature Date

MICHAEL C. MACKEY [redacted] 27/08/03

Coauteur Signature Date

Autorisation des éditeurs pour l'inclusion d'article dans la thèse

Dear Professor Bernard:

Your request is granted under one condition: The original source of publication (with CDS-B) must be properly cited.

Sincerely,

Shouchuan Hu,
Director of AIMS Managing Editor of
"Discrete and Continuous Dynamical Systems"
On the web at http://AIMSciences.org

Professor
Department of Mathematics
Southwest Missouri State University
901 S. National,
Springfield, MO 65804, USA
Tel: (417) 836-5377; Fax: (417) 886-0559

----- Original Message -----
From: "Samuel Bernard" [redacted]
To [redacted]> Sent: Thursday,
August 07, 2003 2:49 PM
Subject: authorization to include article in thesis

Dear Prof. Hu,
I would like to request the authorization to include the following article, by myself and co-workers, in my Ph.D. thesis, entitled
\'Equations diff\'erentielles \'a retard et leur application en

h\'ematopo\"\i\'ese, avec \'etude du cas de la neutrop\'enie cyclique / Delay Differential Equations and Their application in hematopoiesis, with a case study on cyclical neutropenia

Bernard, S., B\'elair, J., et Mackey, M.C., (2001) Sufficient conditions for stability of linear differential equations with distributed delays. Discrete and Continuous Dynamical Systems-Series B. 1: 233-256.

Could you send your authorization letter to the address below

Thank you

Sincerely yours

Samuel Bernard
Département de Mathématiques et statistique
Université de Montréal
CP 6128
succ Centre-Ville Montréal
QC H3C 3J7 Canada

Autorisation de Elsevier

Les articles des chapitres 3 et 4 ont été publiés par Elsevier.

Bernard, S., Bélair, J., Mackey, M.C., (2003) Oscillations in Cyclical Neutropenia : New Evidence Based on Mathematical Modeling, J. Theor. Biol. 223 : 283-298.

Bernard, S., Bélair, J., Mackey, M.C., Bifurcations in a model of blood cell production, accepté en juin 2003 pour publication dans C. R. Biologies.

Extrait du site web du *Journal of Theoretical Biology*[1]

> What rights do I retain as author ?
>
> As an author, you retain rights for large number of author uses, including use by your employing institute or company. These rights are retained and permitted without the need to obtain specific permission from Elsevier.
>
> The right to include the article in a thesis or dissertation provided that this is not to be published commercially.

[1] authors.elsevier.com/getting_published.html ?dc=CI

Autorisation du Biophysical Journal